OPTIMIZATION OF PERVIOUS CONCRETE INCORPORATING COAL FLY ASH, IRON-OXIDE NANOPARTICLES AND WATER REDUCING ADMIXTURES AND ITS APPLICATION FOR THE REMOVAL OF NUTRIENTS AND FECAL COLIFORMS

By

LINOSHKA SOTO PÉREZ

A thesis submitted in partial fulfillment of the requirements for the degree of

MASTER OF SCIENCE

In

CIVIL ENGINEERING

(Environmental and Water Resources Engineering)

UNIVERSITY OF PUERTO RICO

MAYAGÜEZ CAMPUS

May 2015

Approved by:

Sangchul S. Hwang, PhD President, Graduate Committee	Date
Omar I. Molina Bas, PhD Member, Graduate Committee	Date
Moses N. Bogere, PhD Member, Graduate Committee	Date
José Cortés, PhD Representative, Graduate School	Date
Ismael Pagán Trinidad, MSCE Chair, Department of Civil Engineering and Surveying	Date

ABSTRACT

Physicomechanical characteristics and durability of the cement pastes containing fly ash (FA) and iron-oxide nanoparticles (NI) showed that workability was reduced with the FA addition, although it was counterbalanced when NI was added. FA substitution enhanced the durability of the hardened pastes by gaining weight and compressive strength when exposed to tap water. However, in acid solutions, the FA substitution produced a negative effect on the durability of the hardened pastes. In comparison, the addition of NI alone increased the compressive strength of the hardened pastes exposed to acid solutions.

Concrete is the most widely used engineering construction material. There are different cement mixtures with special properties and chemical compositions that are made to specifications for specific applications. Concrete properties such as strength and durability mostly depend on its internal microstructure, which can be modified and improved by adding mineral admixtures and other additives. Several experiments were conducted to assess the physicomechanical and durability properties of cement pastes containing different additives, optimize the combination of different mixture components and, make a reactive Portland cement pervious concrete (PCPC) and evaluate its mechanical and hydrological capabilities, as well as the FC inactivation and nutrients removal from water.

Different curing periods during the development of compressive strength of the cement pastes with FA and NI as admixtures showed that lower compressive strength (CS) was achieved with the increase of FA at early periods of curing. On the other hand, the CS was improved after 90 days of curing. The NI only contribute to the CS at late curing ages. The effect of cement type on the spread percentage (SP) and the compressive strength at 28 days of curing was also evaluated in the cement pastes. The optimum mix ratio of two cement types was obtained for a desired SP and the maximum possible CS. The addition of NI to the mixtures did not play a significant role in the development of the CS at 28 days of curing. The optimum variable settings for the Type IP cement were at 35.1 % W/B, 28.5% FA/B and 1.6% NI/B, while for the Type GU cement the settings were obtained at 35.1% W/B, 40% FA/B and 0.55% NI/B. Slightly higher predictive compressive strength at 64.72 MPa for the Type GU cement was obtained, while for the Type IP

a 62.78 MPa was predicted. Quadratic and interaction effects of the factors resulted in playing a significant role in the development of both of the prediction models of the dependent responses.

The effect of aggregate type and grading size on the manufacture of PCPC and its performance permeability and CS were evaluated. Gravels retained in the sieves with smaller opening size were better for the PCPC production since a higher compressive strength was obtained. At the same time the permeability was kept between the ranges established for PCPC by the American Concrete Institute. Partial clogging due to the drainage of the binder materials was observed for some of the specimens due to an excess in the W/B ratios and the reduction of FA/B in the PCPC.

A green pervious concrete surface (GPCS) capable of removing contaminants from water was developed in a four factor, two level central composite design to investigate the main, quadratic and interaction effects of the independent variables on the permeability and compressive strength. The increment of W/B and the reduction of FA/B independent of the settings of NI/B and WR/B resulted in a decrease of the permeability. The addition of high amounts of FA/B required a large addition NI/B in order to achieve a compressive strength higher than 20.7 MPa, while lower additions of FA/B were found to require less amount of NI/B to achieve similar CS's. Phosphorus and FC removals were achieved at a high pH, with average values for FC inactivation of 74.2, 67.9 and 95.4% at 2 hour contact time, and for phosphorus removal of 92.6, 84.6 and 100% for Opt A, Opt B and Control, respectively. The increase of contact time improved the nitrate reduction, achieving removals up to up to 79.0, 48.8 and 54.3% by the Opt A, Opt B and Control, respectively. Weight increment in all GPCS's was observed when exposed to either water or sulfuric acid, although the increment was more noticeable for the specimens placed in water. On the contrary, GPCS placed in the acetic acid solution resulted in a rapid weight loss from the beginning of the experiment. The simultaneous addition of FA and NI resulted in a higher compressive strength for the GPCS even after the exposure to acids.

RESUMEN

Las características físico-mecánicas y la durabilidad de pastas de cemento que contienen cenizas volantes (FA) y nanopartículas de óxido de hierro (NI) mostraron que la manejabilidad se redujo con la adición de FA, aunque fue contrarrestada cuando se le añadió NI. La sustitución de FA mejoró la durabilidad de las pastas endurecidas mediante el aumento de peso y resistencia a la compresión cuando se expusieron al agua de grifo. Sin embargo, en soluciones ácidas, la sustitución de FA produjo un efecto negativo sobre la durabilidad de las pastas endurecidas. En comparación, la adición de NI solo aumentó la resistencia a la compresión de las pastas endurecidas expuestas a soluciones ácidos.

El hormigón es el material de construcción de ingeniería más ampliamente utilizado. Hay diferentes mezclas de cemento con propiedades especiales y composiciones químicas que se realizan para especificaciones y aplicaciones específicas. Las propiedades del hormigón tales como resistencia y durabilidad dependen principalmente de su microestructura interna, que puede ser modificada y mejorada por la adición de aditivos minerales, entre otros. Se realizaron varios experimentos para evaluar las propiedades físico-mecánicas y de durabilidad de las pastas de cemento que contienen diferentes aditivos, optimizar la combinación de diferentes componentes de la mezcla, hacer un hormigón permeable de cemento Portland reactivo (PCPC) y evaluar sus capacidades mecánicas e hidrológicas, así como la inactivación de coliformes fecales (FC) y la remoción de nutrientes del agua.

Diferentes períodos de curado durante el desarrollo de la resistencia a la compresión de las pastas de cemento con FA y NI mostraron que la menor resistencia a la compresión (CS) se consiguió con el aumento de FA en los primeros períodos de curado. Por otro lado, la CS se mejoró después de 90 días de curado. El NI sólo contribuyó a la CS a edades de curado tardías. El efecto del tipo de cemento en el porcentaje de propagación (SP) y la resistencia a la compresión a los 28 días de curado también se evaluó en las pastas de cemento. La relación de mezcla óptima de los dos tipos de cemento se obtuvo para un SP deseado y la máxima posible CS. La adición de NI a las mezclas no desempeñó un papel importante en el desarrollo de la CS a los 28 días de curado. Los valores de las variables óptimas para el cemento Tipo IP fueron 35.1% W/B, 28.5% FA/B y 1.6% NI/B, mientras que para el cemento Tipo GU los porcentajes fueron 35.1% W/B, 40% FA/B

y 0.5% NI/B. La resistencia a la compresión de predicción para el cemento Tipo GU fue ligeramente mayor, con un valor de 64.72 MPa mientras que para el Tipo IP se predijeron 62.78 MPa. Los efectos cuadráticas y de interacción de los factores resultaron jugar un papel significativo en el desarrollo de ambos modelos de predicción de las respuestas dependientes.

Se evaluó el efecto del tipo de agregado y la clasificación por tamaños en la fabricación de PCPC y en los resultados de permeabilidad y CS. La grava retenida en los tamices con tamaño de apertura más pequeña era mejor para la producción PCPC ya que se obtuvo una resistencia a la compresión superior. Al mismo tiempo, la permeabilidad se mantuvo entre los rangos establecidos para PCPC por el American Concrete Institute (ACI). Se observó obstrucción parcial de los vanos del hormigón permeable debido al drenaje de los materiales aglutinantes para algunas de las muestras debido a un exceso en las proporciones W/B y la reducción de FA/B en el PCPC.

Una superficie verde de hormigón permeable (GPCS) capaz de eliminar contaminantes del agua fue desarrollada en un diseño central de cuatro factores y dos niveles para investigar los efectos principales, cuadráticos y de interacción de las variables independientes sobre la permeabilidad y la resistencia a la compresión. El incremento de W/B y la reducción de FA/B independientemente de los ajustes de NI/B y WR/B resultó en una disminución de la permeabilidad. La adición de altas cantidades de FA/B requirió de una gran adición de NI/B con el fin de lograr una resistencia a la compresión superior a 20.7 MPa, sin embargo se encontró que adiciones inferiores de FA/B requerían menores cantidades de NI/B para lograr similares resultados de CS. La remoción de fosfatos FC se lograron a un pH alto, con valores promedios de inactivación de FC de 74.2, 67.9 y 95.4% para un tiempo de contacto de 2 horas, mientras que para la remoción de fosfato se obtuvieron valores de 92.6, 84.6 y 100% para la muestras Opt A, Opt B y Control, respectivamente. El aumento del tiempo de contacto mejoró la remoción de nitratos, logrando remociones de hasta 79.0, 48.8 y 54.3% en la muestras Opt A, Opt B y Control, respectivamente. Se observó un incremento de peso en todos los de GPCS cuando se expusieron al agua o ácido sulfúrico, aunque el incremento fue más notable para las muestras colocadas en agua. Por el contrario, los GPCS colocados en la soluciones de ácido acético obtuvieron una rápida pérdida de peso desde el inicio del experimento. La adición simultánea de FA y NI resultó en una mayor resistencia a la compresión para la GPCS incluso después de la exposición a los ácidos.

In dedication to my dear God, who gave me the health, strength and knowledge to accomplish my dreams.

To my mother, for making me who I am.

*To my fiancé, for supporting me all the way***.**

ACKNOWLEGEMENTS

I would like to express my gratitude to my God for giving me the strength and guiding me through this journey of my life. Thank God for all of the blessings and for giving me health to achieve this important goal.

I would like to thank my advisor, Dr. Sangchul S. Hwang, for giving me the opportunity to work on this investigation, and for his commitment, his support and guidance during these two years. I would also like to thank my graduate committee, Dr. Omar I. Molina Bas and Dr. Moses N. Bogere for their help and assistance during my college experience and during this investigation.

I want to thank my beloved mother, for her limitless support during my college career and for believing in me and teaching me that no matter what, with God by my side everything is possible. To my family, thanks for your support and encouragement, and for all of your prayers. My deepest thanks to my future husband, for his disinterested support, his unconditional love and for helping me achieve this goal in my life.

I also thank all the people who were involved with me during my years of studies. Thanks to my research group members Juliana, Crystal, Rene, Adriana, Victor, Carlos and Marleisa, Valerie and Minju for your hard work that made possible this research. To Monse, for his help in the materials lab. To my friends Keila, Natalia, Margaret, Joan, Vilda, Isomar, Perla and Irmarie for their laughs, for listening to me and for being with me all the way.

Finally, but not least, I would like to thank for their financial support, in part, to AES Puerto Rico, LLC and the United States Geological Survey through the US Virgin Islands Water Resources Research Institute. Special thanks to Ing. Jesús Davila Scholarship for Master Studies in Environmental Engineering and the Puerto Rico NASA Space Grant Fellowship for their financial support of my studies. I also thank Eng. Ruben Segarra (Essroc San Juan) for his valuable input with the characterization of cement and fly ash and to the civil engineering materials lab technician for his support during the testing of the concrete specimens.

TABLE OF CONTENTS

LIST OF TABLES

LIST OF FIGURES

LIST OF ABBREVIATIONS

A - axial point

a - exposed area

ACI - American Concrete Institute

ACS - American Chemical Society

AF - alumina to iron ratio

ANOVA - analysis of variants

ASTM - American Society for Testing and Materials

C - center point

C_2S - dicalcium silicate

C_3A - tricalcium aluminate

C_3S - tricalcium silicate

C_4AF - tetracalcium aluminoferrite

C-A-H - calcium aluminate hydrate

CCD - central composite design

CCF - face centered central composite design

CFU - colony-forming units

CH - calcium hydroxide

CI - confidence interval

CO_2 - carbon dioxide

COI - loss on ignition

CS - compressive strength

C-S-H - calcium silicate hydrate

d - density

D_f - final diameter of specimen

D_i - initial diameter of specimen

EPA - Environmental Protection Agency

F - factorial point

FA - fly ash

FA/B - fly ash-to-binder

FC - fecal coliforms

g - grams

GPCS - green pervious concrete surface

h - head difference

I - adsorption

k - number of factors

K - permeability

L - length

LSF - lime saturation factor

MH - moderate heat of hydration

m_t - mass change at time t

N - Nitrogen

N_F - number of factorial points

NI - iron-oxide nanoparticles

NI/B - iron-oxide nanoparticles-to-binder

No. - number

NS - not statistically significant

OFAT - one-factor-at-a-time

Opt - optimum

P - Phosphorous

PC - Portland cement

PCPC - Portland cement pervious concrete

RSM - response surface methodology

SEM - Scanning Electron Microscopy

SP - spread percentage

SR - silica ratio

t - time

vol - volume

W/B - water-to-binder

W/C - water-to-cement-ratio

W_f - final weight of specimen

W_i - initial weight of specimen

W_{od} - oven dry weight

WR - water reducer

WR/B - water reducer-to-binder

W_{sd} - surface dry weight

Y - predicted response

α - distance from each axial point to the center of the design space

β - coefficient

ε - error

INTRODUCTION

1. Background

Concrete is the most widely used engineering construction material. It is preferred over other construction materials due to its high resistance to water, versatility in applications, the ability to be cast into any desired shape, low cost and availability. Also, concrete requires less maintenance than other materials and it is resistant to fire and cyclic loadings (Metha and Monteiro, 2014). Portland cement constitutes 10 to 15% of the total concrete mixture by volume (Gagg, 2014), and solidifies due to the hydration reaction that occurs when water is added. According to the American Society for Testing and Materials (ASTM), there are different cements with special properties and chemical compositions that are made to meet particular requirements for specific applications.

Portland cement pervious concrete (PCPC) has been an engineering solution to the arising problem of pollutants in water supplies due to its high porosity and permeability. PCPC is made by eliminating or reducing the fine aggregates and incrementing coarse aggregates, resulting in greater void content and allowing the storm water to infiltrate into the ground, controlling storm water pollution, reducing storm water runoff and recharging groundwater (Deo and Neithalath, 2010). PCPC has been used in the construction of streets, low traffic roads due to its benefits of enhancing of vehicle traction, reducing tire-pavement noise, trapment of the oil spilled by vehicles and reducing the urban heat island effect (Metha and Monteiro, 2014).

The manufacturing of cement is one of the primary contributions to carbon dioxide emissions to the atmosphere. For this reason, substitution of cement with mineral admixtures has been of great interest in order to reduce the cement consumption. Industrial wastes or by-products such as slag, silica fume and fly ash (FA) are some of the most common mineral admixture materials used to replace some of the Portland cement in concrete in order to reduce the cement production/consumption. Some of the benefits of adding mineral admixtures are: reduction of permeability and pore size, and increment in strength and permeability (Chindaprasirt et al., 2005). It also have been reported that concrete properties such as strength and durability mostly depend on its internal microstructure, which can be modified and improved by adding mineral admixtures (Chindaprasirt et al., 2007) and other additives.

2. Justification

Portland cement pervious concrete (PCPC) has been used as an engineering solution to reduce the adverse effects from the increasing problem of pollutants in water supplies due to its high porosity and permeability. This problem is generated as a result of the large amount of impervious surfaces caused by the incremental growth of urban areas. PCPC is made by reducing or eliminating the fine aggregates of the mixture and incrementing the volume of the coarse aggregates. The pores of the PCPC also allow the storm water to infiltrate into the ground, reducing storm water runoff and thereby recharging groundwater (Deo and Neithalath, 2010). PCPC has been used in a wide range of applications such as low traffic volume roads, park surfaces, parking lots, among others. Other advantages include the reduction and elimination of the construction of retention ponds, swales and lagoons as measures for controlling storm water represent a great economic benefit over conventional impervious pavements (Metha and Monteiro, 2014).

Mechanical properties and durability in aggressive environments are very important characteristics of concrete in order to provide a good service life. Early deterioration of concrete structures represents a serious concern for engineers due to the poor acid resistance of Portland cement. More research work is needed in order to understand the concrete chemistry as a key design knowledge. This should lead to efficient selection of the proper materials and parameters that will lead to a strong and durable material. The partial substitution of Portland cement with mineral admixtures has been significantly used due to its positive effects on late strength development and durability enhancement, although no information is available on the use of iron-oxide nanoparticles on high volume FA cements. Chemical admixtures such as water reducers and nanoparticles have also been incorporated in order to enhance the workability and strength of PCPC.

For this reason, the assessment of chemical and physical properties of PCPC such as durability, strength, permeability and workability was conducted by statistical design and analysis where the influential factors have a significant effect on the responses (i.e., strength and permeability). Fly ash, water reducer and iron oxide nanoparticles were incorporated into the PCPC and the optimum combination of these parameters was selected. Also, the water quality enhancement of runoff water focusing on fecal coliform (FC) inactivation and phosphate and nitrate removal was evaluated.

3. Goal and Objectives

The main goal of this investigation was to find the optimum mix design parameters of PCPC in terms of workability, compressive strength and permeability for use in pavements to control and enhance the quality of runoff waters. A water reducer, FA and iron-oxide nanoparticles (NI) coated with a surfactant were incorporated to the mixture to enhance the properties of the PCPC. The specific objectives of the current study were to:

- obtain the low and high levels of water-to-binder (W/B) ratio and FA-to-binder (FA/B) ratio by conducting a one-factor-at-a-time (OFAT) experiment with cement paste specimens;
- test the capillary water absorption, workability, settling time and durability of a two factor, two level (2^2) factorial design with the low and high levels of W/B and FA/B ratios selected and the incorporation of NI-to-binder ratio (NI/B) of cement paste specimens;
- compare the effect of using different cement types on the spread percentage and compressive strength of cement pastes specimens cured for 28 days;
- select the type and size of gravel used in the CCD by conducting a OFAT experiment with PCPC specimens;
- acquire the optimum W/B, FA/B, NI/B and water reducer-to-binder (WR/B) ratios that will give the best compressive strength of a green pervious concrete surface (GPCS) while maintain a good permeability;
- assess the characteristics of filtered runoff water in terms of FC inactivation and nutrient reduction with the optimum mix design of GPCS; and
- evaluate the chemical resistance of the optimum mix design of the GPCS in terms of weight loss and compressive strength change by exposing the specimen to acidic environments.

4. References

Chindaprasirt P, Jaturapitakkul C, Sinsiri T. Effect of fly ash fineness on microstructure of blended cement paste. Construction and Building Materials 2007; 21:1534-1541.

Chindaprasirt P, Jaturapitakkul C, Sinsiri T. Effect of fly ash fineness on compressive strength and pore size of blended cement paste. Cement and Concrete Composites 2005; 27:425-428.

Deo O, Neithalath N. Compressive behavior of pervious concretes and a quantification of the influence of random pore structure. Materials and Science and Engineering A 2010; 528:402-412.

Gagg C. Cement and concrete as an engineering material: An historic appraisal and case study analysis. Engineering Failure Analysis 2014; 40:114-140.

Metha P, Monteiro P. Concrete microstructure, properties and materials, 4th Ed. McGraw-Hill Education, 2014.

CHAPTER 1.

Physicomechanical properties and durability of fly ash cement pastes containing iron-oxide nanoparticles

1.1.Abstract

Physicomechanical characteristics and durability of the cement pastes containing fly ash (FA) (0 and 40% wt.) and iron-oxide nanoparticles (NI) (0 and 3% wt.) were tested. Results showed that workability was reduced with the FA substitution but was offset with the NI addition. The FA substitution and NI addition delayed the setting times. The NI addition reduced the water absorption rate of the hardened pastes but produced a negative effect on the development of compressive and tensile strengths. In general, the FA substitution with and without NI addition enhanced durability of the hardened pastes gaining the weight and compressive strength while exposing in tap water. However, in acid solutions, the FA substitution with and without the NI addition produced a negative effect on the durability of the hardened pastes. In comparison, the addition of NI alone increased the compressive strength of the hardened pastes exposed to acid solutions.

1.2.Literature Review

1.2.1. Cement and Concrete Chemistry

Cement consists of different calcium compounds and its chemical composition is shown in Table 1. The hydration of Portland cement occurs at different rates due to the heterogeneity of the mixture. Silicates react much slower than the aluminates, and they contribute to the strength of the hardened concrete while silicates only contribute to its alkalinity (Metha and Monteiro, 2014). The principal solid phases in hydrated cement paste are: calcium silicate hydrate (C-S-H), calcium hydroxide ($Ca(OH)_2$ or CH) and calcium sulfoaluminate hydrates (ettringite and monosulfate) (Gagg, 2014). The C-S-H gel comprises up to 60% of the total volume of the hardened concrete, and is the principal hydrate contributing to the early strength development of concrete. The formation of the C-S-H gel contributes to the densification of the specimen, preventing the penetration of aggressive agents such as sulfates.

The formation of ettringite and monosulfate depends on the concentration of sulfate ions present in the cement. If the concentration of sulfate ions is high, it's more likely to form ettringite; while if it's low, it tends to form monosulfate. The presence of monosulfates makes concrete more vulnerable to sulfate attack. Sulfates react with the monosulfate in the hardened paste, promoting the delayed ettringite formation, which causes cracking and spalling of the cement paste, thus reducing the mechanical strength and durability of concrete (Setina et al., 2013). On the other hand, CH only occupies 20 to 25% of the hydrated Portland cement volume and is the responsible for the high alkalinity of concrete but does not provide strength to the hardened concrete (Metha and Monteiro, 2014).

Chemical deterioration of concrete is attributed to: a) hydrolysis and leaching of the components of the hardened cement paste, b) cation-exchange reactions between aggressive solutions and the components of the hardened cement paste, and c) the formation of expansive products inside the hardened paste (Metha and Monteiro, 2014). Portland cement concrete does not have high acid resistance because CH is highly soluble in water and leaches out of the concrete, leaving a porous material susceptible to further deterioration due to the interaction with other hostile agents. The removal of calcium from the cement paste is also due to the formation of soluble salts and non-expansible insoluble salts as result of cation-exchange reactions.

Table 1. Chemical composition of Portland cement (Mindess et al., 2003).

Chemical Name	Chemical Formula	Abbreviation	Weight Percent (%)
Tricalcium silicate	$3CaO{\cdot}SiO_2$	C_3S	55 (37-71%)
Dicalcium silicate	$2CaO{\cdot}SiO_2$	C_2S	18 (4-36%)
Tricalcium aluminate	$3CaO{\cdot}Al_2O_3$	C_3A	10 (0-14%)
Tetracalcium aluminoferrite	$4CaO{\cdot}Al_2O_3{\cdot}Fe_2O_3$	C_4AF	8 (4-19%)
Calcium sulfate dihydrate (gypsum)	$CaSO_4{\cdot}2H_2O$	-	6 (1-7%)

1.2.2. Fly Ash

The manufacturing of cement is one of the primary contributions to carbon dioxide (CO_2) emissions to the atmosphere. Approximately 0.54 tons of CO_2 are released to the atmosphere for every ton of Portland cement produced: cement formation involves comples decomposition of calcite. In addition, large amounts of energy are required for the production of cement, increasing CO_2 emissions to 0.34 and 0.09 tons due to fuel and electricity consumption, respectively (Ma et al., 2014). For this reason, substitution of cement with mineral admixtures has been of great interest in order to reduce the cement consumption.

Industrial wastes or by-products such as slag, silica fume and FA are some of the most common mineral admixture materials used to replace some of the Portland cement in concrete in order to reduce the cement production/consumption. Some of the benefits of adding mineral admixtures are: reduction of permeability and pore size, and increment in strength and permeability (Chindaprasirt et al., 2005). It also have been reported that the addition of these admixtures to cement can benefit the final product in terms of technical, economic and environmental improvements (Toledano-Prados et al., 2013).

Coal FA is a by-product produced during the combustion process of coal burning power plants (Zeng et al., 2012). Approximately 500 million tons of FA were produced annually, by the year of 2010 estimates (Ahmaruzzaman, 2010). Fly ash is a fine spherical powder, with a particle size raging between 10 to 100 μm (Pando and Hwang, 2006). Its chemical composition depends on the chemical composition of the coal used and how it is burned in the combustion process. Fly ash can be divided into two different categories depending on its calcium content: Class F ($< 10\%$ by weigth) and Class C ($> 20\%$ by weight).

Table 2 shows the chemical requirements for each class of FA established by ASTM C 618.

Table 2. Chemical requirements for FA established in ASTM C 618.

Chemical Requirements		Class	
		F	C
$SiO_2 + Al_2O_3 + Fe_2O_3$	min %	70	50
SO_3	max %	5	5
Moisture Content	max %	3	3
Loss on Ignition	max %	6	6

The disposal of FA is of serious environmental concern since it contains potentially toxic trace elements (Ahmaruzzaman, 2010). Nevertheless, utilizing its characteristics under controlled environment, FA has been applied as nutrient for plant growth, gas absorbent, and phosphate removal from water (Can and Yildiz, 2006). It has also been found that FA addition to concrete has a positive impact on the internal microstructure and durability of concrete (Deschner et al., 2012). The SiO_2 found in FA reacts with the portlandite available in the hydrated paste to form more C-S-H gel (Deschner et al., 2012), thus reducing the amount of leachable CH and densifying the mixture, producing a stronger concrete. However, some standards limit its uses from 10 to 25% in structural concrete, even though it has been demonstrated that high volume FA cements significantly improve the mechanical and durability properties of concrete (Aydın et al., 2007).

The greatest limitation of using FA in concrete is that the strength improvement is slow and is developed at higher rates after long curing times. It has been found that increasing the temperature of the curing medium helps the pozzolanic reaction to start at early ages (Hanehara et al., 2001).

1.2.3. Nanoparticles

The use of nanoparticles in cement specimens have shown better results by filling voids and increasing the kinetics and hydration process in concrete compared to other mineral admixtures such as FA and silica fume. The most commonly used oxide nano-powders in concrete are: nano-SiO_2, nano-Al_2O_3 and nano-Fe_2O_3 (Oltulu and Sahin, 2013). Other nano-powders, for example nano-ZnO_2 and nano-TiO_2 have been studied for the removal of pollutants in air, degradation of organic pollutants, bacteria and viruses (Lucas et al., 2013; Shen et al., 2012).

Oltulu and Sahin (2013) studied the effect of adding different proportions and combination of nano-SiO_2, nano-Al_2O_3 and nano-Fe_2O_3 to cement mortars that contained FA. They found that the addition of nano-powder enhanced the compressive strength of cement mortars and that the strength increment depends on the proportion of nano-powder added. In their study, the addition of nano-Fe_2O_3 resulted in a higher strength enhancement in comparison to the other nano-powders. They also found that pozzolanic activity was increased by the addition of binary powder combinations. Khoshakhlagh et al. (2012) also found that the addition of up to 4 wt% of Fe_2O_3 nanoparticles increased the compressive and flexural strengths but reduced water permeability of concrete specimens.

1.3. Materials and Experimental Methodology

1.3.1. Materials

Portland cement Type IP in compliance with ASTM C595 was used and FA was obtained from a local coal-fueled power plant (AES Puerto Rico). Detailed descriptions of the physiochemical properties of the cement and FA are shown in Table 3. It should be noted that the FA complies with the Class C FA for the most of the chemical characteristics, except for its SO_3 content that is much higher than the maximum percentage (5%) specified in ASTM C618.

Table 3. Physiochemical properties of fly ash and Portland cement.

Properties	Fly Ash	Portland Cement Type IP
Mineralogical composition (% wt.)		
SiO_2	30.84	27.14
Al_2O_3	9.93	6.68
Fe_2O_3	5.01	3.71
CaO	39.61	55.47
MgO	0.35	1.62
K_2O	1.01	0.48
Na_2O	0.90	0.59
SO_3	11.43	3.48
TiO_2	0.45	0.32
P_2O_5	0.11	0.11
Loss-on-Ignition (% wt.)	7.62	5.52
Blaine (m^2/kg)	441	554
Fineness (% wt.)[a]	73.7	92.6
Specific gravity	2.55	2.86
Lime Saturation Factor (LSF)[b]	0.39	0.64
Silica Ratio (SR)[c]	2.06	2.61
Alumina to Iron Ratio (AF)[d]	1.98	1.80

[a] Wet sieve percentage passing the No. 325 (45 μm) sieve (ASTM C430)

[b] LSF = $CaO/(2.8 \cdot SiO_2 + 1.2 \cdot Al_2O_3 + 0.65 \cdot Fe_2O_3)$

[c] SR = $SiO_2/(Al_2O_3 + Fe_2O_3)$

[d] AF = Al_2O_3/Fe_2O_3

The iron-oxide nanoparticles (NI) were purchased from the Ferrotec (Bedford, NH) and is composed of nominal 10-nm magnetite, proprietary surfactant and water. Its chemical and physical characteristics can be found in Table 4. Certified ACS-grade sulfuric acid and acetic acid were purchased from the Fisher Scientific and were diluted with DI water to make acid solutions at pH 3 to test durability of the paste specimens under acidic environments.

Table 4. Chemical and physical properties of NI.

Parameter		**Value or Description**
Composition (% by vol.)	Magnetite	2.8 - 3.5
	Surfactant	2.0 - 4.0
	Water	92.5 - 95.2
Appearance		black fluid
Nominal particle diameter (nm)		10
Density (g/mL)		1.245
pH		> 10

1.3.2. Specimen design and preparation

An OFAT experiment, which is based on varying one factor at a time over a certain range to determine the setting that best affects the response variable was done in triplicate in order to select the maximum cement substitution with FA while maintaining an allowable mechanical strength of the specimens. Two factors were considered, the FA/B substitution and the W/B ratio. The proportions of these factors can be found in Table 5.

The purpose of the second experimental design was to determine the physical and chemical properties of cement paste specimens when adding NI. Cement paste specimens were made in duplicates with two levels of the FA substitution (0 and 40 % wt. in binders) and two levels of the NI addition (0 and 3% wt. in binders). The binders are defined in this study as the summation of Portland cement and FA. The paste specimens are coded as FA*x*NI*y*, where *x* is the percentage of FA substitution and *y* the percentage of NI addition. The water-to-binders (W/B) was fixed at 35% wt. based on the results from the OFAT studies.

Table 5 . Design for the selection of low and high levels of FA substitution.

W/B	FA/B
0.30	0.0
	0.10
	0.20
	0.40
	0.60
0.35	0.0
	0.10
	0.20
	0.40
	0.60
0.40	0.0
	0.10
	0.20
	0.40
	0.60

The specimens were prepared in accordance to the American Society for Testing and Materials (ASTM). A mechanical mixer was used to prepare the specimens in accordance to the ASTM C192. Mixed paste was cast to the plastic mold of 2-in in diameter and 4-in in height. The standard rodding consolidation method was used for compaction of each specimen in accordance to the ASTM C192. After 24 hours, the specimens were demolded and cured in a tank filled with lime-saturated tap water at ambient temperature (24±2 ^{o}C), unless otherwise specified.

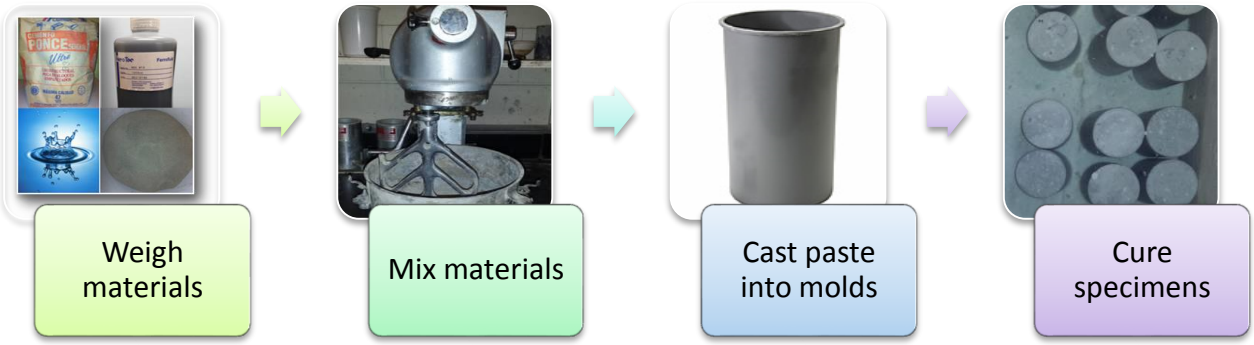

Figure 1. Procedure for preparing cement paste specimens.

1.3.3. Testing and Analysis

All testing was done in accordance to the ASTM's shown in Table 6 unless otherwise specified.

Table 6. ASTM standard test methods.

Test method	ASTM designation
Making and Curing Concrete Test Specimens in the Laboratory	C192 / C192M-02
Standard Specification for Flow Table for Use in Tests of Hydraulic Cement	C230 / C230M-13
Flow of Hydraulic Cement Mortar	C1437-13
Time of Setting Time of Hydraulic Cement by Vicat Needle	C191-13
Measurement for Rate Absorption of Water by Hydraulic Cement Concretes	C1585-13
Chemical Resistance of Mortars, Grouts, and Monolithic Surfacings and Polymer Concretes	C267-06
Compressive Strength of Cylindrical Concrete Specimens	C39/C39M - 12a

1.3.4. Spread percentage and setting time

Spread percentages of the fresh cement pastes of the second experimental design were determined using a flow table in accordance with ASTM C230 and C1437. A conical mold with a bottom diameter of 10 cm was placed at the center of the flow table and was filled with two layers of fresh cement paste. Twenty tamps per layer were applied to ensure a uniform fill in the mold. After removing the excess cement paste, the conical mold was removed and the flow table was dropped 25 times in 15 seconds as shown in Figure 2. The increase in base diameter was recorded and the spread percentage of the fresh cement paste was calculated.

Setting times were measured with the Vicat Needle (Figure 3) according to ASTM C191. Periodic penetration of a 1-mm needle to the cement paste was performed until no circular impression was observed on the paste surface. Henceforth, the initial and final setting times of the cement paste were determined.

Figure 2. Flow table test procedure.

Figure 3. Vicat Needle instrument.

1.3.5. Water absorption rate

Water absorption rate through the exposed surface due to capillary rise was quantified by measuring the weight increase of the paste specimens of the second experimental design in accordance to the ASTM C1585-13. The paste specimens cured for 28 days in calcium-saturated tap water at ambient temperature were used in this experiment. The specimens were placed in an oven for three days at a temperature of 50±2℃.The specimens were transferred to a closed container and kept there for 15 days at a temperature of 23±2℃. Before the starting the absorption experiment, the samples were weighed and then the side surfaces of the specimens were sealed with epoxy in order to allow water absorption only through the bottom side of the specimen. The top surface was covered with a plastic sheet. Before starting the experiment, the specimens were weighed again and then placed in a pan filled with tap water. The water level of the pan was kept at 2±1mm from the bottom of the specimen. Upon first contact with water, time was and mass were recorded at different intervals for a total of 9 days. The absorption, I, was calculated using equation (1) (ACI, 2010):

$$I = \frac{m_t}{a \cdot d} \tag{1}$$

where I is the absorption (mm), m_t is the change in specimen mass at time t (g), a is the exposed area of the specimen (mm^2) and d the density of the water (g/mm^2).

1.3.6. Compressive and tensile strengths

The specimens for the OFAT design were only tested for compressive and tensile strength after 7 and 28 days of curing, in accordance to ASTM C39. The specimens of the second experimental design were tested for compressive and tensile strengths after the paste specimens were cured for 3, 7, 28, 56 and 90 days in order to determine a long-term strength development of the paste. Capping rubber pads (Gilson HM-370) and wood veneer (1-in wide, 4-in long, 1/8-in thick) were placed on the top and bottom sides of the specimens during the compressive and tensile strength tests, respectively, to provide a uniform load distribution by a 3000 kN Forney universal testing machine as shown in Figure 4.

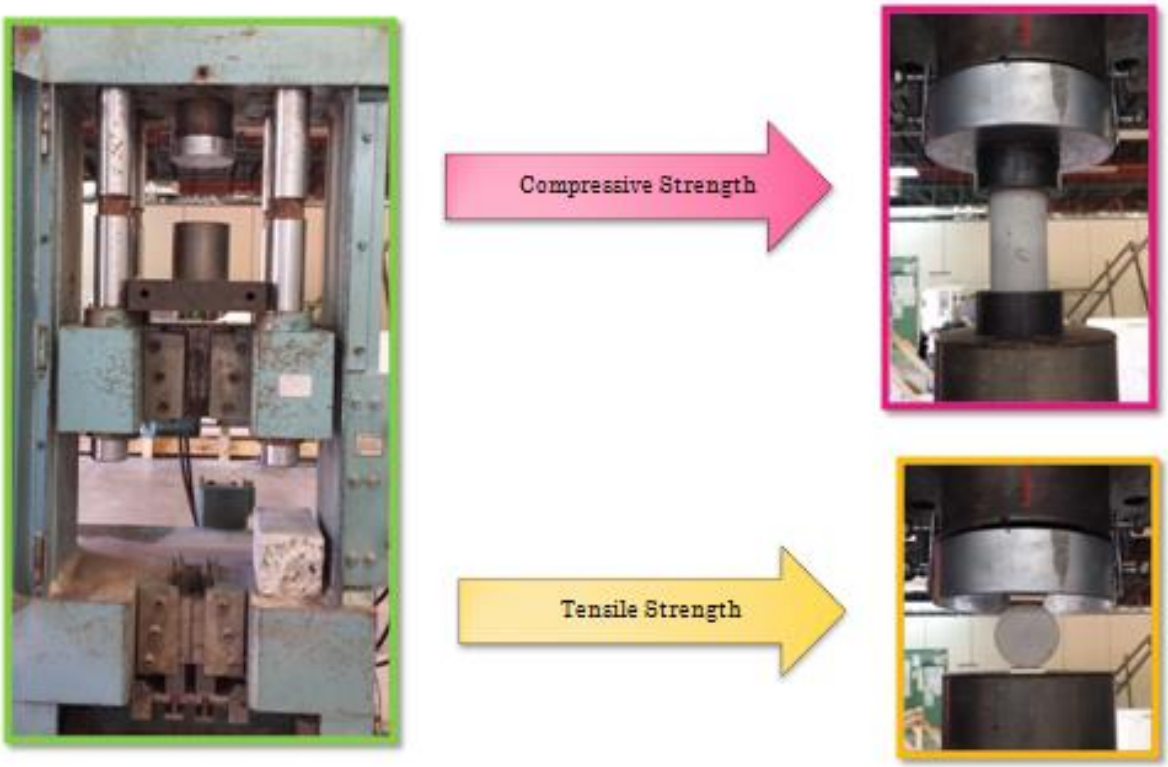

Figure 4. Compressive and tensile strength test representation in the Forney universal testing machine

1.3.7. Durability

The method for testing chemical resistance of concrete mortars (ASTM C267) was modified to accommodate the experiment with cement pastes. The changes in the weight and compressive strength was assessed by exposing the hardened pastes of the second experimental design in tap water at pH 7.5 and two different acid solutions at pH 3: sulfuric acid and acetic acid. Two paste specimens per mixture were placed in a container filled with 6 liters of the test solution. Weight monitoring was done after 1, 3, 7, 28, 56, and 90 days of immersion and the system was replenished with the fresh test solution after each monitoring. When the specimens were taken out of the acid solutions, they were shortly rinsed three times with running DI water and blot dried with a paper towel between each rinse. Saturated weight was then recorded and cumulative mass loss/gain was calculated between each monitoring period. The solution pH was also recorded during the period of durability experiment.

1.4. Results and Discussion

1.4.1. Compressive and Tensile Strengths of the OFAT experiment

Figure 5 and 6 shows the results for the compressive and tensile strengths of the OFAT study for 7 and 28 days of curing. At late curing ages (28 days), all of the pastes resulted in higher compressive and tensile strengths independently of their composition. Figure 5a shows that the pastes FA0 and FA10 reached the highest compressive strengths at 7 days of curing, while the pastes FA20, FA40 and FA60 obtained results significantly lower due to the high amount of FA that was incorporated into the pastes. However, after a longer curing period the specimen all of the specimens obtained similar to for the compressive strength. The slow development of the mechanical strength in the paste containing FA is attributed to slow pozzolanic reactions of FA occurring at late ages after CH is formed with hydration of cement (Donatello et al., 2013; Zeng et al., 2012).

The maximum compressive strength was found for the FA0WB30 paste at 44.2 and 60.4 MPa for the 7 and 28 days of curing, respectively. This is in agreement Abram's law of concrete, which states that the compressive strength varies inversely with the W/B (Appa, 2001). This behavior is attributed to the reduction of the pore sizes in the cement paste structure, consequently increasing the compressive strength and durability of the specimens (Banfill, 2011).

Since all of the measurements were done in % wt., the substitution of cement with FA resulted in a higher volume of the total binders since the specific gravity of the FA is lower than the cement (Table 3). This caused that a higher amount of water was needed to achieve a complete hydration of the binding materials. The lack of water in the mixtures resulted in an incomplete hydration and consequently the reduction of the compressive strength of the specimens as observed for specimens FA40 and FA60, which obtained very low compressive strengths at low W/B ratios. When the W/B was increased to 40%, similar results of compressive strength were obtained for all the pastes after 28 days of curing.

Similarly to the compressive strength, the tensile strength of the specimens with high amounts of FA resulted in low values of strength at the early ages of curing (Figure 6a), but similar strengths at the 28 days of curing due to the low pozzolanic reactions of the FA (Figure 6b). In

general, the increase of FA in the mixtures resulted in low mechanical strength at 7 days of curing, but similar strengths after the 28 days. The highest mechanical strengths for most of the mixture combinations were found at 35% W/B, thus this factor was fixed at this level for the second set of cement paste experiment.

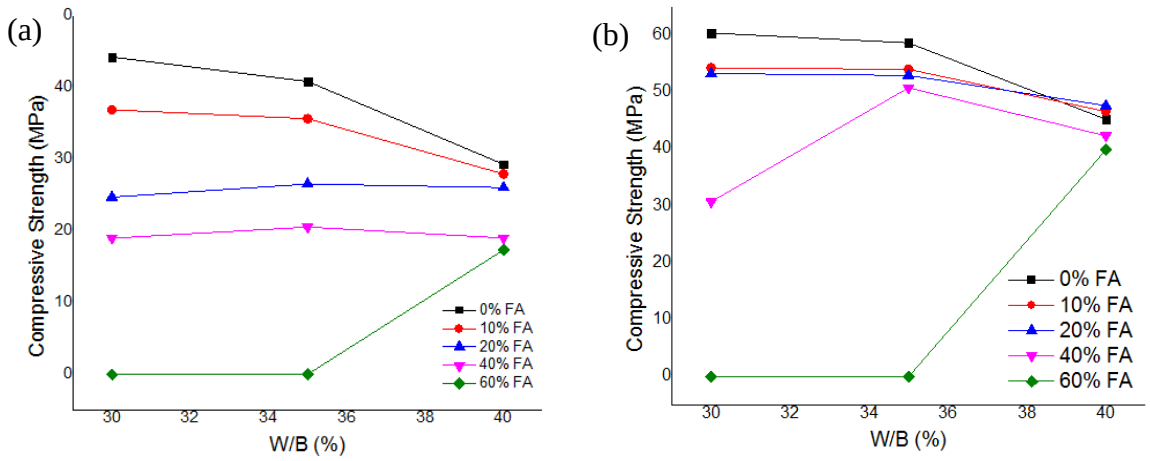

Figure 5. Compressive strength vs W/B for different percentages of FA/B addition at (a) 7 day and (b) 28 days of curing

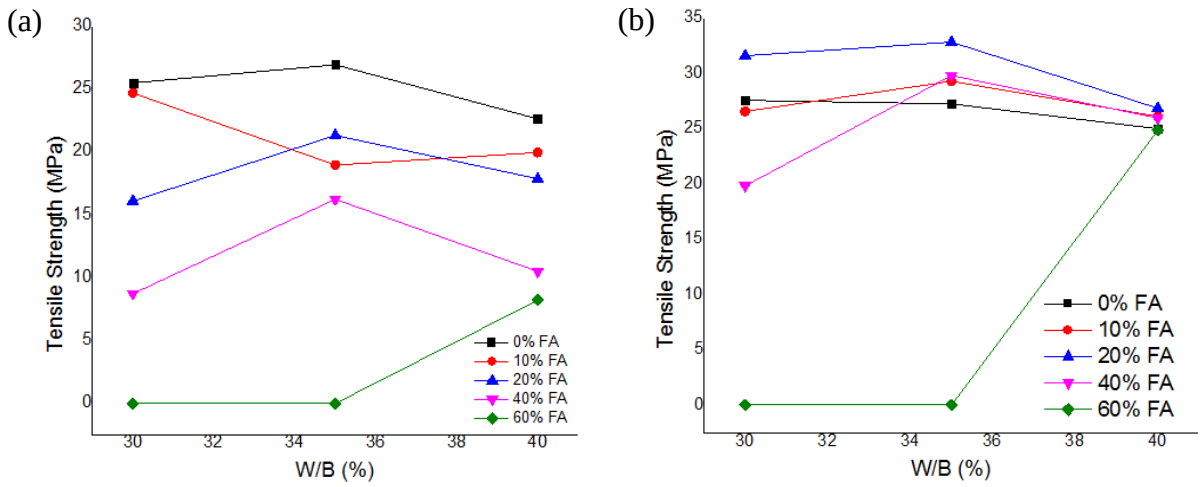

Figure 6. 28 day tensile strength vs W/B for different percentages of FA/B addition at (a) 7 day and (b) 28 days of curing

1.4.2. Spread percentage and setting time

As shown in Table 7, the control paste FA0NI0 had a spread percentage of 111%, similar to the spread percentage of cement mortars of 107% (Jiménez-Quero et al., 2013). When NI was added at 3% to the paste mixture (i.e., FA0NI3), spread percentage was increased by 23%. This increase of spread percentage could be attributed to an enhanced fluidity caused by the surfactants that was coated on NI. A similar enhancement of fluidity was reported by Ouyang et al. where the addition of synthetic surfactants up to $4x10^{-3}$% wt. of the cement increased the mortar fluidity by ~15% (Ouyang et al., 2008).

Conversely, the FA substitution decreased the spread percentage by 41%. Since FA had lower specific gravity than the cement (Table 3), the paste FA40NI0 had a greater amount of binders in the mixture and therefore more water would have been required in order to obtain the same spread percentage that the paste FA0NI0 had. Also, a relatively high loss-on-ignition (LOI) value of FA (Table 3) might be responsible for the decreased spread percentage of the paste FA40NI0. An increase in the requirement of water for the mortars containing high LOI additives was also reported by other researchers (Jimenez-Quero et al., 2013; Chandara et al., 2010). The significant decrease in spread percentage of the paste FA40NI0 was counteracted with 3% NI additions to the paste, where spread percentage was increased by 25%.

Table 7. Spread percentages and settling time of specimens tested with a flow table and vicat needle.

Factor/Level		Spread Percentage	Setting Time (minutes)		Water Absorption Rate (10^{-3} mm/$\sqrt{s}$)	
FA (%)	NI (%)	(%)[a]	Initial[b]	Final[c]	Initial[d]	Secondary[e]
0	0	111	183	330	15.9	5.5
0	3	136	260	540	10.9	5.8
40	0	66	169	450	20.5	5.4
40	3	83	247	515	14.2	6

[a] $\left(D_f - D_i\right)/D_i \times 100\%$, D_f and D_i are the final and initial diameter of the specimen, respectively.
[b] the time elapsed until the penetration of the Vicat needle is at 25 mm.
[c] the time when the Vicat needle does not sink visibly into the paste.
[d] the linear slope of water absorption from 1 minute to 6 hours.
[e] the linear slope of water absorption from 1 day to 7 days.

Figure 7 shows the penetration depth of the Vicat needle to the pastes and Table 7 contains the initial and final setting times of the pastes. Compared to the control paste FA0NI0, the paste FA0NI3 had delayed initial and final setting times by 42 and 64%, respectively. Surfactants have been utilized as water reducers and set retarders (Metha and Monteiro, 2014). As was the case for the increased spread percentage, the surfactants on NI seemed to play a role as set retarders. The contribution of nanoparticles to hydration of cementitious paste depended on the type of nanoparticle. For example, the addition of surfactant-free, nano$CaCO_3$ by 5% to the paste completely offset the delayed setting times in the paste with 50% FA substitution (Kawashima et al., 2013).

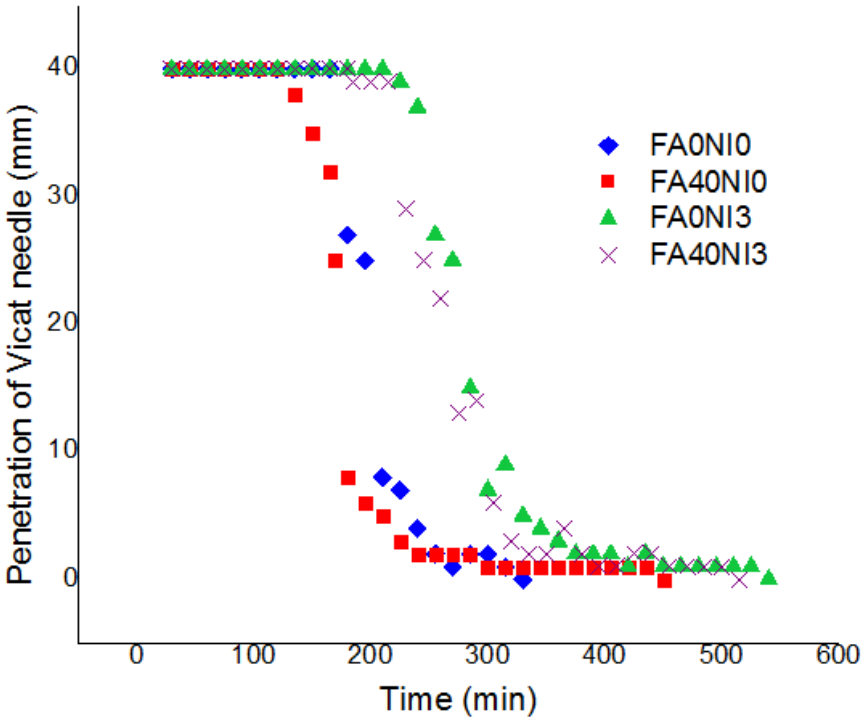

Figure 7. Trend of the Vicat needle penetration to the fresh pastes.

Despite a slightly shortened initial setting time by 7%, the paste FA40NI0 had a delayed final setting time by 36% (Table 7). It is generally accepted that FA substitution for cement delays setting times due to slow pozzolanic reactions of FA and thereby lowers early-age strengths (Bentz, 2014). For the paste FA40NI3, the initial and final setting times were delayed by 35 and 56%, respectively.

1.4.3. Water absorption

In general, the paste FA40NI0 had the fastest initial rate of water absorption compared to others. It should be noted that According to the ASTM C1585-13, the initial rate of water absorption is defined as the linear slope of water absorption from 1 min to 6 hours (ASTM C1585-13). The paste FA40NI0 had an initial rate of water absorption 29% faster than the control paste FA0NI0 (Figure 8 and Table 7). Li also reported an increase of water absorption rate due to higher pore size and porosity in the FA concrete specimens (Li, 2004). The paste FA0NI3 had a reduced initial rate of water absorption by 31% compared to the control paste FA0NI0. Thereby, when the paste contained both FA and NI (i.e., the paste FA40NI3), the initial rate of water absorption was very similar to that of the control paste FA0NI0 (i.e., 15.9×10^{-3} vs. 14.2×10^{-3} mm/$\sqrt{sec}$).

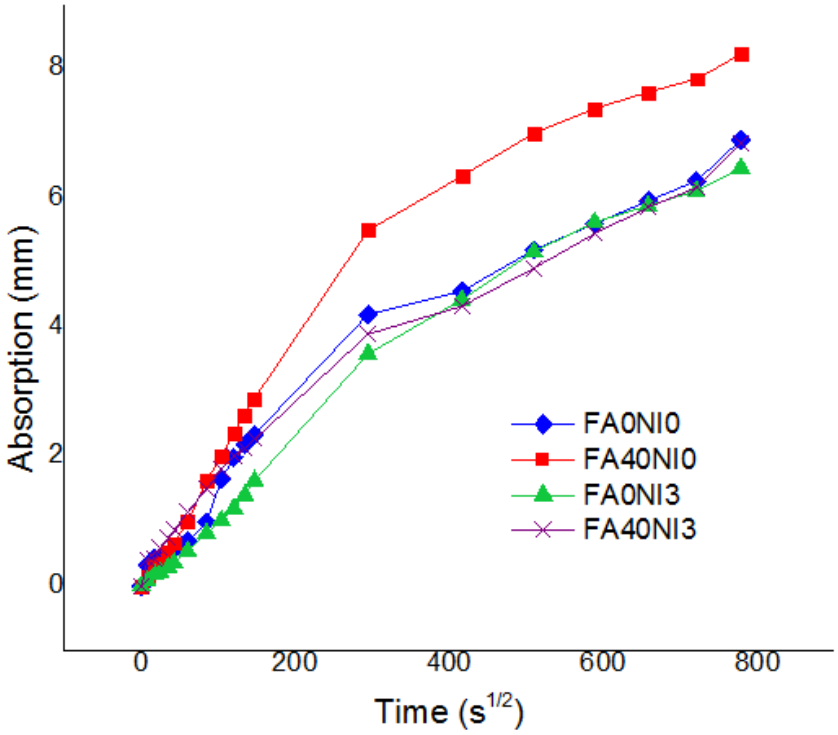

Figure 8. Water absorption of the hardened pastes.

The secondary rates of water absorption were in the range of 5.4×10^{-3} to 6.0×10^{-3} mm/$\sqrt{sec}$. It should be noted that the secondary rate of water absorption is defined as the linear slope of water absorption from 1 day to 7 days (ASTM C1585-13). The reduction from the initial rate to the secondary rate of water absorption was found in the decreasing order of the paste FA40NI0 (74%),

the control paste FA0NI0 (65%), the paste FA40NI3 (58%) and the paste FA0NI3 (47%). The greatest rate reduction for the FA-substituted paste was likely attributed to slow pozzolanic reactions of FA filling the pores at a later time in the paste mixture (Joseph and Ramamurthy, 2009).

Portland cement contains iron-rich ferrite phases such as calcium aluminoferrite (C_4AF) and the hydration of C_4AF produces either $C_6A(F)\underline{S}_3H_{32}$ or $C_4A(F)\underline{S}H_{18}$ hydrate, depending on the sulfate concentration (Kar et al., 2012). The addition of NI to the paste mixture seemed to contribute to the formation of these hydrates to fill the capillary pores of the paste. Furthermore, the addition of NI appeared to accelerate the time for the pozzolanic reaction of FA to take place since the water absorption rate of the paste FA40NI3 was significantly lower than the paste FA40NI0.

1.4.4. Long-term strength development

Figure 9 and 10 shows the trend of the compressive and tensile strength development of cementitious pastes for a period of 90 days of curing. At early curing ages (< 7 days), the pastes FA40NI0 and FA40NI3 resulted in lower compressive and tensile strengths than the pastes FA0NI0 and FA0NI3. However, the pastes FA40NI0 and FA40NI3 kept developing the strengths during 90 day curing and reached the compressive and tensile strengths of ~70 and ~30 MPa, respectively, similar to those of the pastes FA0NI0 and FA0NI3. For the pastes FA0NI0 and FA0NI3, the maximum strengths were not developed at 90 days of curing. Instead, they reached the maximum compressive and tensile strengths at 56 days and 28 days, respectively, of curing and then decreased afterwards.

As mentioned before, the slow development of the mechanical strength in the paste containing FA is attributed to slow pozzolanic reactions of FA occurring at late ages (Donatello et al., 2013). The addition of NI alone to the paste (i.e., FA0NI3) produced a negative effect on the development of compressive strength. However, such a negative effect caused by NI addition on the compressive strength was not found for the paste containing both NI and FA (i.e., FA40NI3). In general, the addition of NI induced a negative effect on the development of tensile strength whether or not FA substituted the cement.

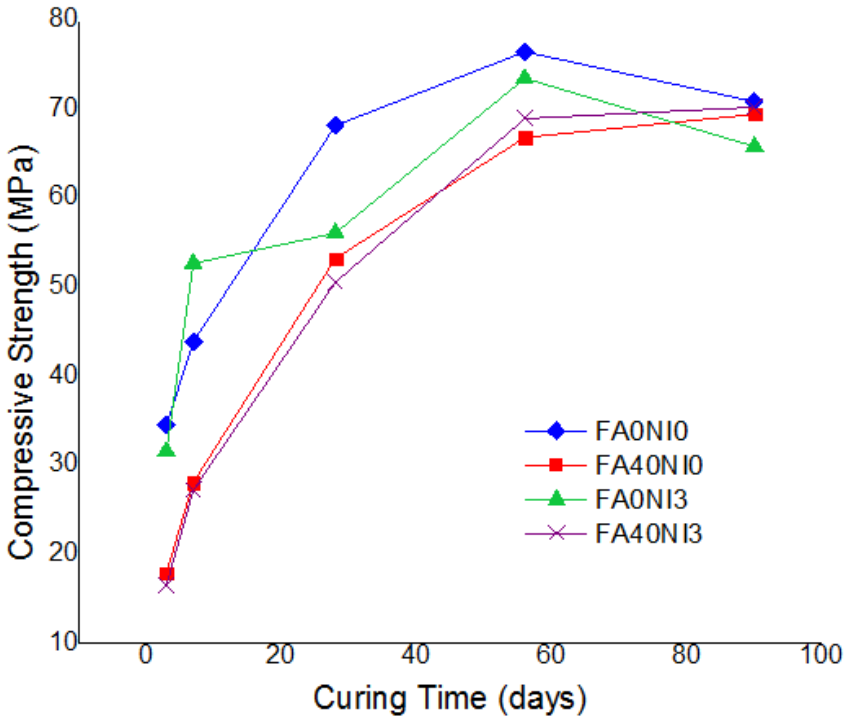

Figure 9. Development of the compressive strength during 90-day of curing.

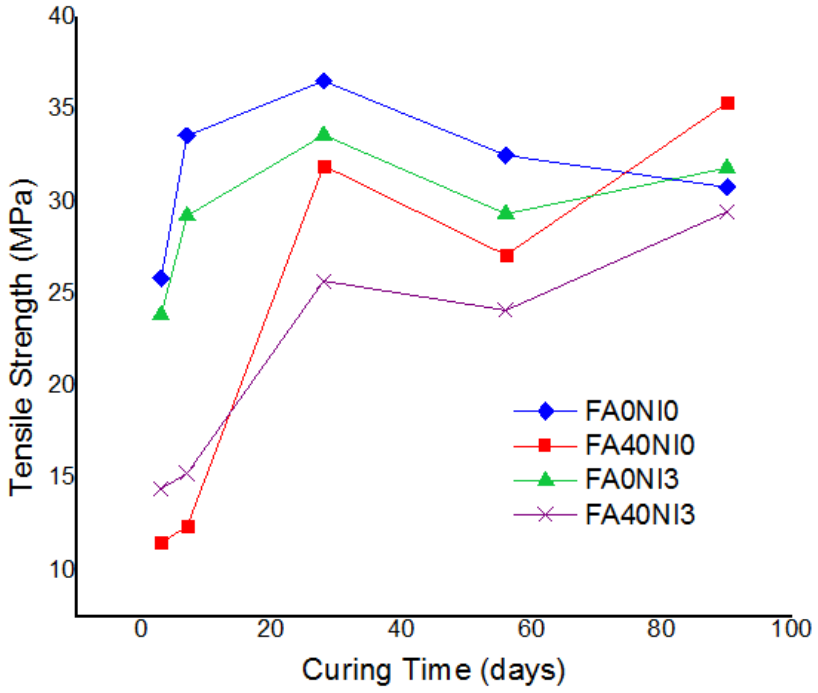

Figure 10. Development of the tensile strength during 90-day of curing.

1.4.5. Durability (Changes in the weight)

Figure 11 shows the weight changes when the pastes were placed in tap water at pH 7.5 and acid solutions at pH 3.0. It is important to note that the pastes were cured for 28 days prior to the durability experiment. In tap water, the pastes FA40NI0 and FA40NI3 had a faster weight gain than the pastes FA0NI0 and FA0NI3. After 90 days of exposure, the pastes FA40NI0 and FA40NI3 gained more weight than the pastes FA0NI0 and FA0NI3. This can be ascribed to the ongoing hydration of cement and to the pozzolanic reactions to form more C-S-H and calcium aluminate hydrate (C-A-H) gels. Makholoufi et al. (2012) found a higher and faster weight gain in the specimens containing natural pozzolana, resulting in a denser material due to pore reduction and thus enhancing the durability of the concrete specimens. Hossain and Lachemi (2006) also reported that the concrete specimens containing pozzolanic additives contained less CH due to their reactions by pozzolana to form more gels that lowered porosity and increased resistance to chloride ions.

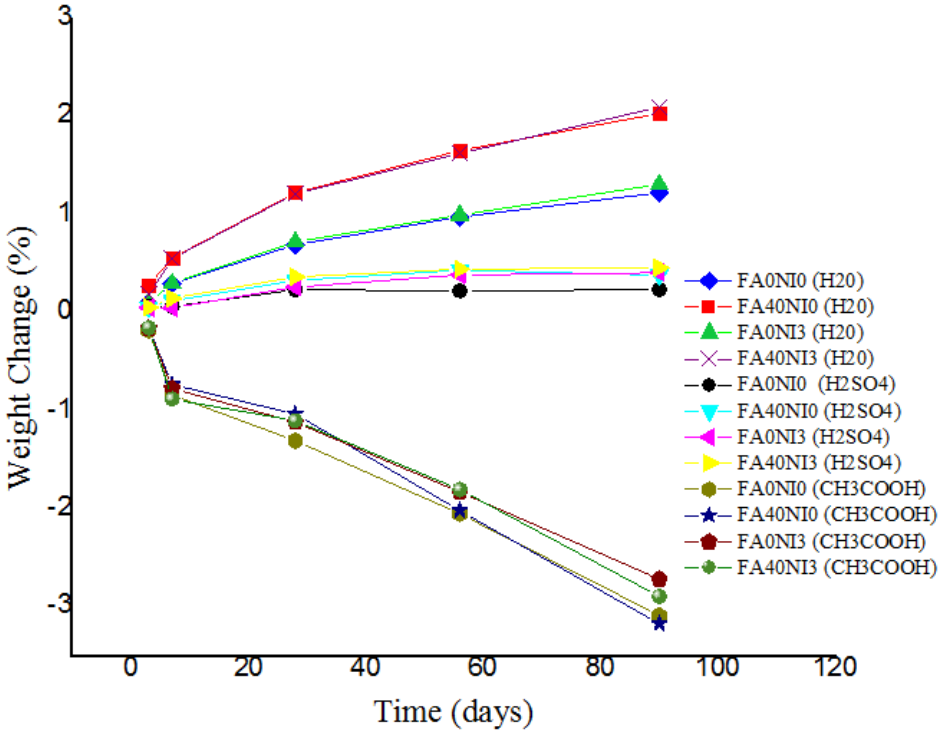

Figure 11. Weight changes of the paste specimens in water and acid solutions.

All the pastes in the sulfuric acid solution gained weight, although the magnitude of weight gain was less than 0.5%. The least weight gain was found for the control paste FA0NI0. The weight gain in contact with the sulfuric acid solution can be attributed to the fast formation of expansive products such as gypsum ($C\underline{S}H_2$) and ettringite ($C_3A{\cdot}C\underline{S}H_{32}$) under sulfate-rich environment (Metha and Monteiro, 2014):

$$CH_{(s)} + H_2SO_{4(aq)} \rightarrow CaSO_4{\cdot}2H_2O_{(s)} \quad (1)$$

$$C_3S_2H_{3(s)} + H_2SO_{4(aq)} \rightarrow CaSO_4{\cdot}2H_2O_{(s)} + C_2S_2H_{2(s)} \quad (2)$$

The extent of gypsum formation depends on sulfate concentration. Gypsum is easily formed by sulfate attack on CH and C-S-H gel at a high sulfate concentration (reactions 1 and 2), whereas ettringite is likely produced at a low sulfate concentration (Girardi and Maggio, 2011) as shown in reactions 3 and 4:

$$\text{Calcium aluminate hydrates (CAH)} + H_2SO_4 \rightarrow C_3A{\cdot}C\underline{S}H_{32} \text{ (ettringite)} \quad (3)$$

$$\text{Monosulfate hydrates } (C_3A{\cdot}C\underline{S}H_{12\text{-}18}) + H_2SO_4 \rightarrow C_3A{\cdot}C\underline{S}H_{32} \quad (4)$$

Early ettringite formation by sulfate attack on monosulfate hydrates ($C_3A{\cdot}C\underline{S}H_{12\text{-}18}$) can be responsible for weight increase at the beginning of the exposure. However, delayed ettringite formation at a later time may cause cracking and spalling due to internal stress in the specimen (Makholoufi et al., 2012). Spalling was visually noticed on the surface of all the paste specimens after 90 days in sulfuric acid solution.

All the specimens exposed to acetic acid at pH 3 immediately started to lose weight (Figure 11). After 90 days in acetic acid, the pastes FA0NI3 and FA40NI3 showed a slightly lesser weight loss than the pastes FA0NI0 and FA40NI0. This implies again that NI helped to improve the durability of the specimens when exposed to acids due to pore size reduction (Makholoufi et al., 2012; Hossain and Lachemi, 2006). Similarly to the sulfuric acid solution, all the paste specimens had noticeable spalling on the surface after 90 days in acetic acid solution.

Unlike the effect of sulfuric acid to form less water-soluble (1.3 mg/100 mL at 25 ^{o}C) but expansive calcium salts ($C\underline{S}H_2$), acetic acid tends to form calcium salts (calcium acetate,

$Ca(CH_3COO)_2$), which are highly soluble in water (34.7 g/100 mL at 20 ^oC) and easily leach out of the paste specimens resulting in weight loss (Metha and Monteiro, 2014):

$$CaCO_{3(s)} + 2CH_3COOH_{(aq)} \rightarrow Ca(CH_3COO)_{2(aq)} + H_2O_{(aq)} + CO_{2(g)}$$

$$Ca(OH)_{2(s)} + 2CH_3COOH_{(aq)} \rightarrow Ca(CH_3COO)_{2(aq)} + 2H_2O_{(aq)}$$

Bertron et al. (2005) obtained a very high porosity and a weak mechanical strength for cementitious paste exposed to a mixture of organic acids including acetic acid. All of their specimens, with and without furnace slag, resulted in the decalcification of the paste. Senhadji et al. (2014) also reported that it was more likely to obtain a higher weight loss in cement mortar specimens when the products of the acidic reaction were soluble calcium salts.

1.4.6. pH changes during exposure in tap water and acid solutions

In tap water, pH rapidly increased from 7.5 to ~10.5 at day 3 and then quickly stabilized at ~8.5 for all the pastes regardless of FA substitution or NI addition (Figure 12). Increase of pH was due to the water absorption/transport through the pores, dissolving and leaching CH to the solution.

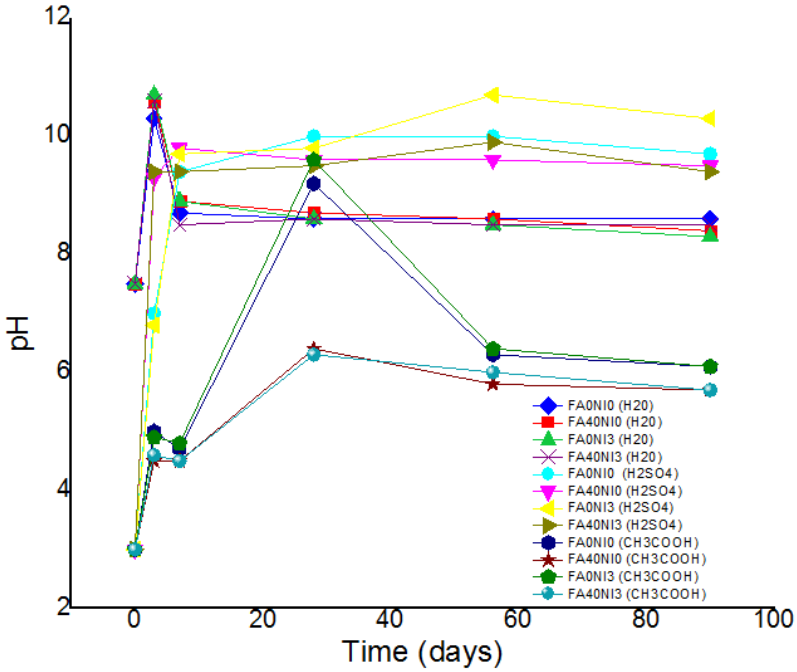

Figure 12. pH profiles when the paste specimens were in contact with tap water and acid solutions.

In the sulfuric acid solution, the pH of the pastes FA40NI0 and FA40NI3 increased from 3.0 to ~9.3 at day 3, whereas the pastes FA0NI0 and FA0NI3 from 3.0 to ~7.0 (Figure 12). However, pHs after day 7 were developed in an opposite to those at day 3. The pastes FA40NI0 and FA40NI3 maintained slightly lower pH than the pastes FA0NI0 and FA0NI3 (i.e., ~9.5 vs. ~10.0). The highest pHs of ~10.5 were observed for the paste FA0NI3 at later days of the experiment. Similarly, Makholoufi et al. (2012) found that pH of sulfuric acid solutions increased during the first 30 days of exposure, and then pH remained constant due to lower decalcification of CH.

A much lower pH development was found in acetic acid solution than in the sulfuric acid (Figure 12). More importantly, the pastes FA40NI0 and FA40NI3 had lower pHs in acetic acid solution than the paste FA0NI0 and FA0NI3. The highest pHs at ~6.4 were found at day 28 for the pastes FA40NI0 and FA40NI3 and at ~9.5 for the pastes FA0NI0 and FA0NI3. After day 56, the pastes FA40NI0 and FA40NI3 had slightly lower pHs than the pastes FA0NI0 and FA0NI3, although the pHs were near 6 for both cases.

1.4.7. Durability (Changes in the compressive strength)

Changes in compressive strength of the pastes were tested after exposure in tap water and acid solutions for 90 days (Figure 13). The 28-day compressive strengths of the pastes measured prior to the durability experiment were used as the initial values for this purpose.

The type of chemical solution influenced the changes in the compressive strength. For example, all fours pastes that had been exposed in tap water gained the compressive strength, whereas two pastes (FA0NI3 and FA0NI0) gained the compressive strength in sulfuric acid solution (Figure 13). Only one paste (FA0NI3) gained the compressive strength in acetic acid. This was consistent with the trend of weight changes (Figure 11) where the pastes in tap water gained the weight the most and those in sulfuric acid solution the second, whereas those in acetic acid solution lost the weight. Formation of highly soluble calcium salts ($Ca(CH_3COO)_2$) by the reaction of acetic acid with hydration products such as CH and C-S-H gel would have facilitated leaching of these soluble salts, leaving a more porous material, and therefore reducing the compressive strength as well as the weight.

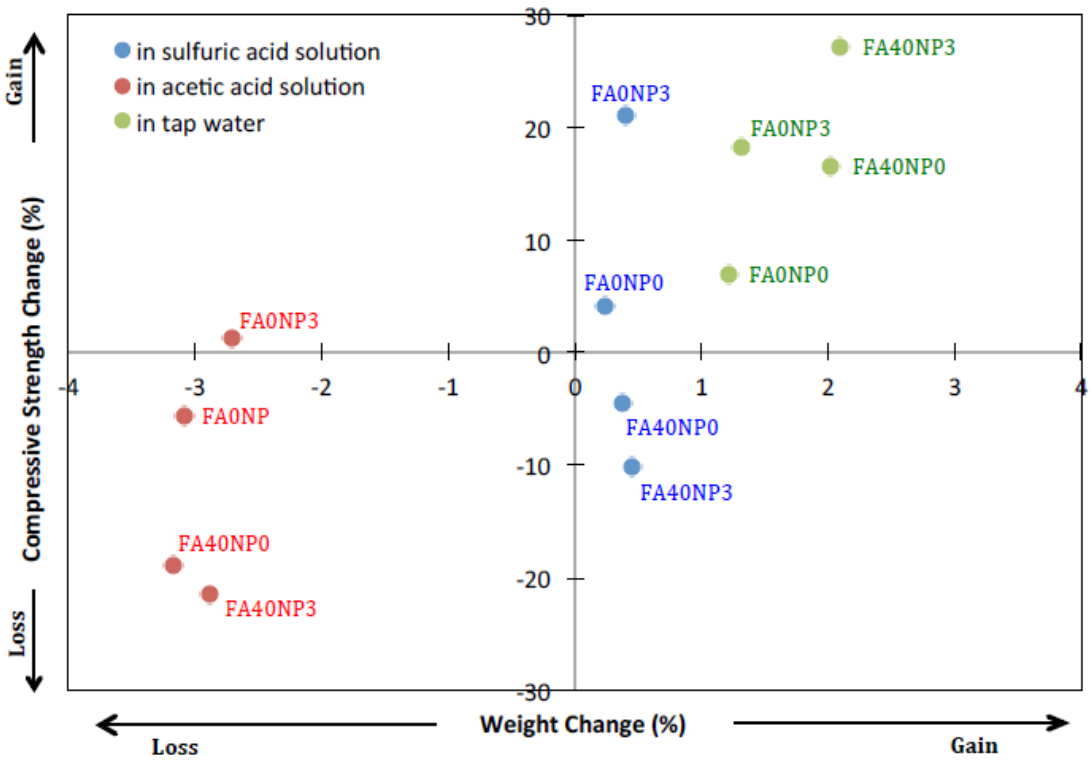

Figure 13. Changes in the compressive strength and weight of the specimens after a 90 day exposure in tap water and acid solutions.

Additionally, depending on the type of chemical solution, the FA substitution and NI addition produced a mixed effect on the changes in the compressive strength. For example, when the pastes had been exposed in tap water, the greatest gain of the compressive strength was found for the paste FA40NI3 followed by the paste FA0NI3. The control paste (FA0NI0) gained the compressive strength the least. In this regard, the FA substitution with and without NI addition were beneficial since it helped the paste gain the compressive strength and weight while exposing in tap water.

In sulfuric acid solution, the greatest gain of the compressive strength was for the paste FA0NI3, which was also the only paste that gained the compressive strength in acetic acid solution. Therefore, it can be said that the NI addition alone to the cement pastes were beneficial due to the enhancement of durability by increasing the compressive strength in acid solutions. On the

contrary, the FA substitution with and without the NI addition deteriorated durability of the cement pastes by reducing the compressive strength in acidic solutions, especially in acetic acid solution.

Figure 13 also shows a mixed effect of FA and NI on the correlation between the changes in compressive strength and the changes in weight. For example, in acetic acid solution, the paste FA40NI3 lost the compressive strength the most; however, its weight lost not the most. Similarly, in sulfuric acid solution, the paste FA0NI3 gained the compressive strength much more than others, but its weight gain was not the greatest but similar to others.

1.5. Conclusions

The effect of FA substitution (0 and 40% wt.) and NI addition (0 and 3% wt.) on physicomechanical properties and durability of cement pastes was evaluated. The following conclusions can be drawn based on the experimental results:

- The increment of W/B resulted in a reduction of the compressive and tensile strength of the specimens.
- The FA substitution had a negative effect on the mechanical strength at early ages of curing.
- The FA substitution after long term of curing was beneficial as the pastes increased both the weight and compressive strength while immersed in tap water (i.e., the pastes FA40NI0 and FA40NI3), although the pastes containing FA had a lower fluidity, a delayed setting time, a faster initial water absorption rate, and a slower development of the mechanical strengths.
- The NI addition compensated the negative effect caused by the FA substitution so as to enhance workability and reduce water absorption rate, although the addition of NI hindered the development of mechanical strengths of the fresh pastes.
- The FA substitution with and without the NI addition deteriorated durability of the hardened pastes in acid solutions, whereas the NI addition alone enhanced durability, increasing the compressive strength.

1.6. References

Ahmaruzzaman M. A review on the utilization of fly ash. Progress in Energy and Combustion Science 2010; 36:327-363.

Appa, G. Role of water-binder ratio on the strength development in mortars incorporated with silica fume. Cement and Concrete Research 2001; 31:443-447.

Banfill, PFG. Additivity effects in the rheology of fresh concrete containing water-reducing admixtures. Construction and Building Materials 2011; 25:2955-2960.

Bertron A, Duchesne J, Escadeillas G. Attack of cement pastes exposed to organic acids in manure. Cement and Concrete Composites 2005; 27:898-909.

Can MY, Yildiz E. Phosphate removal from water by fly ash: Factorial experimental design. Journal of Hazardous Materials 2006; B135:165-170.

Chandara C, Sakai E, Azizli KAM, Ahmad ZA, Hashim SFS. The effect of unburned carbon in palm oil fuel ash on fluidity of cement pastes containing superplasticizer. Construction and Building Materials 2010; 24:1590-3.

Chindaprasirt P, Jaturapitakkul C, Sinsiri T. Effect of fly ash fineness on compressive strength and pore size of blended cement paste. Cement and Concrete Composites 2005; 27:425-428.

Deschner F, Winnefeld F, Lothenbach B, Seufert S, Schwesig P, Dittrich S, Goetz-Neunhoeffer F, Neubauer J. Hydration of Portland cement with high replacement by siliceous fly ash. Cement and Concrete Research 2012; 42(10):1389-400.

Donatello S, Palomo A, Fernández-Jiménez A. Durability of very high volume fly ash cement pastes and mortars in aggressive solutions. Cement and Concrete Composites. 2013; 38:12-20.

Gagg C. Cement and concrete as an engineering material: An historic appraisal and case study analysis. Engineering Failure Analysis 2014; 40:114-140.

Girardi F, Di Maggio R. Resistance of concrete mixtures to cyclic sulfuric acid exposure and mixed sulfates: Effect of the type of aggregate, Cement and Concrete Research 2011; 33:276-285.

Hanehara S, Tomosawa F, Kobayakawa M, Hwang K. Effects of water/powder ratio, mixing ratio of fly ash, and curing temperature on pozzolanic reaction of fly ash in cement. Cement and Concrete Research 2001; 31:31-39.

Hossain KMA, Lachemi M. Performance of volcanic ash and pumice based blended cement concrete in mixed sulfate environment. Cement and Concrete Research 2006; 36:1123-33.

Jiménez-Quero VG, León-Martínez FM, Montes-García P, Gaona-Tiburcio C, Chacón-Nava JG. Influence of sugar-cane bagasse ash and fly ash on rheological behavior of cement pastes and mortars. Construction and Building Materials 2013; 40:691-701.

Joseph G, Ramamurthy K. The influence of fly ash on strength and sorption characteristics of cold-bonded fly ash aggregate concrete. Construction and Building Materials 2009; 23:1862-70.

Kar A, Ray I, Unnikrishnan A, Davalos J. Estimation of C–S-H and calcium hydroxide for cement pastes containing slag and silica fume. Construction and Building Materials 2012; 30:505-15.

Kawashima S, Hou P, Corr DJ, Shah SP. Modification of cement-based materials with nanoparticles, Cement and Concrete Composites 2013; 36:8-15.

Khoshakhlagh A, Nazari A, Khalaj G. Effects of Fe_2O_3 nanoparticles on water permeability and strength assessments of high strength self-compacting concrete. Journal of Materials and Science Technologies 2012; 28:73-82.

Li G. Properties of high-volume fly ash concrete incorporating nano-SiO_2. Cement and Concrete Research 2004; 34:1043-9.

Lucas SS, Ferreira VM, Barroso de Aguiar JL. Incorporation of titanium dioxide nanoparticles in mortars – Influence of microstructure in the hardened state properties and photocatalytic activity. Cement and Concrete Research 2013; 43:112-120.

Ma B, Ma M, Shen X, Li X, Wu X. Compatibility between a polycarboxylate super-plasticizer and the belite-rich sulfoaluminate cement: Settling time and the hydration properties. Construction and Building Materials 2014; 51-47-54.

Makholoufi Z, Kadri EH, Bouhicha M, Benaissa A. Resistance of limestone mortars with quaternary binders to sulfuric acid solution. Construction and Building Materials 2012; 26:497-504.

Metha P, Monteiro P. Concrete microstructure, properties and materials, 4th Ed. McGraw-Hill Education, 2014.

Oltulu M, Sahin R. Effect of nano-SiO_2, nano-Al_2O_3, nano-Fe_2O_3 powders on compressive strength and capillary water absorption of cement mortar containing fly ash: A comparative study. Energy and Buildings 2013; 58:292-301.

Ouyang X, Guo Y, Qiu X. The feasibility of synthetic surfactant as an air entraining agent for the cement matrix. Construction and Building Materials 2008; 22:1774-9.

Pando M, Hwang S. *Possible applications for circulating fluidized bed coal combustion by-products from the Guayama AES power plan.* Civil and Infrastructure Research Center, University of Puerto Rico at Mayagüez, Puerto Rico, 2006.

Setina J, Gabrene A, Juhnevica I. Effect of Pozzolanic Additives on Structure and Chemical Durability of Concrete. Procedia Engineering 2013; 57:1005-1012.

Shen S, Burton M, Jobson B, Haselbach L. Pervious concrete with titanium dioxide as a photocatalyst compound for greener urban road environment. Construction and Building Materials 2012; 35:874-883.

Toledano-Prados M, Lorenzo-Pesqueira M, González-Fonteboa B, Seara-Paz S. Effect of polycarboxylate super-plasticizers on large amounts of fly ash cements. Construction and Building Materials 2013; 48:628-635.

Zeng Q, Li K, Fen-chong T, Dangla P. Determination of cement hydration and pozzolanic reaction extents for fly-ash cement pastes. Construction and Building Materials 2012; 27:560-9.

CHAPTER 2

Response Surface Methodology for the optimization of fly ash cement pastes with iron-oxide nanoparticles

2.1. Abstract

The purpose of this study was to quantify the significance of the curing period during the development of compressive strength of the cement pastes with FA and iron-oxide nanoparticles (NI) as admixtures. To this end, a global optimization of the mixture was made in order to find the mix design possessing the desired workability of the fresh pastes and the achievable maximum time-dependent compressive strength of the hardened pastes. A three factor, two level, face centered central composite design was developed in order to assess the main, quadratic and interactions effects of the independent variables of water-to-binder (W/B), FA-to-binder (FA/B) and NI-to-binder (NI/B), on the dependent response variables. The compressive strengths (CS) were measured in the range of 14.2-37.4, 27.9-64.3 and 56.5-79.3 MPa for the hardened pastes cured for 3, 28 and 90 days, respectively, while the spread percentages (SP) of the fresh pastes ranged between 84.8 and 150 %. SP was found to increase with the increase of NI/B and W/B and the reduction of FA/B. Lower CS were found with increase of FA at early ages of curing, while it improved after 90 days of curing. The NI/B only contribute to the CS at late curing ages. The optimum variable settings were found at 36% W/B, 29.5% FA/B and 0.78% NI/B and responses were predicted with good accuracy.

2.2. Literature Review

2.2.1. The curing time in concrete

Structural design of ordinary Portland cement concrete is typically based on the strength of the concrete specimens cured for 28 days in controlled laboratory settings. However, in practice, such a long curing period is not provided mainly to reduce the cost of construction (Termkhajornkit et al., 2006). Not to mention that proper curing ensures concrete structures meet the specifications for their design life, thus, improper curing generally causes concrete failures at most of the field sites (Cusson et al., 2010; Poole, 2005).

Cement hydration is a chemical reaction of cement with water to form the hydration products, calcium silicate hydrate (C-S-H) gel and portlandite ($Ca(OH)_2$). The C-S-H gel is the principal hydration product of cement contributing to the early strength development of concrete. The rate and extent of cement hydration is governed mainly by the type of cementing materials, the presence of admixtures and mixture proportions. Pozzolanic reaction by FA with the formed $Ca(OH)_2$ produce additional C-S-H gel. Therefore, the curing period should be prolonged for FA-cement concretes due to a slower pozzolanic reaction, especially when a high volume of FA is used. For example, evidence of FA reaction, determined by $Ca(OH)_2$ consumption, was noticed after 7 days of curing and a significant increase of compressive strength in FA-cement pastes was observed after 28 days (Deschner et al., 2012). Similarly, pore filling effect and pozzolanic reaction in FA cement concrete occurred after 28 days of curing and a significant contribution of FA addition to the strength was noticed after 91 days of curing (Cheng et al., 2011).

Nano-sized SiO_2, Al_2O_3 and Fe_2O_3 have also been added to cement and concrete as nuclei and/or filler to its microstructure (Oltulu and Sahin, 2013; Sanchez and Sobolev 2010; Singh et al., 2013). It is known that these metal oxide nanoparticles react with $Ca(OH)_2$ increasing the C-S-H gel production, leading to a denser microstructure, thereby not only decreasing permeability but also improving durability and mechanical strength (Hanus and Harris, 2013). As they are involved in the chemistry of cement hydration and pozzolanic reactions for FA cement concretes, the rate and extent of nano-sized metal oxide contribution to the strength development would also depend on the curing period.

2.2.2. Response Surface Methodology (RSM)

In the engineering world, experiments are widely used for understanding what happens to the output response of a process if the levels of a factor are changed. A factor is defined as a controllable variable that is believed to have an effect on the response, and a level refers to an experimental setting at which a factor will be evaluated (Montgomery, 2013). Experiments are conducted with the purpose of characterization and optimization, evaluation of properties of a certain material, and determine the tolerance of a system, among others.

There are several strategies of experimentation for determining the influence of changing a certain factor on a system. A very common practice used by engineers is the best-guess approach, which works well only if the operator of the experiment has experience and knowledge on the area and can predict the results that a certain change may produce. Another strategy is the one-factor-at-a-time (OFAT), which also needs a lot of technical experience and it's based on varying one factor at a time over a certain range to determine the setting that best affects the response variable. The disadvantage of this method is that it is based on trial and error and if the guess does not provide a positive effect on the response variable, a new set of conditions must be done. The biggest disadvantage of the aforementioned approaches is that it doesn't consider the effect that the interaction of certain factors may have on the response (Montgomery, 2013).

In order to consider the effect that several factors may have on a response, and optimize this response, the response surface methodology (RSM) is used. Montgomery (2013) defines an RSM as a collection of mathematical and statistical techniques that are used to analyze and model the effect that will cause changing several variables at the same time, with the objective of optimizing the response. One of the biggest advantages of RSM is that a large amount of information can be obtained by doing fewer experiments, in comparison to other experimental processes techniques. RSM experiments have been used to analyze, improve and optimize biochemical processes, enzymatic synthesis of fatty acids, determination of reaction parameters and kinetic constants among others (Baş and Boyacı, 2007). Other applications such as determining the effect of design parameters on conventional and pervious concrete have also been studied with RSM (Sonebi and Bassuoni, 2013).

The first step before running an RSM is to make preliminary experiments in order to select the range of low and high levels (represented by the plus (+) and minus (-) signs, respectively, in Figure 14) that will be tested for a certain independent variable or factor. The biggest error when doing this type of experiment is the selection of the wrong range. As a result, the optimum value will be one of the extreme levels (Baş and Boyacı, 2007) and it is not the optimum indeed. Factorial designs are used to study the effects of two or more factors, and it considerate all possible combinations of the levels and factors under study. It is also capable of identifying if there is any significant effect made by the interaction of the factors under study. The regression model is a linear equation and the response surface plot of the factorial analysis is represented by a linear plane. If the interaction of the factors is significant, a curvature is observed in the plane. Central points, which are runs at the middle range of each factor, are used to account for the curvature effects in the response. A strong curvature effect means that a linear model is not feasible to predict the response (Montgomery, 2013).

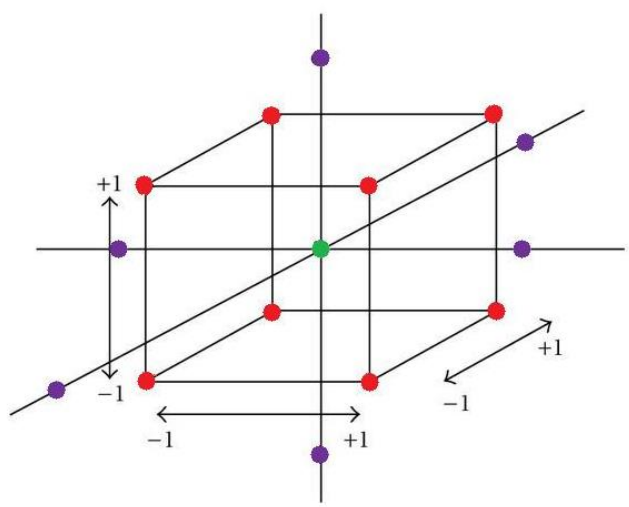

Figure 14. Central composite design diagram where the red dots are the factors, the purple dots are the axial points and the green dot is the central point.

Second order models such as central composite designs (CCD) are used to better represent the curvature of a response that cannot be predicted with linear models. CCD involves the use of a two-level of full or fractional factorial points (8 points for a 3 factor design (i.e., k=3)), *2k* axial points, and center points. Axial points are the levels that go off the limits established as low and high levels, as represented by the purple dots in Figure 14. The number of center points depends on the replication. CCD can have different design properties by controlling the value of α that is

the distance from each axial point to the center of the design space. A more common choice of α is $\alpha = k^{1/2}$ or $\alpha = (N_F)^{1/4}$, where N_F is the number of factorial points in a k factor design. The factorial points contribute to the estimation of the interaction terms. The center points provide information about the existence of curvature in the system, with which the axial points allow to estimate the quadratic terms (Montgomery, 2013).

Since the location of the optimum factor combination is unknown, it is important to have the same estimation precision in all directions of the experimental region. Rotatability is the term used to imply that the variance of the predicted response is the same in all points that are at the same distance from the center. Spherical designs possess this characteristics and the rotatability depends on the value of α.

$$\alpha = \sqrt{k} \tag{2}$$

CCDs have been the most commonly used design method with RSM in statistically assessing the mathematical relationship between the independent variables and the responses. For example, CCDs with RSM were employed to optimize the amount of the Portland cement and silica fume to yield an acceptable mechanical strength of ultra-high-performance-fiber reinforced concrete (Aldahdooh et al., 2013).

Another common design method is the face centered central composite design (CCF), which is a special case of CCD where α is equal to one. This forces the axial points of CCF to locate on the surface of the cubic, instead on the sphere space as in CCD, and therefore makes CCF a three-level CCD. The second-order polynomial equation (3) was used to fit the data of the CCF:

$$Y = \beta_0 + \sum_{i}^{k} \beta_i x_i + \sum_{i=1}^{k} \beta_{ii} x_i^2 + \sum \sum_{i<j}^{k} \beta_{ii} x_i x_j + \varepsilon \tag{3}$$

where Y represents the predicted response (i.e., compressive strength) in MPa, β_0 is the intercept, β_i the first-order (linear) coefficient, β_{ii} the second-order (quadratic) coefficient, β_{ij} the coefficient of interaction effect, x_i and x_j the coded levels of the independent variables X_i and X_j, respectively, and **ε** the associated random error (Montgomery, 2013).

2.3. Materials and Experimental Methodology

2.3.1. Cement, FA and NI

Portland cement Type IP in compliance with ASTM C595 was used and FA was obtained from a local coal-fueled power plant (AES Puerto Rico) (Table 3).The NI solution was purchased from the Ferrotec (Bedford, NH) (Table 4, Chapter 1).

2.3.2. Specimen design and preparation

This study was designed in a three factor, two level (2^3) face centered, central composite design aiming to assess the main, quadratic and interaction effects of the independent variables, the percentages of water-to-binder (W/B), FA-to-binder (FA/B) and NI-to-binder (NI/B), on the dependent response variables, spread percentage (SP) of the fresh pastes and compressive strength (CS) of the hardened pastes (Table 8). In this study, the binder is defined as the total amount of Portland cement and FA. Response Surface Methodology (RSM) was utilized to optimize the mix design in order to obtain a time-dependent maximum compressive strength of cement pastes cured for 3, 28 and 90 days and achieve the desired spread percentage of the fresh pastes simultaneously. The mixing, casting and curing of the cement paste specimens were done as describe in Chapter 1, section 1.3.2.

2.3.3. Response Surface Methodology

Mathematical and statistical interpretations of the data were done with Minitab 17 for the spread percentage and the compressive strength after 3, 28 and 90 days of curing. A total of 20 combinations of independent variable settings were run with 6 replicates at the center points. The significance of each of the independent variables to the dependent variable and their interactions were determined by an analysis of variance (ANOVA). Factors with a p-value of 0.05 or lower were determined to be statistically significant, and therefore considered for the predictive regression model. The relationship between the independent variables and the response variable was evaluated by contour plots. Numerical optimization of the independent variables for the cement pastes was also performed to identify the combination of variable settings that maximize the compressive strengths and at the same time meeting a desired spread percentage.

Table 8. Matrix of 2^3 face centered central composite design and the measured dependent response variables.

Run	Point[a]	Independent Variables						Dependent Variables			
		Coded			Actual (% wt.)			Spread (%)	Compressive Strength (MPa)		
		W/B	FA/B	NI/B	W/B	FA/B	NI/B		3 day	28 day	90 day
1	F	-1	-1	-1	35	20	0.5	89.5	20.6	59.6	78.8
2	F	1	-1	-1	37	20	0.5	110.0	21.1	47.5	69.2
3	F	-1	1	-1	35	40	0.5	84.8	17.8	49.3	64.6
4	F	1	1	-1	37	40	0.5	97.3	14.2	46.6	69.0
5	F	-1	-1	1	35	20	3.0	137.3	18.9	54.6	72.1
6	F	1	-1	1	37	20	3.0	135.5	22.7	27.9	56.5
7	F	-1	1	1	35	40	3.0	106.8	19.5	55	64.8
8	F	1	1	1	37	40	3.0	115.8	16.3	47.8	60.1
9	A	-1	0	0	35	30	1.75	97.0	26.4	59.5	64.8
10	A	1	0	0	37	30	1.75	120.3	27.1	51.1	63.7
11	A	0	-1	0	36	20	1.75	126.8	37.4	46.1	57.8
12	A	0	1	0	36	40	1.75	101.8	21.3	49.3	64.1
13	A	0	0	-1	36	30	0.5	97.3	26.8	60.3	79.1
14	A	0	0	1	36	30	3.0	121.5	31.2	52.3	79.3
15	C	0	0	0	36	30	1.75	113.5	17	60.8	60.6
16	C	0	0	0	36	30	1.75	115.8	16.5	62.4	75.5
17	C	0	0	0	36	30	1.75	150.0	16.7	60.5	76.1
18	C	0	0	0	36	30	1.75	119.0	26.7	64.3	76.8
19	C	0	0	0	36	30	1.75	114.0	27.9	42.8	72.2
20	C	0	0	0	36	30	1.75	115.3	27.8	53.4	74.7

[a]F: factorial point, A: axial point, C: center point

2.3.4. Testing of the dependent variables

Spread percentages of the fresh cement pastes were determined using a flow table in accordance with ASTM C230 and C1437, as described in Chapter 1, section 1.3.4. The compressive strengths of the hardened cement pastes were tested in triplicate in accordance to ASTM C39, as described in Chapter 1, section 1.3.6.

2.3.4. Scanning Electron Microscopy (SEM) imaging

The microstructure of the cement pastes at different curing times was observed by SEM (JEOL JSM-6390 Scanning Electron Microscope) operated at 5 keV. SEM samples were coated with gold using a Denton Vacuum Desk IV sputter-coater to improve the conductivity of the samples and thus the quality of the images. Four different cement paste combinations were analyzed with two levels of the FA substitution (0 and 40 % wt. in binders) and two levels of the NI addition (0 and 3% wt. in binders) at 3-, 28- and 90-days of curing in lime-saturated tap water.

2.4. Results and Discussion

2.4.1. Responses of the RSM

The spread percentages of the fresh pastes ranged between 84.8 and 150 % (Table 8). A recommended spread percentage of cement pastes is not available in the literature. For this reason, 110±5% of cement mortars (Jimenez-Quero et al., 2013) were used as the reference value for the spread percentage of cement pastes in the CCF analysis.

The compressive strengths were measured in the range of 14.2-37.4, 27.9-64.3 and 56.5-79.3 MPa for the hardened pastes cured for 3, 28 and 90 days, respectively. These results clearly showed that the development of compressive strength was time dependent and FA cement pastes gained additional compressive strength during late age of curing (i.e., 90 days) (Table 8).

2.4.2. Statistical models of the RSM

The ANOVA for each dependent variable is shown in Table 9. The suitability of the model was validated by checking residual plots and the lack-of-fit at a significance level of 0.05. Residual plots confirmed that the residuals were independent, were normally distributed, and had equal variances. Lack-of-fit for each response resulted in p-values much greater than 0.05, indicating that the models accurately fit the data. The high regression coefficients (R^2) of 85.5% for spread percentages and of 79.9, 85.2 and 74.5 % for 3, 28 and 90 day compressive strengths, respectively, also described the adequacy of the model.

The main and interactive effects of independent variables on the dependent variables were also assessed at a significance level of 0.05 (Table 9). The estimated regression models after removing insignificant terms for the spread percentage response and the time-dependent compressive strength responses are given in equations 4 to 7:

$$SP_1 = 122.1 - 0.928FA/B + 11.04NI/B \tag{4}$$

$$CS_{3d} = 31.58 - 0.316FA/B \tag{5}$$

$$CS_{28d} = 164.8 - 5.71W/B + 6.48FA/B - 0.1059FA/B^2 \tag{6}$$

$$CS_{90d} = -8.3 + 6.60FA/B - 18.10NI/B - 0.1119FA/B^2 + 4.53NI/B^2 \tag{7}$$

Table 9. ANOVA and full regression models statistics.

Term	Spread Percentage		Compressive Strength					
			3 day		28 day		90 day	
	p-value	coefficient	p-value	coefficient	p-value	coefficient	p-value	coefficient
Constant		122.1		31.58		164.8		-8.3
W/B	0.071	NS	0.906	NS	0.007	-5.71	0.184	NS
FA/B	0.016	-0.928	0.042	-0.316	0.466	6.48	0.538	6.60
NI/B	0.002	11.04	0.549	NS	0.148	NS	0.166	-18.10
W/B^2	0.265	NS[a]	0.526	NS	0.586	NS	0.136	NS
FA/B^2	0.815	NS	0.726	NS	0.017	-0.1059	0.031	-0.1119
NI/B^2	0.315	NS	0.837	NS	0.823	NS	0.033	4.53
W/B*FA/B	0.922	NS	0.366	NS	0.078	NS	0.163	NS
W/B*NI/B	0.372	NS	0.762	NS	0.221	NS	0.384	NS
FA/B*NI/B	0.264	NS	0.755	NS	0.059	NS	0.529	NS
Lack-of-Fit	0.668		0.798		0.296		0.515	
R^2 (%)	85.5		79.9		85.2		74.5	

[a] NS: The contribution of the terms was not statistically significant

It should be noted that the coefficient values were for the terms of uncoded independent variables. As shown in equation (4), only two linear terms of FA/B and NI/B factors significantly affected the SP with the NI/B influencing the most. Thereby, the smaller FA/B and the greater NI/B the fresh pastes had, the greater SP was predicted. A significant increase of the spread percentage could be attributed to an enhanced fluidity caused by the surfactants coated on the iron-oxide nanoparticles. An enhanced fluidity of cement due to the addition of synthetic surfactants was reported previously (Ouyang et al., 2008).

For the CS_{3d}, the linear term of FA/B was the only factor affecting the response significantly, although its coefficient was small (equation 5). In other words, the compressive strength after 3 days of curing was predicted to decrease by the replacement of Portland cement with FA, but only slightly. This could be due to slow development of compressive strength in FA cement pastes (Deschner et al., 2012).

Unlike the CS_{3d}, the CS_{28d} and CS_{90d} were predicted with second order polynomial models. Although the linear term of W/B and the quadratic term of FA/B were only statistically significant for the CS_{28d} (Table 9), the linear term of FA/B was also incorporated to the regression model in order to maintain the hierarchy of the model (equation 6) (Montgomery, 2013). Thereby, the CS_{28d} was predicted as a function of the linear terms of W/B and FA/B and also of the quadratic term of FA/B. The independent variable, NI/B, did not significantly contribute to the CS_{28d}.

However, the NI/B produced significant impacts for the CS_{90d} (equation 7). Although the quadratic terms of FA/B and NI/B were the only statically relevant to the CS_{90d} (Table 9), the linear terms of FA/B and NI/B were also included in the prediction model to maintain the hierarchy of the model (Montgomery, 2013). The contribution of W/B to the CS_{90d} was insignificant and not included in the prediction model. No interactions between the independent variables were found to be statistically relevant to any of the dependent variables (Table 9). Thereby, they were not factored in the prediction models.

2.4.3. Response optimization of the cement pastes

Table 10 summarizes optimization goals of the RSM to find the best combination of independent variable settings that could produce the highest compressive strength while meeting a desirable spread percentage. As mentioned in the before, the spread percentage of 110% was

chosen as a target optimality criterion. The maximum achievable compressive strengths (Table 8) were selected as the optimality criteria of 3, 28 and 90 day compressive strengths.

The response optimizer tool of Minitab 17 was utilized to simultaneously optimize the responses. As shown in Figure 15 the optimum independent variable setting at 36% W/B, 29.5% FA/B and 0.78% NI/B resulted in the 3, 28 and 90 day compressive strengths at 22.1, 60.4 and 79.8 MPa, respectively, while meeting the desirable spread percentage at 107%. This was attained with the global desirability value at 0.72 and with the response-specific desirability values at 0.89 for the spread percentage and 0.34, 0.89 and 1.00 for the 3, 28 and 90 day compressive strengths, respectively. It should be noted that the optimization goals could be assigned at different weight and importance. In the current study, however, the target responses had equal weight and importance.

Table 10. Optimization criteria for each dependent variable.

Dependent variable	Measured		Optimization	
	Lower	Upper	Goal	Target
Spread Percentage (%)	84.75	150	Target	110
Compressive Strength (MPa)				
3 day	14.24	37.44	Maximum	37.44
28 day	27.93	64.27	Maximum	64.27
90 day	56.48	79.30	Maximum	79.30

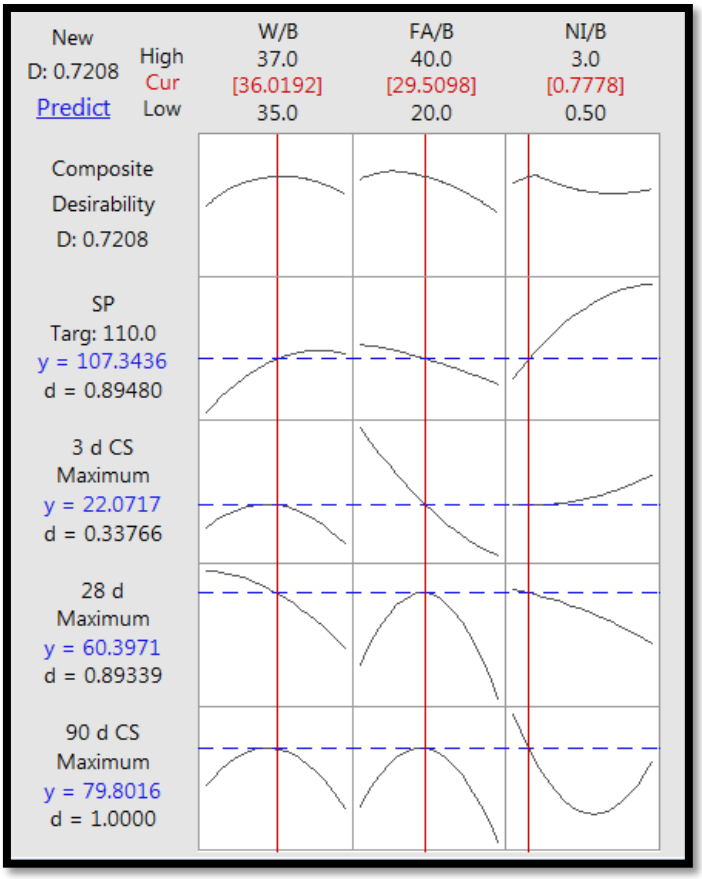

Figure 15. Response optimization plot for the RSM.

2.4.4. Contour plots for RSM at the optimum settings

Contour plots of the responses were drawn in a function of two independent variables while the third independent variable was held at its optimal value. As shown in Figure 16, the dependent response SP increased with the decrease of FA/B and increase of NI/B at the same time, while the W/B was held at the optimum level of 30%. When the FA/B was held at the optimum 29.5%, increasing with W/B and NI/B increased the SP. With the NI/B held at the optimum level of 0.78%, an enhanced SP was found with the increase of FA/B and the increase of W/B at the same time.

Overall, a greater SP was found with a greater W/B or NI/B but with a lesser FA/B. The increase of NI/B would facilitate fluidity of the cement pastes attributed to the surfactants coated on the NI. This was in agreement with Ouyang et al. (2008) who documented an increased fluidity of cement with the addition of surfactants. As shown in Table 3, the FA had a lower specific gravity

than the Portland cement used in the study. Therefore, more volume of FA was required for making the same weight to the Portland cement, consuming more water in hydration resulting in a reduced SP. This effect was counteracted with an increase of the W/B and NI/B in the mixture.

The extent of contribution that independent variables had on the CS was time dependent (Figure 16-19). The NI/B did not play a significant role in the development of compressive strength at the 3 day curing (i.e., CS_{3d}) (Figure 17a-16a). However, a decreased CS_{28d} was found with an increase of the NI/B and an increase/a decrease of the FA/B from the middle level, while the W/B was held at its optimum level of 36% (Figure 17b). The CS_{90d} was decreased with increasing of the W/B and NI/B at the same time. The greatest CS_{90d} was obtained when both the W/B and NI/B were at lower levels while the FA/B held at the optimum level of 29.5% (Figure 18b). A minimax pattern was observed for the contribution of NI/B to the CS_{90d}. That is, from the saddle points near the center of the design, increasing or decreasing of the NI/B increased the CS_{90d}, whereas increasing of decreasing of the W/B decreased it (Figure 17c and 18c). Increasing CS_{90d} with the increase of NI/B implies that the addition of NI was effective in supporting the chemistry in cement paste at later curing stages and probably the reaction of calcium ferrite minerals to produce siliceous hydrogarnet ($C_3(A,F)S_yH_{6-2y}$) was favored. This resulted in higher strength development due to densification of the cement pastes (Dilnesa et al., 2014).

When the NI/B held at its optimum level of 0.78%, increasing FA/B reduced the CS_{3d}, whereas the changes in W/B had a small influence on it (Figure 19a). In a rising ridge pattern, the increase or decrease of the FA/B from the middle levels of the design and the increase of W/B at the same time decreased the CS_{28d} (Figure 19b). A simple maximum pattern was observed for the CS_{90d} when the W/B was in a function with FA/B: the CS_{90d} was the highest near the center of the design from which the changes of W/B and/or FA/B decreased it (Figure 19c). The enhanced CS_{28d} with the increase of W/B could be attributed to the slow pozzolanic reaction of FA that occurs at late ages after $Ca(OH)_2$ is formed by the hydration of cement (Senhadji et al., 2014).

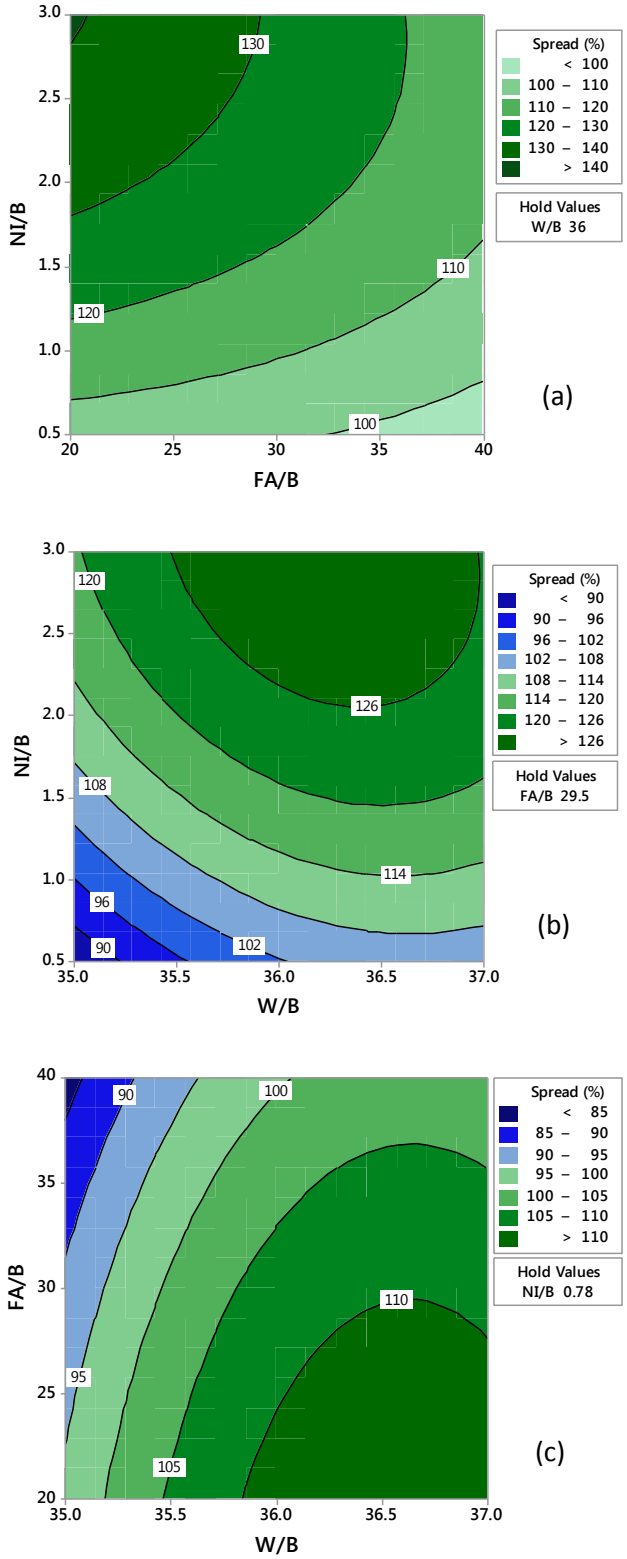

Figure 16. Contour plots of the SP in a function of two independent variables while the third one was held at its optimum level.

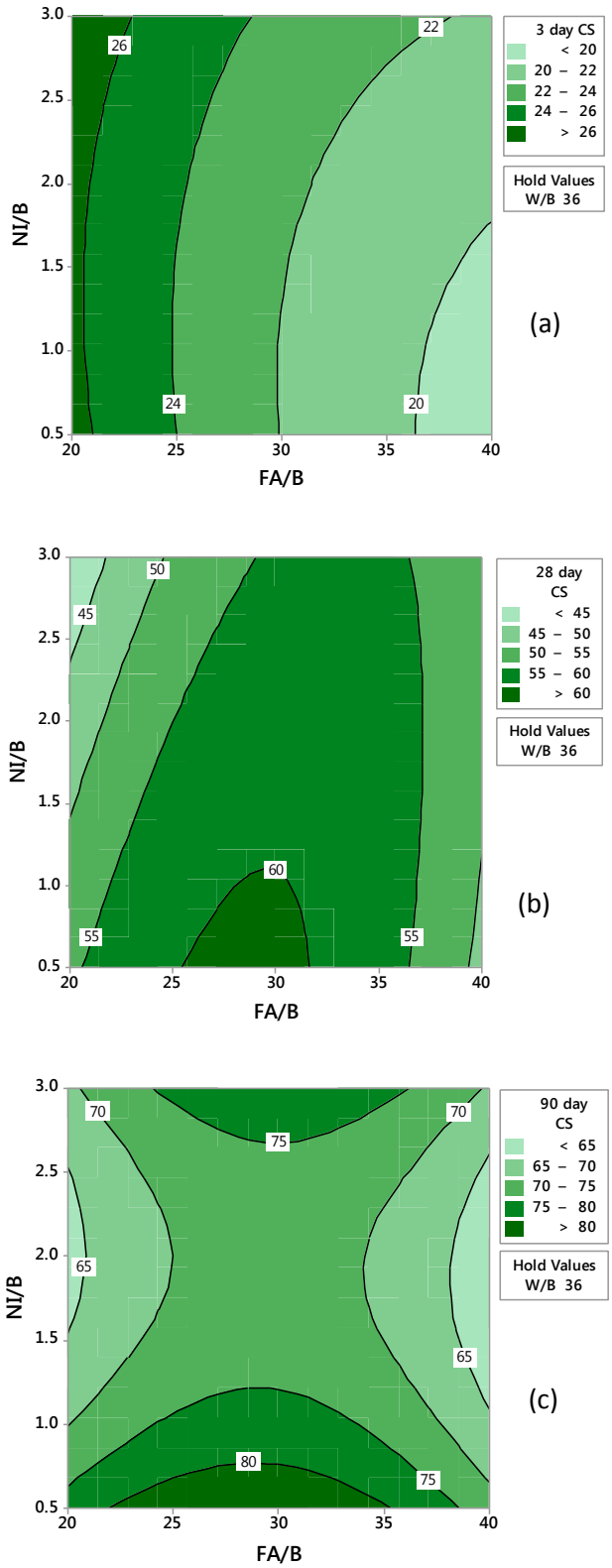

Figure 17. Contour plots of the CS in a function of FA/B and NI/B while the W/B was held at its optimum level of 36%: (a) CS_{3d}, (b) CS_{28d}, and (c) CS_{90d}.

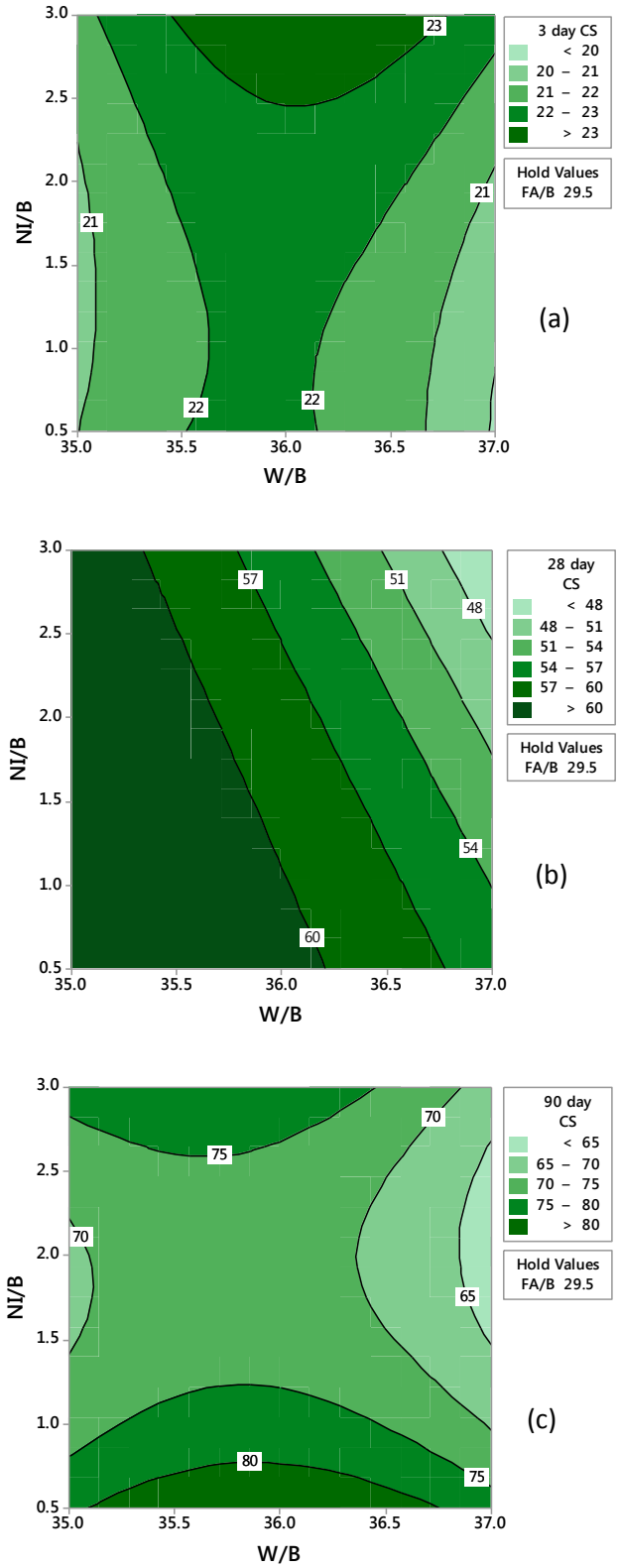

Figure 18. Contour plots of the CS in a function of W/B and NI/B while the FA/B was held at its optimum level of 29.5%: (a) CS_{3d}, (b) CS_{28d} and (c) CS_{90d}.

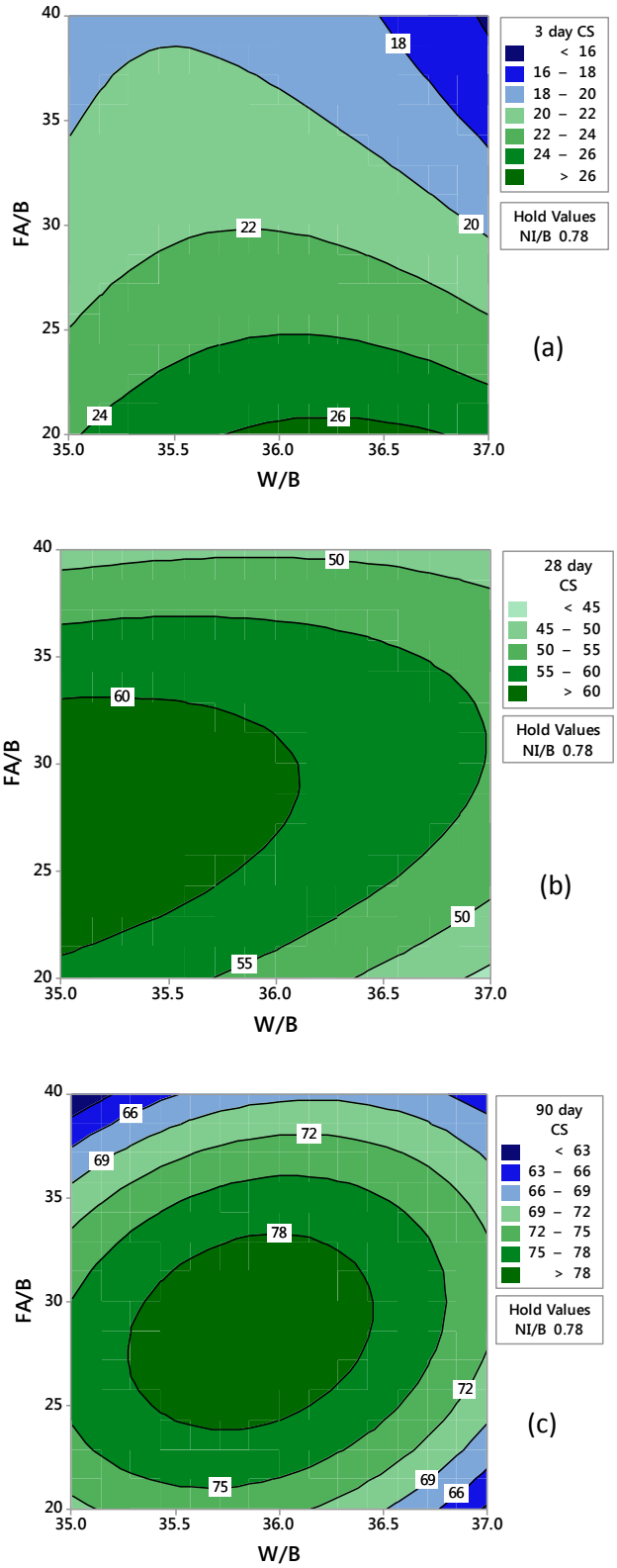

Figure 19. Contour plots of the CS in a function of W/B and FA/B while the NI/B was held at its optimum level of 0.78%: (a) CS_{3d}, (b) CS_{28d} and (c) CS_{90d}.

2.4.5. Overlay contour plots for the RSM at optimum settings

As previously shown in Table 8, the CS's were measured in the range of 14.2-37.4, 27.9-64.3 and 56.5-79.3 MPa for the hardened pastes cured for 3, 28 and 90 days, respectively, while the SP ranged between 84.8 and 150 %. The overlay plots of the responses in a function of two independent variables while the third independent variable was held at its optimum level were made to find the regions where the hardened paste had the maximum possible CS while the SP of the fresh pastes was in the desirable ranges. In this regard, the desired SP was set at 105-115% and the maximum possible CS_{3d}, CS_{28d} and CS_{90d} were set in the ranges of 20-40, 50-70 and 70-85 MPa, respectively (Figure 20).

As shown in Figure 20a, when the W/B was held at its optimum level of 36%, all the responses could be obtained in the desired ranges with a simultaneous increase of the FA/B from 0.5 to 1.5% and the NI/B from 20 to 35%. On the other hand, when the FA/B was fixed at its optimum level of 29.5%, the desirable responses could be obtained with the increase of W/B from 35 to 37% and the simultaneous decrease of NI/B from 2.3 to 0.5 % (Figure 20b). A wider region on the right half of the design was predicted for the desired responses for the W/B from 35.5 to 37% and the FA/B from 20 to 35%, while the NI/B was held at its optimum level of 0.78% (Figure 20c).

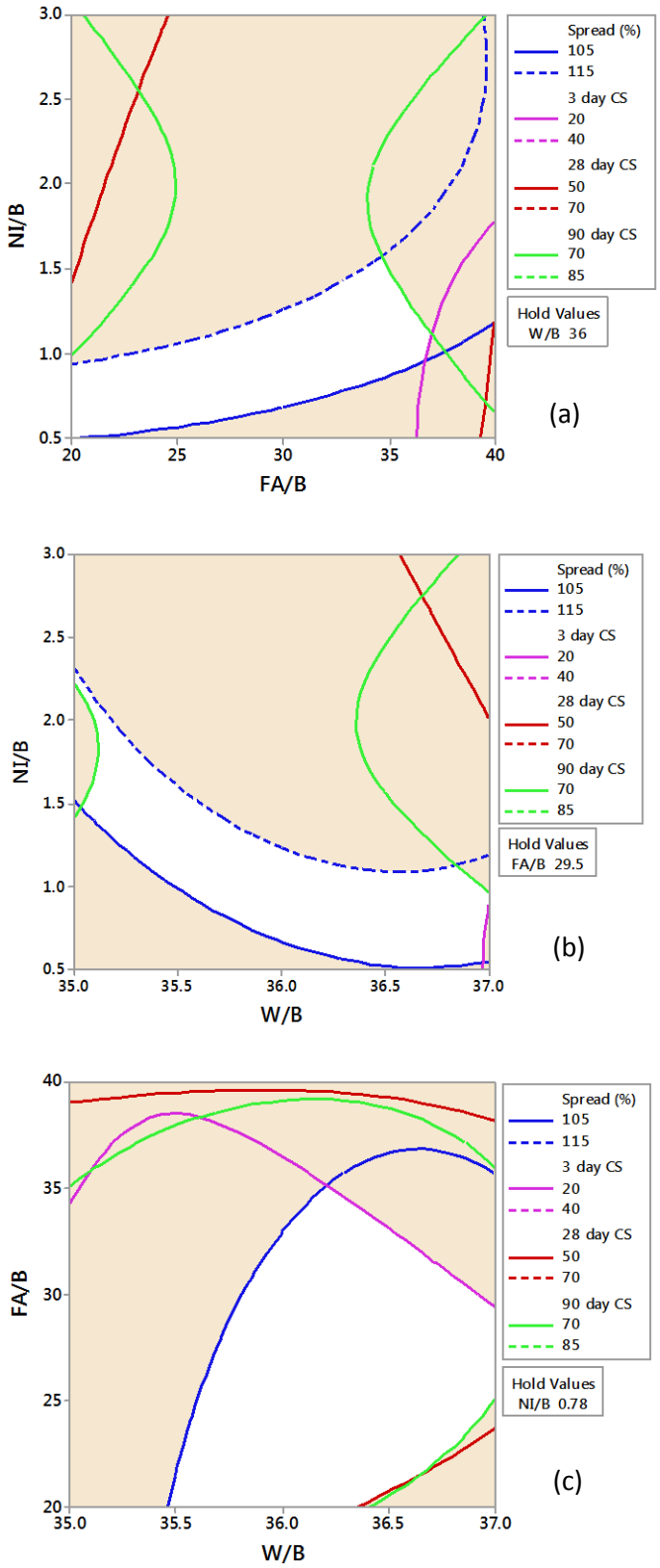

Figure 20. Overlay contour plot of the response variables in a function of two independent variables while the third one was held at its optimum level.

2.4.6. Model validation

The accuracy of the prediction model was validated by performing another set of experiment where the specimens were made at the global optimum mix ratio obtained in the Section 2.4.2 and by comparing the predicted and measured responses to each other. As shown in Table 11, the measured values were in good agreement with the values predicted by the model since they all were in between the 95% confidence interval values.

Table 11. Values for the predicted, observed and confidence intervals of the dependent responses.

Response	Statistical Values		
	Predicted	Observed	95% CI
Spread (%)	107.34	102.5	95.8 - 118.9
Compressive Strength (MPa)			
3 days	22.07	20.7	17.1 - 27.0
28 days	60.4	60.7	54.3 - 66.5
90 days	79.8	68.1	72.9 - 86.7

2.4.7. Scanning Electron Microscopy (SEM)

SEM pictures were taken in order to observe the microstructure of the cement pastes at different curing times. For the FA0NI0 and FA0NI3 specimens, early ettringite formation as needle shape was observed at 3-day curing (Figure 21a and 22a) while a denser microstructure was observed after longer curing times (e.g. 28- and 90 days). In Figure 22 it was observed that the addition of NI to the cement pastes resulted in a denser microstructure after the 28-day curing period. On the other hand, the presence of unreacted FA was observed in the specimen FA40NI0 (Figure 23a and b). At the 28-day curing time, it was observed that the boundaries of the FA spheres were starting to react with the rest of the structure, in contrast with the 3-day curing where no binding was observed (Figure 23a and b). A unique microstructural property was found for the FA40NI3 paste (Figure 24). It is uncertain at this moment what mechanisms with which the FA40NI3 paste has been developed. Further investigation on this matter is warranted.

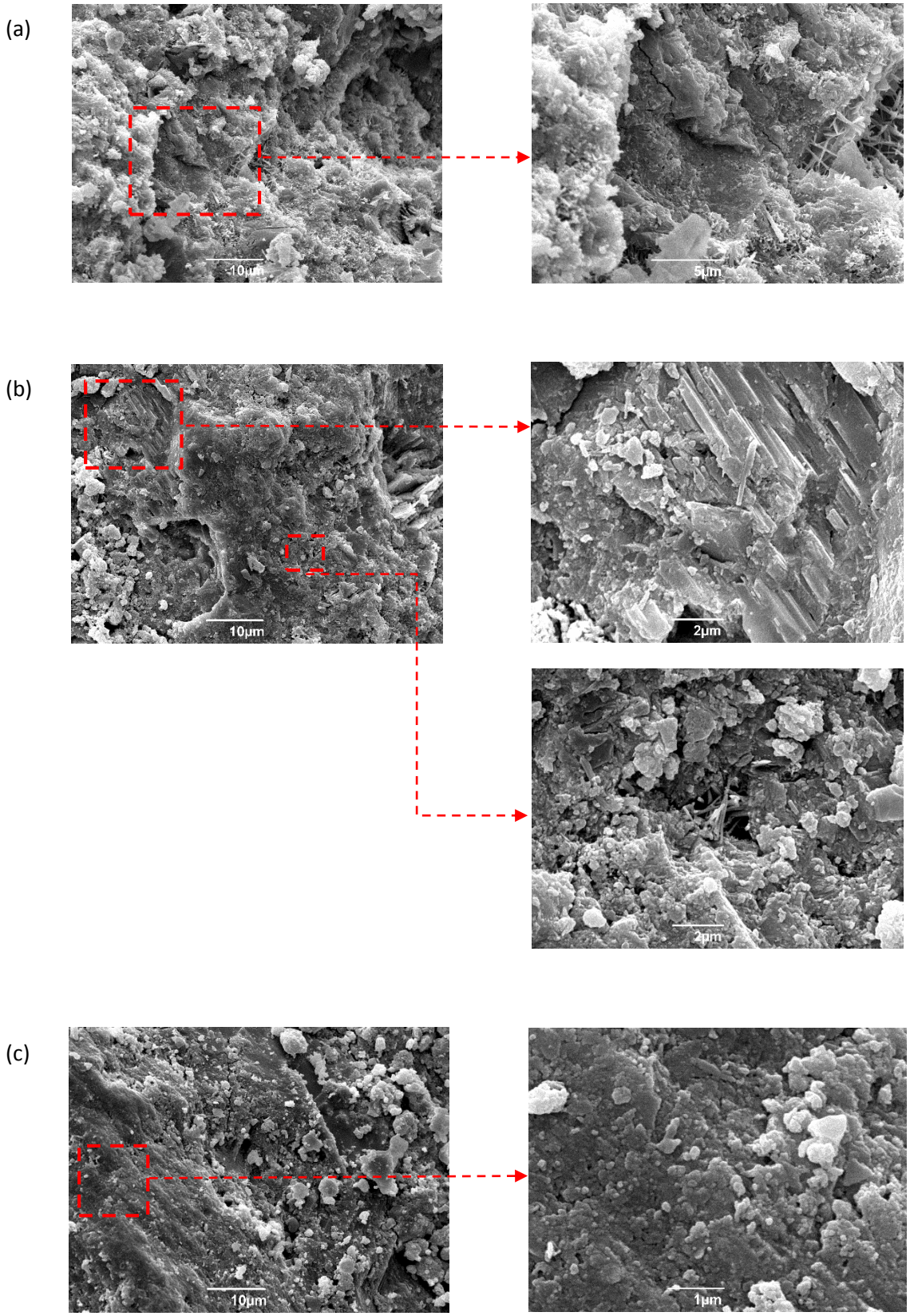

Figure 21. SEM images of the FA0NI0 specimen at (a) 3-day, (b) 28-day and (c) 90-day curing.

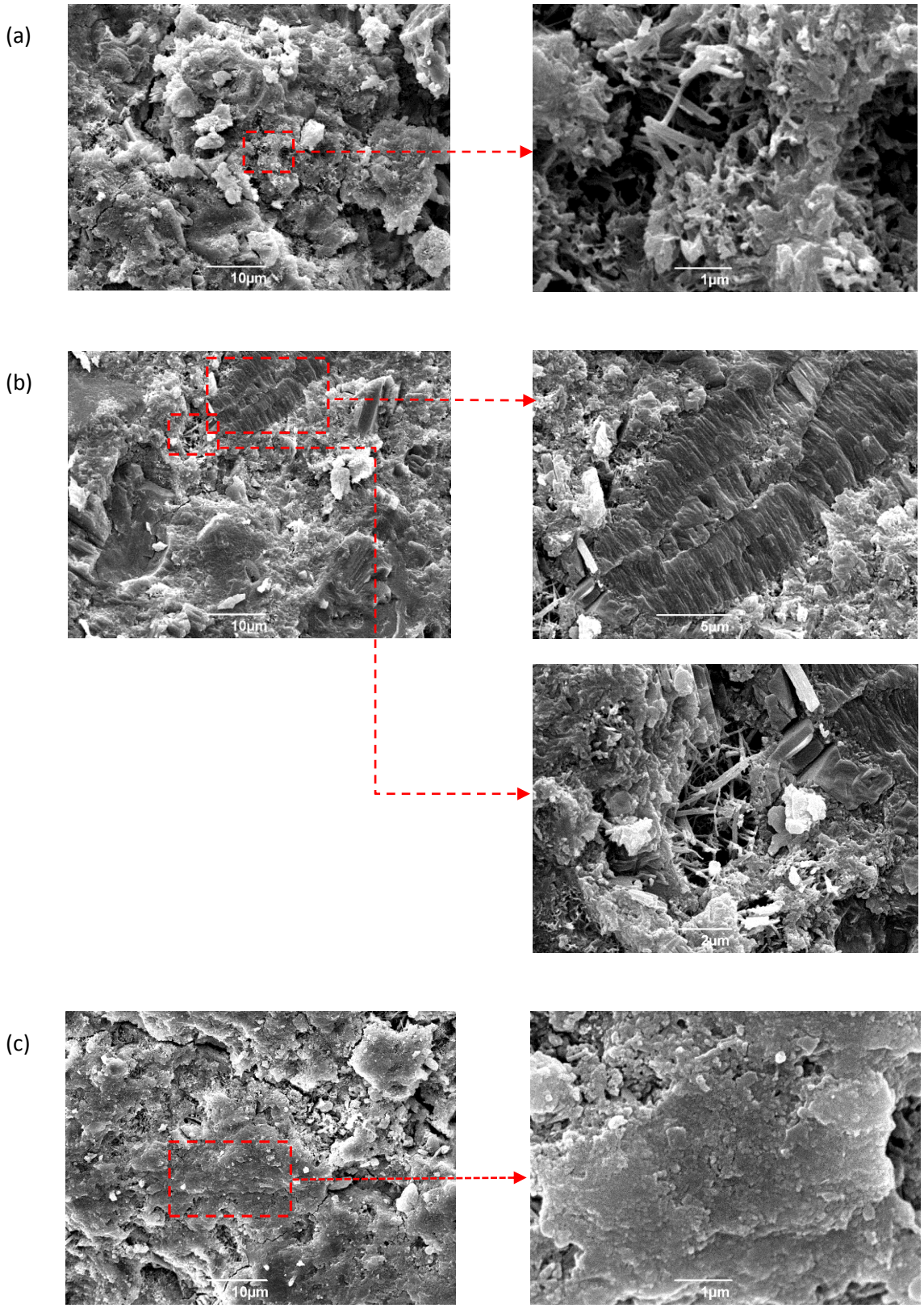

Figure 22. SEM images of the FA0NI3 specimen at (a) 3-day, (b) 28-day and (c) 90-day curing.

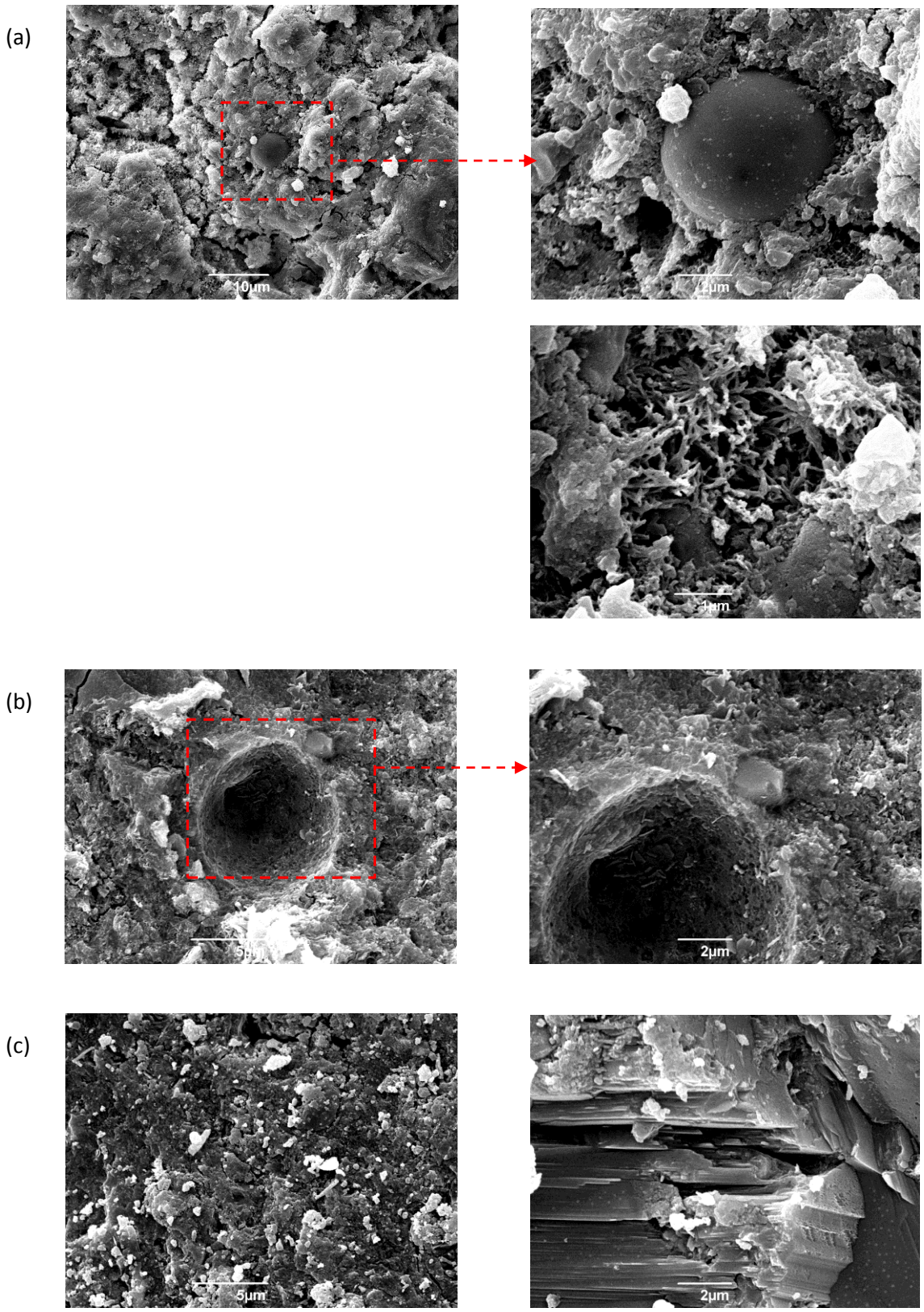

Figure 23. SEM images of the FA40NI0 specimen at (a) 3-day, (b) 28-day and (c) 90-day curing.

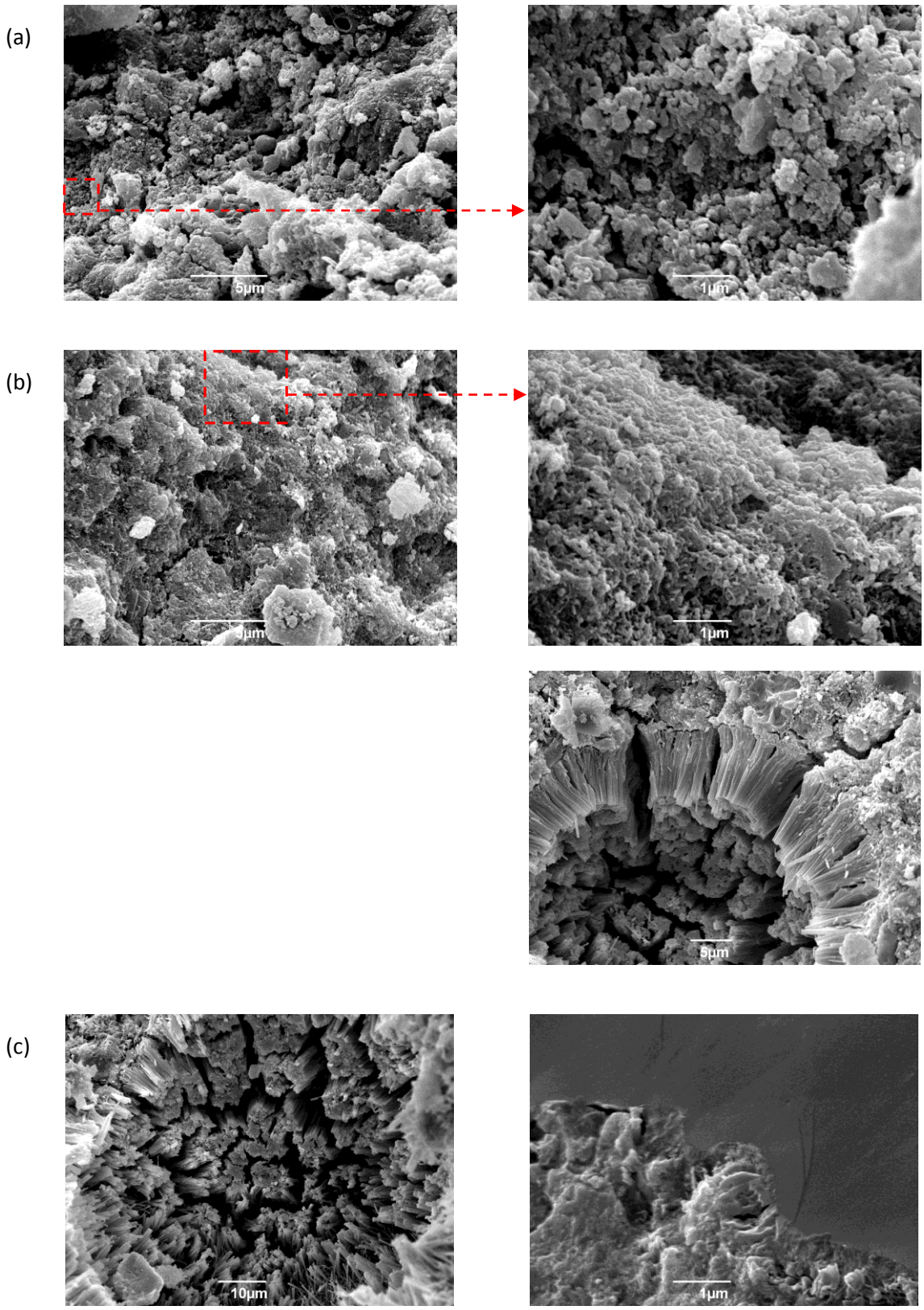

Figure 24. SEM images of the FA40NI3 specimen at (a) 3-day, (b) 28-day and (c) 90-day curing.

2.5. Conclusions

In this investigation, mix ratio of the cement paste was optimized for the desired spread percentage of the fresh paste and the maximum possible compressive strengths of the hardened pastes for 3, 28 and 90 days. The following conclusions can be made from the experimental results:

- The compressive strengths were measured in the range of 14.2-37.4, 27.9-64.3 and 56.5-79.3 MPa for the hardened pastes cured for 3, 28 and 90 days, respectively, while the spread percentages of the fresh pastes ranged between 84.8 and 150 %.
- D-optimal with desirability functions found that the optimum independent variable setting at 36% W/B, 29.5% FA/B and 0.78% NI/B resulted in the 3-, 28- and 90- day compressive strengths of 22.1, 60.4 and 79.8 MPa, respectively, while satisfying the desirable spread percentage at 107%.
- The spread percentage of fresh pastes increased with the increase of NI/B or W/B but with the decrease of FA/B.
- Increasing FA/B generally decreased the compressive strength at early age of curing (i.e., 3-day) but either increasing or decreasing FA/B from the optimum level decreased the response at late age after 28 day. This attributed to the slow pozzolanic reaction of FA that occurs at late ages after $Ca(OH)_2$ is formed by the hydration of cement.
- NI/B did not play a significant role in the development of compressive strength at early age (i.e., 3-day), whereas the addition of NI was found effective in supporting the chemistry in cement paste at later curing stages, especially after 90-day curing.
- The statistical model predicted the dependent variables of spread percentage and compressive strength with good accuracy.
- SEM images showed that a denser microstructure was obtained at a longer curing time, especially for the specimens containing NI as an additive. Pozzolanic reaction was observed to have already taken place at the 28-day curing.

In summary, the extent of contribution that W/B, FA/B and NI/B had on the compressive strength responses was time-dependent for the cement pastes containing FA and NI as admixtures. Specifically, FA began to play a major role in the development of compressive strength at late age of curing (>28 days), whereas NI did after 90 days of curing. Such a time-dependency of the

cement chemistry with FA and NI should be taken into consideration with caution. Translating laboratory research results, typically based on a 28-day strength results, to field practice where a shorter curing period is typically provided for cost reasons can lead to failure to meet the design life requirements of concrete structures.

2.6. References

Aydın S, Yazıcı H, Yiğiter H, Baradan B. Sulfuric acid resistance of high-volume fly ash concrete. Building and Environment 2007; 42:717-721.

Aldahdooh MAA, Bunnori NM, Johari MA. Evaluation of ultra-high-performance-fiber reinforced concrete binder content using the response surface method. Materials & Desiggn 2013; 52:957–65.

Baş D, Boyacı IH. Modeling and optimization I: Usability of response surface methodology. Journal of Food Engineering 2007; 78:836-845.

Cheng AS, Huang CH, Yen T, Luo YL. Influences of slag and fly ash on themicrostructure property and compressive strength of concrete. Advanced Materials Research 2011; 146:1690-7.

Cusson D, Lounis Z, Daigle L. Benefits of internal curing on service life and life-cycle cost of high-performance concrete bridge decks – A case study. Cement and Concrete Composites 2010; 32:339-50.

Deschner F, Winnefeld F, Lothenbach B, Seufert S, Schwesig P, Dittrich S, Goetz-Neunhoeffer F, Neubauer J. Hydration of Portland cement with high replacement by siliceous fly ash. Cement and Concrete Research 2012; 42(10):1389-400.

Deo O, Neithalath N. Compressive behavior of pervious concretes and a quantification of the influence of random pore structure. Materials and Science and Engineering A 2010; 528:402-412.

Dilnesa BZ, Wieland E, Lothenbach B, Dähn R, Scrivener KL. Fe-containing phases in hydrated cement. Cement and Concrete Research 2014; 58:45-55.

Hanus MJ, Harris AT. Nanotechnology innovations for the construction industry. Progress in Materials Science 2013; 58:1056-102.

Jiménez-Quero VG, León-Martínez FM, Montes-García P, Gaona-Tiburcio C, Chacón-Nava JG. Influence of sugar-cane bagasse ash and fly ash on rheological behavior of cement pastes and mortars. Construction and Building Materials 2013; 40:691-701.

Montgomery D. Design and Analysis of Experiments. 8th Ed. John Wiley & Sons, Inc.; 2013.

Oltulu M, Sahin R. Effect of nano-SiO_2, nano-Al_2O_3, nano-Fe_2O_3 powders on compressive strength and capillary water absorption of cement mortar containing fly ash: A comparative study. Energy and Buildings 2013; 58:292-301.

Ouyang X, Guo Y, Qiu X. The feasibility of synthetic surfactant as an air entraining agent for the cement matrix. Construction and Building Materials 2008; 22:1774-9.

Poole TS. Curing Portland Cement Concrete Pavements, Volume I. FHWA-RD-02-099. Federal Highway Administration, McLean, VA; 2005.

Sanchez F, Sobolev K. Nanotechnology in concrete – A review. Construction and Building Materials 2010; 24:2060-2071.

Shehadji Y, Escadeillas G, Mouli M, Khelafi H, Benosman. Influence of natural pozzolan, silica fume and limestone fine on strength, acid resistance and microstructure of mortar. Powder Technoly 2014; 254:314-23.

Singh LP, Karade SR, Bhattacharyya SK, Yousuf MM, Ahalawat S. Beneficial role of nanosilica in cement based materials. Construction and Building Materials 2013; 47:1069-1077.

Sonebi M, Bassuoni MT. Investigating the effect of mixture design parameters on pervious concrete by statistical modeling. Construction and Building Materials 2013; 38:147-154.

Termkhajornkit P, Nawa T, Kurumisawa K. Effect of water curing conditions on the hydration degree and compressive strengths of fly ash–cement paste. Cement and Concrete Composites 2006; 28:781-9

CHAPTER 3

Assessment of the optimum mix design of two types of cements by Response Surface Methodology

3.1. Abstract

In this study, the effect of cement type on the spread percentage and the compressive strength at 28 days of curing was evaluated in a cement paste mixture containing FA and NI as admixtures. The optimum mix ratio of two cement types were optimized for a desired SP and the maximum possible CS. A three factor, two level, face centered central composite design was developed in order to assess the main, quadratic and interactions effects of the independent variables of water-to-binder (W/B), FA-to-binder (FA/B) and NI-to-binder (NI/B), on the dependent response variables. The CS's were measured in the range of 27.9-64.3 MPa and 52.7-66.7 MPa for the hardened pastes, while the SP's ranged in between 84.8-150% and 111.5 to 154% for the fresh paste of the Type IP and GU cements, respectively. The spread percentage of fresh pastes increased with the increase of NI/B or W/B but with the decrease of FA/B for both types of cements. On the other hand, the addition of NI/B the mixtures did not play a significant role in the development of the CS at 28 days of curing. The optimum variable settings at for the Type IP cement were at 35.1 % W/B, 28.5% FA/B and 1.6% NI/B, while for the Type GU cement the settings were obtained at 35.1% W/B, 40% FA/B and 0.55% NI/B. Slightly higher predictive compressive strength at 64.72 MPa for the Type GU cement were obtained, while for the Type IP a 62.78 MPa were predicted. Quadratic and interaction effects of the factors resulted to play a significant role in the development of both of the prediction models of the dependent responses.

3.2. Literature Review

3.2.1. Cement types and specifications

According to the American Society for Testing and Materials (ASTM), there are different cements with special properties and chemical compositions that are made to meet particular requirements for specific applications. Under the category of Portland cements there are ten different types of cements. Some cements are designed with a combined type of specification (e.g., Type I/II) in order to meet the requirements indicated for both types of cements and have the flexibility in use when either type is desired. The specifications for the hydraulic cements for general and special applications are covered by the ASTM C1157, and cover 7 different types of cement. On the other hand, blended hydraulic cements only have four types of cements and they consists of Portland cement mixed with either a slag cement, a pozzolan or a limestone, or a combination of these. The standard composition requirements of the different types of Portland cement can be found in Table 12 while the standard physical requirements are listed in Table 13.

Table 12. Standard composition requirements of Portland cements (Modified from ASTM C150).

Cement Type	I and IA	II and IIA	II(MH) and II(MH)A	III and IIIA	IV	V
Al_2O_3, (max %)	-	6.0	6.0	-	-	-
Fe_2O_3, (max %)	-	6.0[a]	6.0[a,b]	-	6.5	-
MgO, (max %)	6.0	6.0	6.0	6.0	6.0	6.0
SO_3, (max %)						
When C_3A is ≤ 8%	3.0	3.0	3.0	3.5	2.3	2.3
When C_3A is > 8%	3.5	[c]	[c]	4.5	[c]	[c]
C_3S, (max %)	-	-	-	-	35[b]	-
C_2S, (min %)	-	-	-	-	40[b]	-
C_3A, (max %)	-	8	8	15	7[b]	5[a]
$\sum C_3S + 4.75\ C_3A$, (max %)	-	-	100[b]	-	-	-
$\sum C_4AF + 2(C_3A)$ or $\sum C_4AF + C_2F$, (max %)	-	-	-	-	-	25[a]
$Na_2O + 0.658K_2O$, (max %)[d]	0.60	0.60	0.60	0.60	0.60	0.60
Loss on ignition, (max %)	3.0	3.0	3.0	3.0	2.5	3.0
Insoluble residue, (max %)	0.75	0.75	0.75	0.75	0.75	0.75

[a]Does not apply when the sulfate resistance limit is specified.
[b]Does not apply when the heat of hydration limit is specified.
[c]Not applicable.
[d]Optional composition requirements for low alkali cements.

As previously mentioned, each type of cement possesses specific characteristics in order to be used for a specific application. The Type I cement is the most frequently used in the field, since it is used when there is no special property specified. When the letter A is added at the end of the type of cement it means that it is intended to be used when air entrainment is also desired. The Type II is used when moderate sulfate resistance is desired. The Type II(MH) cement is used when moderate heat of hydration and sulfate resistance are desired. When high early strength is desired, the Type III cement is used. The last two types of cement, Type IV and V, are used when a low heat of hydration is desired and when high sulfate resistance is desired, respectively.

Table 13. Standard physical requirements for Portland cements (Modified from ASTM C150).

Cement Type	I	IA	II	IIA	II(MH)	II(MH)A	III	IIIA	IV	V
Air content of mortar, (vol %)										
max	12	22	12	22	12	22	12	22	112	12
min	-	16	-	16	-	16	-	16	-	-
Fineness, specific surface, air permeability test, (m^2/kg)										
max	260	260	260	260	260	260	-	-	260	260
min	-	-	-	-	430[a]	430[a]	-	-	430	-
Autoclave expansion, (max %)	0.8	0.8	0.8	0.8	0.8	0.8	0.8	0.8	0.8	0.8
Strength[b], (MPa)										
1 day	-	-	-	-	-	-	12.0	10.0	-	-
3 days	12.0	10.0	10.0	8.0	10.0	8.0	24.0	19.0	-	8.0
7 days	19.0	16.0	17.0	14.0	17.0	14.0	-	-	7.0	15.0
28 days	-	-	-	-	-	-	-	-	17.0	21.0
Time of setting, (min)										
not less than	45	45	45	45	45	45	45	45	45	45
not more than	375	375	375	375	375	375	375	375	375	375

[a]Maximum fineness limits do not apply if the sum of $C_3S+4.75C_3A$ is ≤ 90.
[b]Shall be not less that the specified at any test age.

The standard physical requirements for the hydraulic cements covered in the ASTM C1157 are given in Table 14. The Type GU is a hydraulic cement for general construction, and is used when more than one of the special types are not required. The Type HE is a cement that possess high early strength. The Types MS and HS are for moderate and high sulfate resistance, respectively. On the other hand, the blended cement Type MH is used when moderate heat of hydration is desired, while the Type LH is used when low heat of hydration is required.

Table 14. Standard physical requirements for hydraulic cements.

Cement Type	GU	HE	MS	HS	MH	LH
Fineness	[a]	[a]	[a]	[a]	[a]	[a]
Autoclave length change, max (%)	0.80	0.80	0.80	0.80	0.80	0.80
Time of setting[b], (min)						
not less than	45	45	45	45	45	45
not more than	420	420	420	420	420	420
Air content, max (%)	12	12	12	12	12	12
Strength, (MPa)						
1 day	-	12.0	-	-	-	-
3 days	13.0	24.0	11.0	11.0	5.0	-
7 days	20	-	18	18	11	11
28 days	28.0	-	-	25.0	-	21.0
Heat of Hydration, (max, kJ/kg)						
7 days	-	-	-	-	290	250
28 days	-	-	-	-	-	290
Mortar bar expansion, max (%)						
14 days	0.020	0.020	0.020	0.020	0.020	0.020
Sulfate expansion[c], max (%)						
6 months	-	-	0.10	0.05		
1 year	-	-	-	0.10		

[a]Both amount retained when wet sieve on the 45-µm (No.325) sieve and specific surface area by air permeability apparatus in m^2/kg shall be reported on all certificates of test results.
[b]Time of setting refers to initial setting time of Vicat needle experiment.
[c]In the testing of HS cement, testing of one year shall not be required when the cement meets the 6-month limit. An HS cement failing the 60month limit shall not be rejected unless it also fails the 1-year limit.

The blended hydraulic cements are divided into binary or ternary blended cements. Binary blended cements consist of Portland cement with either a slag cement, a pozzolan or a limestone. On the other hand, ternary blended cements (Type IT) consists of Portland cement and a combination of either two different pozzolans, slag cement and a pozzolan, a pozzolan and a limestone or a slag cement and a limestone. The characteristics of the different types of blended hydraulic cements are listed in Table 15. Similarly to the Portland cements, air entrainment cements are available for each of their blended cement equivalents. The Portland blast-furnace slag cement (Type IS) is a hydraulic cement in which the slag cement constituent is up to 95% by mass of the blended cement. As stated by the ASTM C595-13, any binary or ternary cement that contains slag cement equal to or more than 70% by mass, is allowed to contain hydrated lime. The Portland-pozzolan cement (Type IP) contains pozzolans up to 40% by mass of the blended cement, while the Portland-limestone cement (Type IL) has a limestone content in the range of 5 to 15 % by mass of the blended cement. The physical requirements of each type of the blended cements are listed in Table 16.

Table 15. Chemical requirements of blended hydraulic cement (Modified from ASTM C595-13).

Cement Type[a]	IS(<70), IT (P<S<70), IT(L<S<70)	IS(≥70), IT(S≥70)	IP, IT(P≥S), IT(P≥L)	IL, IT(L≥S), IT(L≥P)
MgO, (max %)	-	-	6.00	-
SO_3, (max %)[b]	3.0	4.0	4.0	3.0
S^{2-}, (max %)	2.0	2.0	-	-
Insoluble residue, (max %)[c]	1.0	1.0	-	-
Loss on ignition, (max %)	3.0[d]	4.0[d]	5.0[d]	10.0

[a] Chemical requirements are also applicable to all air-entrained cement equivalents.
[b] It is permissible to exceed these values since in the Test Method C1038 was demonstrated that cements with higher SO_3 content will not develop expansion exceeding 0.020% at 14 days.
[c]Does not apply for ternary cements.
[d]Ternary blended cements with limestone must not exceed 10% by mass.

Table 16. Physical Requirements of blended hydraulic cements (Modified from ASTM C595).

Cement Type[a]	IP, IS(<70), IL, IT(P≥S), IT(P>L), IT(L≥S), IT(L≥P), IT(P<S<70), IT(L<S<70)	IP(MS), IS(<70)(MS), IT(P≥S)(MS), IT(P<S<70)(MS)	IP(HS), IS(<70)(MS), IT(P≥S)(MS), IT(P<S<70)(HS)	IS(≥70), IT(S≥70)	IP(LH), IL(LH), IT(P≥S)(LH), IT(L<S<70)(LH), IT(P>L)(LH), IT(L≥S)(LH), IT(L≥O)(LH)[b]
Autoclave expansion, (max %)	0.8	0.8	0.8	0.8	0.8
Autoclave contraction, (max %)[c]	0.2	0.2	0.2	0.2	0.2
Time of setting, Vicat test					
Set, minutes, not less than	45	45	45	45	45
Set, hours, not less than	7	7	7	7	7
Mortar air content, (Max vol %)	12	12	12	12	12
Min Compressive Strength, (Mpa)[a]					
3 days	13.0	11.0	11.0	-	-
7 days	20.0	18.0	18.0	5.0	11.0
28 days	25.0	25.0	25.0	11.0	21.0
Heat of Hydration, (max, kJ/kg)					
7 days	290[d]	290[d]	290[d]	-	250
28 days	330[d]	330 [d]	330[d]	-	290
Water requirement, (max weight % of cement)	-	-	-	-	64
Drying shrinkage, (max %)	-	-	-	-	0.15
Mortar expansion, (max %)[e]					
14 days	0.02	0.02	0.02	0.02	0.02
8 weeks	0.06	0.06	0.06	0.06	0.06
Sulfate resistance, (max %)[f]					
Expansion at 180 days	-	0.10	0.05	-	-
Expansion at 1 year	-	-	0.10	-	-

[a]Air-entrained cements shall have a mortar air content of 19 ± 3% by volume and the minimum CS shall be no less 80% of the comparable non-air-entrained cement type.
[b]Applicable only when strengths at early ages are not required or when low heat is required.
[c]The specimens shall remain firm and hard and show no signs of distortion, cracking, checking pitting or disintegration.
[d]Applicable only when moderate heat of hydration (MH) is specified.
[e]Is optional and not required unless the cement will be used with alkali-reactive aggregate.
[f]In the testing of HS cement, testing at one year is not required when it meets the 180-day limit.

3.2.2. Effect of cement type on the performance of mineral admixtures

The performance of mineral admixtures (e.g., fly ash and slag) on concrete frequently depends on the characteristics of the cement used. Studies have shown that these materials have an effect on the hydration of the cement, and their efficiency is strongly affected by the type and composition of the cement clinker (Cyr et al., 2014). An experimental study where the Type I cement was compared against the Type III cement showed that mortars with 30% replacement of cement with FA had the interaction between cement type and fineness significantly affect the flow and strength development of the specimens (Popovics, 1993).

High level of alkalis in cement have been found to increase the reaction rate of mixtures containing silica fume (Meng et al., 1998). Sybertz (1989) also studied the effect of cements with different alkali content on the strength of mortars containing fly ash and found that the fineness and the alkali contents of the cement significantly affected the mortars that contained high amounts of FA.

3.3. Materials and Experimental Methodology

3.3.1. Cement, FA and NI

Two types of cement were used for the purposes of this experiment, blended hydraulic cement Type IP in compliance with ASTM C595 and Portland cement Type GU in compliance with ASTM C1157 (Table 17). Both cements were purchased from local suppliers in Puerto Rico. The FA was obtained from a local coal-fueled power plant (AES Puerto Rico) (Table 17) and the NI solution was purchased from the Ferrotec (Bedford, NH) (Table 4, Chapter 1).

Table 17. Physiochemical properties of fly ash and cement.

Properties	Fly Ash		Cement	
	1	2	Type IP	Type GU
Mineralogical composition (% wt.)				
SiO_2	30.84	28.82	27.14	19.8
Al_2O_3	9.93	11.03	6.68	5.1
Fe_2O_3	5.01	4.62	3.71	3.1
CaO	39.61	38.73	55.47	67.3
MgO	0.35	0.38	1.62	0.8
K_2O	1.01	0.97	0.48	-[a]
Na_2O	0.9	1.43	0.59	-
SO_3	11.43	12.98	3.48	2.7
TiO_2	0.45	0.49	0.32	-
P_2O_5	0.11	0.15	0.11	-
Loss-on-Ignition (% wt.)	7.62	8	5.52	6.8
Blaine (m^2/kg)	441	478	554	488
Fineness (% wt.)	73.7	76.3	92.6	92.5
Specific gravity	2.55	-	2.86	-
Lime Saturation Factor (LSF)	0.39	0.4	0.64	-
Silica Ratio (SR)	2.06	1.84	2.61	-
Alumina to Iron Ratio (AF)	1.98	2.39	1.8	-

[a]Information was not available.

3.3.2. Specimen design and preparation

This study was designed in a three factor, two level (2^3) face centered, central composite design aiming to assess the main, quadratic and interaction effects of the independent variables, the percentages of water-to-binder (W/B), FA-to-binder (FA/B) and NI-to-binder (NI/B), on the dependent response variables, spread percentage (SP) of the fresh pastes and compressive strength (CS) of the hardened pastes. Response Surface Methodology (RSM) was utilized to optimize the mix design in order to obtain the maximum compressive strength of cement pastes cured for 28 days and achieve the desired spread percentage of the fresh pastes simultaneously, and compare the optimization results for each type of cement. The mixing, casting and curing of the cement paste specimens were done as describe in Chapter 1, section 1.3.2.

3.3.3. Response Surface Methodology

Mathematical and statistical interpretations of the data were done with Minitab 17 for the spread percentage and the compressive strength. A total of 20 combinations of independent variable settings were run with 6 replicates at the center points, for each of the cement types. The significance of each of the independent variables to the dependent variable and their interactions were determined by ANOVA, as described in Chapter 2. Numerical optimization of the independent variables for the cement pastes of the two types of cement was also performed to identify the combination of variable settings that maximize the compressive strengths and at the same time meeting a desired spread percentage.

3.4. Results and Discussion

3.4.1. Responses of the RSM

The spread percentages of the fresh pastes ranged between 84.8 and 150 % for the Type IP and from 111.5 to 154 % for the Type GU cement (Table 18). A recommended spread percentage of cement pastes is not available in the literature. For this reason, 110±5% of cement mortars (Jimenez-Quero et al., 2013) were used as the spread percentage reference value of cement pastes in the CCF analysis.

Table 18. Matrix of 2^3 CCF and the measured dependent response variables.

Run	Independent variables			Dependent variables			
	Actual (% wt.)			Type IP cement		Type GU cement	
	W/B	FA/B	NI/B	Spread (%)	CS (MPa)	Spread (%)	CS (MPa)
1	35	20	0.5	89.5	59.6	136.8	57.2
2	37	20	0.5	110	47.5	143.5	54.9
3	35	40	0.5	84.8	49.3	111.5	66.7
4	37	40	0.5	97.3	46.6	118.0	56.6
5	35	20	3.0	137.3	54.6	154.0	60.9
6	37	20	3.0	135.5	27.9	154.0	55.4
7	35	40	3.0	106.8	55.0	143.5	62.4
8	37	40	3.0	115.8	47.8	154.0	58.4
9	35	30	1.75	97.0	59.5	124.0	61.4
10	37	30	1.75	120.3	51.1	141.5	59.7
11	36	20	1.75	126.8	46.1	133.8	52.7
12	36	40	1.75	101.8	49.3	119.5	61.3
13	36	30	0.5	97.3	60.3	118.0	53.2
14	36	30	3.0	121.5	52.3	135.0	62.2
15	36	30	1.75	113.5	60.8	123.3	57.4
16	36	30	1.75	115.8	62.4	125.3	58.6
17	36	30	1.75	150	60.5	123.3	55.6
18	36	30	1.75	119	64.3	122.8	61.9
19	36	30	1.75	114	42.8	127.8	61.3
20	36	30	1.75	115.3	53.4	122.8	61.4

The compressive strengths were measured in the range of 27.9-64.3 MPa and 52.7-66.7 MPa for the cements Type IP and GU, respectively (Table 18). These results clearly showed that compressive strength of the cements pastes made with the Portland cement Type GU resulted in higher values for most of the combinations tested at the 28 days of curing.

3.4.2. Statistical models of the RSM

The ANOVA for each dependent variable is shown in Table 19. The suitability of the model was validated by checking residual plots and the lack-of-fit at a significance level of 0.05. Residual plots confirmed that the residuals were independent, were normally distributed, and had equal variances. Lack-of-fit for each response resulted in p-values greater than 0.05, indicating that the models accurately fit the data. The adequacy of the model can also be described by the high regression coefficients (R^2) of 85.5 and 96.7 % for spread percentages and of 85.2 and 63.0 % for the 28 day compressive strengths of the Type IP and GU cements, respectively.

The main and interactive effects of independent variables on the dependent variables can also be found in Table 19. The estimated regression models after removing insignificant terms for the spread percentage response and the compressive strength responses are given in the equations 8 to 11 as follows:

$$SP_{Type\ IP} = 122.1 - 0.928FA/B + 11.04NI/B \quad (8)$$

$$SP_{Type\ GU} = 16788 - 928W/B - 1.459FA/B - 3.05NP/B + 12.95W/B^2 + 0.402FA/B * NI/B \quad (9)$$

$$CS_{Type\ IP} = 164.8 - 5.71W/B + 6.48FA/B - 0.1059FA/B^2 \quad (10)$$

$$CS_{Type\ GU} = 144.1 - 2.37W/B \quad (11)$$

Table 19. ANOVA and full regression models statistics.

Term	Spread Percentage				28 day Compressive Strength			
	Type IP cement		Type GU cement		Type IP cement		Type GU cement	
	p-value	coefficient	p-value	coefficient	p-value	coefficient	p-value	coefficient
Constant		122.1		16788		164.8		144.1
W/B	0.071	NS	0.003	-928	0.007	-5.71	0.032	-2.37
FA/B	0.016	-0.928	0.000	-1.459	0.466	6.48	0.280	NS
NI/B	0.002	11.04	0.000	-3.050	0.148	NS	0.281	NS
W/B^2	0.265	NS[a]	0.001	12.950	0.586	NS	0.267	NS
FA/B^2	0.815	NS	0.146	NS	0.017	-0.1059	0.452	NS
NI/B^2	0.315	NS	0.161	NS	0.823	NS	0.681	NS
W/B*FA/B	0.922	NS	0.298	NS	0.078	NS	0.469	NS
W/B*NI/B	0.372	NS	0.774	NS	0.221	NS	0.737	NS
FA/B*NI/B	0.264	NS	0.002	0.402	0.059	NS	0.448	NS
Lack-of-Fit	0.668		0.062		0.296		0.277	
R^2 (%)	85.5		96.7		85.2		63.0	

[a] NS: The contribution of the terms was not statistically significant

It should be noted that the coefficient values were for the terms of uncoded independent variables. For the predicted regression equation of the Type IP cement (equation 8), only the linear terms of FA/B and NI/B significantly affected the SP with the NI/B influencing the most. Thereby, the smaller FA/B and the greater NI/B the fresh pastes had, the greater SP was predicted. A significant increase of the spread percentage could be attributed to an enhanced fluidity caused by the surfactants coated on the iron-oxide nanoparticles. An enhanced fluidity of cement due to the addition of synthetic surfactants was reported previously (Ouyang et al., 2008). On the other hand, the Type GU cement resulted to follow a second order polynomial model in which all of the linear terms, the quadratic term of W/B^2 and the interaction between the FA/B and NI/B factors were significant as shown in equation (9).

The CS of the Type GU cement was also predicted with a second order polynomial model. Although, the linear term of W/B and the quadratic term of FA/B were only statistically significant (Table 19), the linear term of FA/B was also incorporated to the regression model in order to maintain the hierarchy of the model (equation 10) (Montgomery, 2013). Thereby, the CS was predicted as a function of the linear terms of W/B and FA/B, and by the quadratic term of FA/B. The independent variable NI/B did not significantly contribute to the $CS_{Type\ IP}$ response, although the interaction of the NI/B with FA/B resulted to have a relatively marginal effect on the response since its p-value was 0.059. On the contrary, the $CS_{Type\ GU}$ cement resulted to only be influenced by the linear term of W/B.

3.4.3. Response optimization of the cement pastes

For the response optimization, the spread percentage of 110% was chosen as the target and the compressive strength was selected to be the maximum possible. The response optimizer tool of Minitab 17 was utilized to simultaneously optimize the responses. As shown in Figure 25a, for the Type IP cement the model optimum independent variable setting at 35.1% W/B, 28.5% FA/B and 1.6% NI/B resulted in the 28 day compressive strength at ~62.8 MPa, while meeting the desirable spread percentage at 109.2%. This was attained with the global desirability value at 0.964 and with the response-specific desirability values at 0.970 for the spread percentage and 0.959 for 28 day compressive strength. It should be noted that the optimization goals could be assigned at different weight and importance. In the current study, however, the target responses had equal weight and importance.

(a)

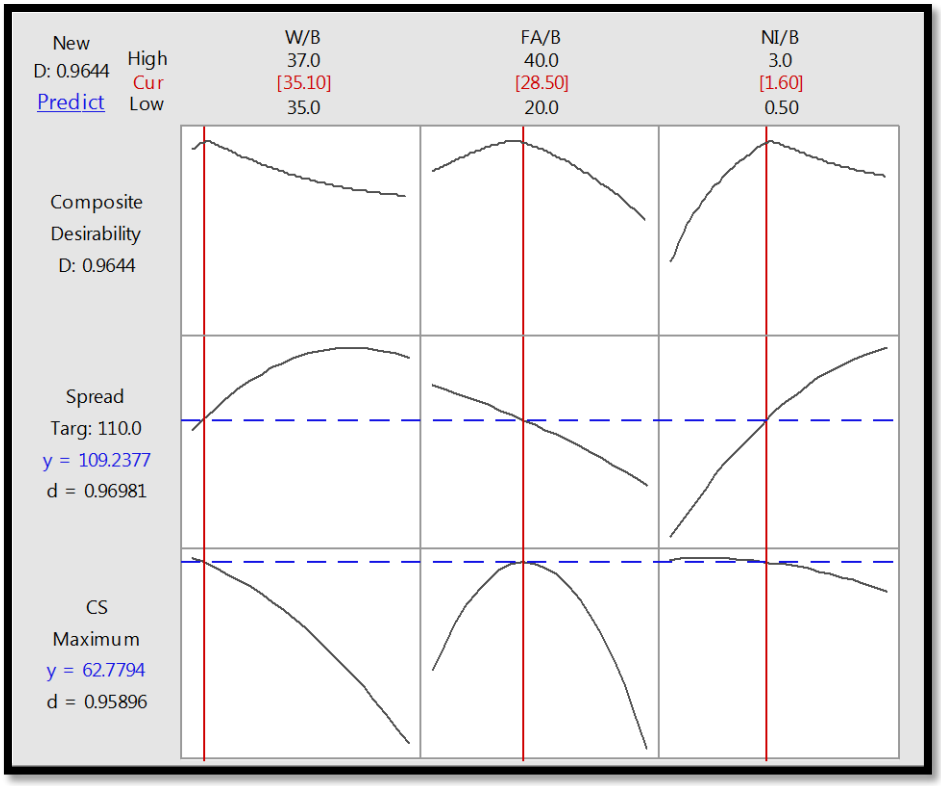

(b)

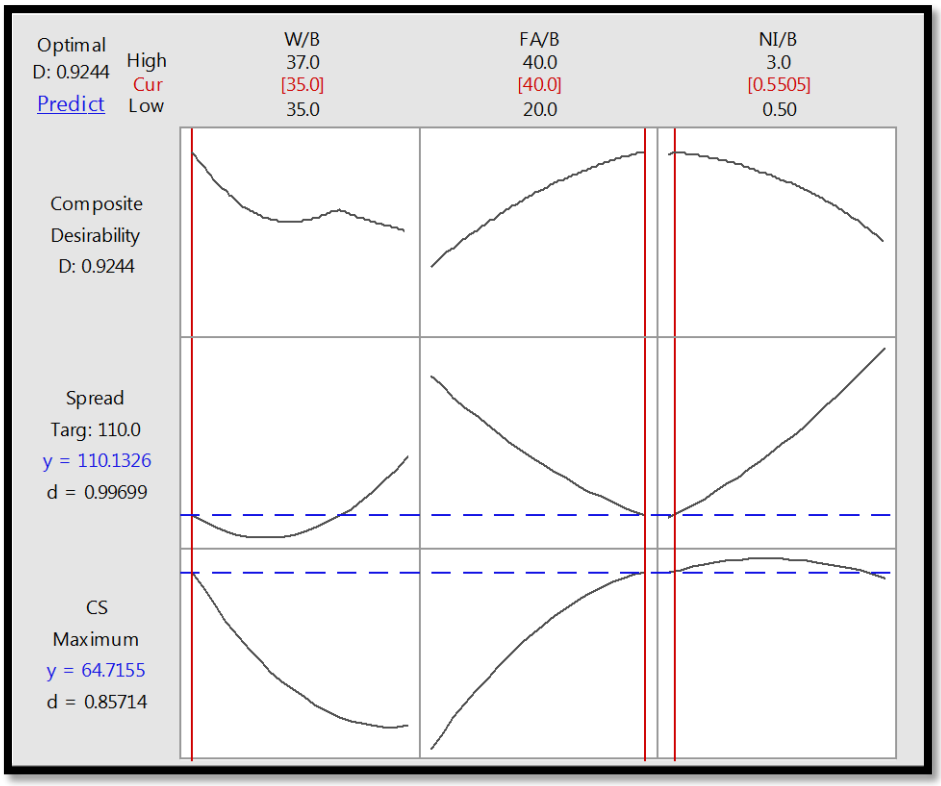

Figure 25. Response optimization plot for the RSM of (a) Type IP and (b) Type GU cements.

The response optimization of the Type GU cement (Figure 25b) resulted in two of the independent variables at their lowest and highest levels for the W/B and the FA/B, respectively; while for the NI/B the variable setting was very near its low level at 0.55%. This showed that the optimum variable settings when using this type of cement might not exist between the levels selected (Baş and Boyacı, 2007), and the optimum given by the response optimizer might not be the actual optimum. As shown in Figure 25b, the model optimization with the independent variable setting at 35 % W/B, 40% FA/B and 0.55% NI/B predicted at 28 day CS of 64.7 MPa and an SP of 110.1%. These results were attained at a global desirability at 0.924 and the specific desirability of 0.857 and 0.996 for the CS and SP, respectively.

Since the $CS_{Type\ GU}$ was described by a linear model (equation 11), a factorial design with center points was developed in order to investigate a broader range to find the optimum variable settings for the Type GU cement. The spread percentages of the fresh pastes for the new measured range were between the values of 67.5 to 111.5 % for the Type GU cement (Table 20). As for the compressive strength, the measured values were in the range of 29.4 to 49.0 MPa. These results showed that reducing the W/B and the NI/B, while increasing the FA/B negatively affected the workability and the strength of the specimens.

Table 20. Matrix of 2^3 factorial design and the measured dependent response variables.

Run	Independent variables			Dependent variables	
	Actual (% wt.)			Type GU cement	
	W/B	FA/B	NI/B	Spread (%)	28 day Compressive Strength (MPa)
1	33	40	0	82.3	45.4
2	35	40	0	102.8	40.2
3	33	50	0	67.5	31.6
4	35	50	0	89.3	29.4
5	33	40	0.5	106.5	45.1
6	35	40	0.5	111.5	49.0
7	33	50	0.5	98.3	35.8
8	35	50	0.5	103.8	30.3
9	34	45	0.25	93.0	37.5
10	34	45	0.25	88.0	33.4
11	34	45	0.25	96.5	41.3
12	34	45	0.25	85.5	39.2

The model response optimization for the factorial design predicted the independent variables settings at 35 % W/B, 40% FA/B and 0.50% NI/B (Table 21), which were the same for the CCD. The predicted value for the 28 day CS was 39.45 MPa, which was lower than for the CCD design, while the SP resulted in very similar results at 111.41%. As shown in

Table 22, all of the linear terms of the independent variables resulted to be significant for the prediction of the SP. On the contrary to the CCD, the interaction between FA/B and NI/B was not found to be relevant to the SP response. On the other hand, no significant effects by the independent variables were found to be statistically significant to the 28 day CS response (

Table **22**).

Table 21. Predicted values at the factorial design optimum settings.

Optimum variable settings			Spread (%)		28 day CS (MPa)	
W/B	FA/B	NI/B	Predicted	95% CI	Predicted	95% CI
35	40	0.5	111.41	100.29-122.53	39.45	23.26-55.65

Table 22. ANOVA and full regression models statistics of the factorial design.

Term	SP		28 day CS	
	p-value	coefficient	p-value	coefficient
Constant		-89.0		-
W/B	0.012	6.59	0.385	NS
FA/B	0.022	-1.106	0.400	NS
NI/B	0.003	39.12	0.179	NS
W/B*FA/B	0.892	NS	0.382	NS
W/B*NI/B	0.059	NS	0.532	NS
FA/B*NI/B	0.369	NS	0.587	NS
Lack-of-Fit	0.961		0.448	
R^2 (%)	95.5		64.8	

[a] NS: The contribution of the terms was not statistically significant

3.4.4. Contour plots for RSM at the optimum settings

Contour plots of the responses were drawn in a function of two independent variables while the third independent variable was held at its optimal value. Figure 26 shows the contour plots for the responses of SP and CS of the Type IP cement. As shown in Figure 26a, the dependent response SP was enhanced when the FA/B was reduced and the W/B was increased and NI/P was held at its optimal level of 1.6%. The CS (Figure 26b) followed a rising ridge pattern, where the increment or reduction of the reduction of the FA/B from the middle levels of the design and the increase of the W/B reduced the CS.

When the FA/B was held at the optimum of 28.5%, the simultaneous increase of NI/B and W/B increased the SP (Figure 26c). On the contrary, the increase of the W/B resulted in the decrease of the CS, whereas the increase of the NI/B did not play a significant role in the development of the CS (Figure 26d). However, the CS resulted in the greatest when both the NI/B and the W/B were at their lower levels.

The SP resulted to be the lowest when the FA/B was at the highest level and NI/B was at its lower level while the W/B was held at 35.1% (Figure 26e). On the other hand, the compressive strength decreased with the reduction/increase of the FA/B, while it was not affected by the NI/B when the W/B was held at its optimum of 35.1%.

Overall, a greater SP was found with a greater W/B or NI/B but with a lesser FA/B. The increase of NI/B would facilitate fluidity of the cement pastes attributed to the surfactants coated on the NI (Ouyang et al., 2008). As previously mentioned, the FA had a lower specific gravity than the Portland cement used in the study (Table 17). Therefore, more volume of FA was required to achieve the same weight to the Portland cement's, consuming more water in hydration resulting in a reduced SP. This effect was counteracted with an increase of the W/B and NI/B in the mixture.

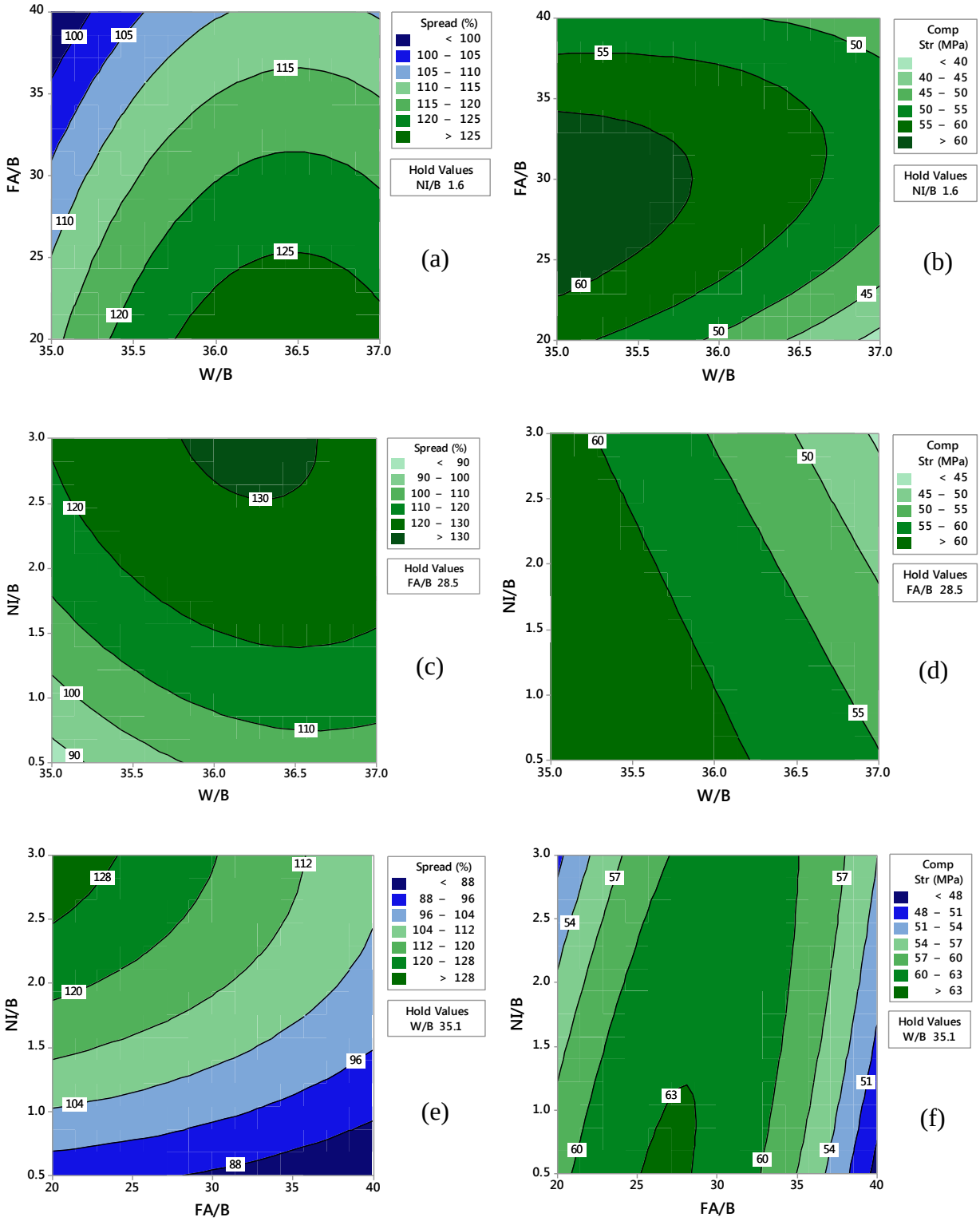

Figure 26. Contour plots of the SP and CS of the Type IP cement in a function of two independent variables while the third one was held at its optimum level.

Figure 27 shows the contour plots for the responses of spread percentage and compressive strength of the Type GU cement drawn from the CCD. As shown in Figure 27a, the dependent response SP was enhanced with the simultaneous increase or decrease of W/B from it's meddle setting and the reduction of the FA/B, when holding the NI/B at 0.55%. The CS (Figure 27b) was obtained to be the highest with the increment of FA/B and the reduction of W/B, while the lowest CS was obtained when increasing the W/B and decreasing the FA/B. This results showed that pozzolanic reactions of the FA/B already occurred at the 28 days of curing, improving the CS of the specimens. On the other hand, although the increment of W/B resulted in an enhancement of the workability of the fresh paste, the excess of water resulted in a decrease of the CS of the hardened cement pastes. These results are in agreement with Nematzadeh and Naghipour (2012), who reported that the water in concrete gradually evaporates with aging of the specimen, leaving pores in the concrete structure which results in a decrease of its mechanical properties.

When the FA/B was held at the optimum of 40.0%, the SP was enhanced with the increment of NI/B and the increase or reduction of the W/B from its meddle setting (Figure 27c). On the other hand, the increment in the NI/B did not play a significant role in the development CS of the cement pastes, whereas the increase of the W/B resulted in the decrease of the CS (Figure 27d).

Figure 27e shows that the increase of the NI/B resulted in an increase of the SP when the W/B was held at the optimum setting of 35%, whereas the increment of the FA/B counteract the effect by reducing the SP. Similarly to Figure 27d, in Figure 27f it is observed that the addition of NI/B did not affected the CS response, while the increase of the FA/B improved the CS, achieving the maximum at the higher level of the FA/B.

Overall, similarly to the pastes made with the Type IP cement, for the Type GU cement the greater SP was found with a greater W/B or NI/B but with a lesser FA/B. The increase of NI/B also facilitated the fluidity of the cement pastes due to the surfactants coated on the NI (Ouyang et al., 2008). This behavior has also counteracted with an increase of the FA/B in the mixture.

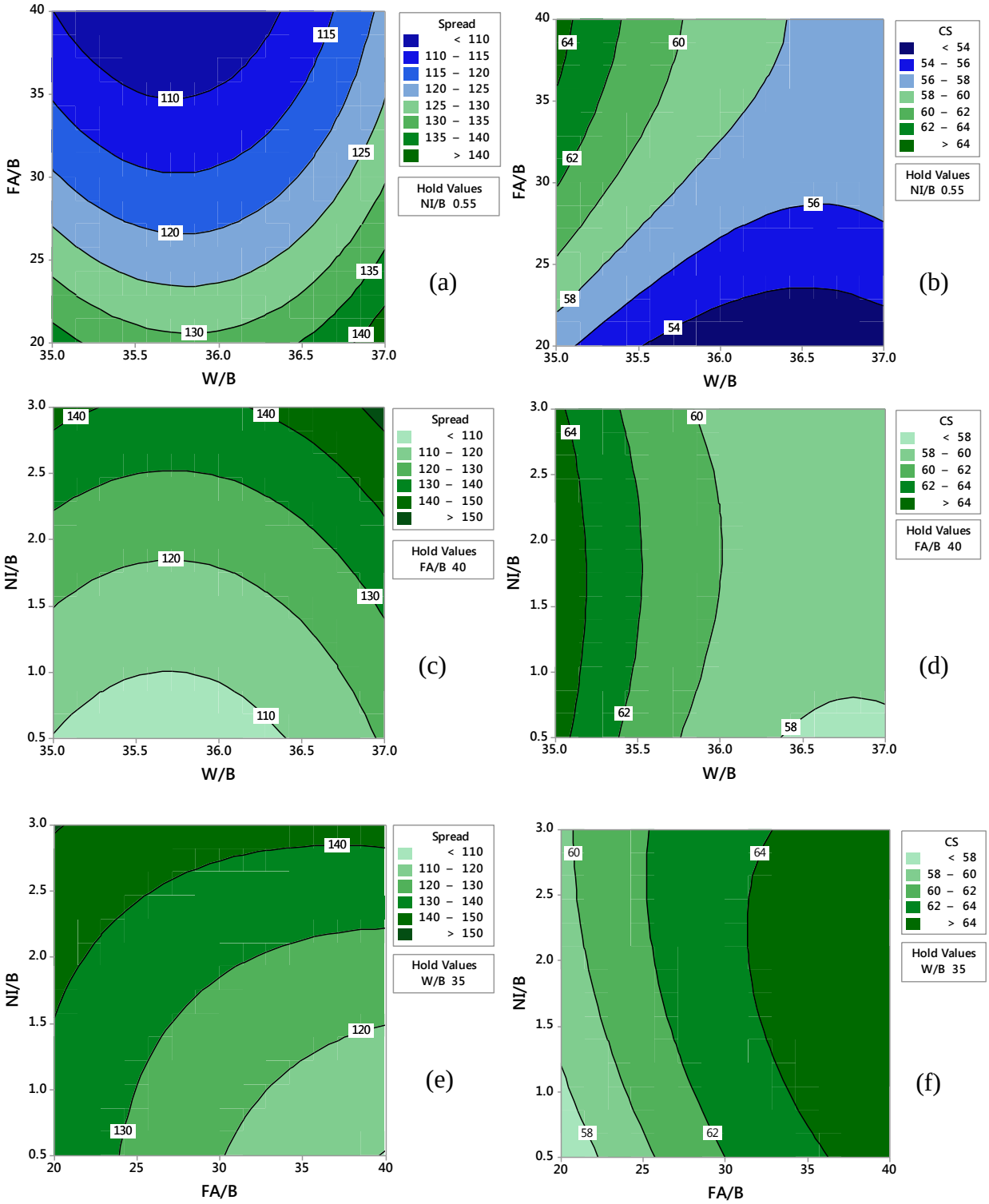

Figure 27. Contour plots of the SP and CS of the Type GU cement in a function of two independent variables while the third one was held at its optimum level.

3.4.5. Overlay contour plots for the RSM at optimum settings

The overlay plots of the responses in a function of two independent variables were plotted while the third independent variable was held at its optimum levels in order to find the regions where the hardened paste had the maximum possible CS while the SP of the fresh pastes was in the desirable range of 110±5%. In this regard, the desired SP was set at 105-115% and the maximum possible CS was set in the range of 55-60 MPa and 58-64MPa for the Type IP and GU cements, respectively (Figure 28 and 25).

As shown in Figure 28a, when the NI/B was held at its optimum level of 1.6%, the responses for the Type IP cement achieved the desired ranges at two different regions. The first region was when both the FA/B and the NI/B were at their lower levels, while the second region was wider and between the ranges of ~34-38 % and ~35-36% for the FA/B and the W/B, respectively. As for Figure 28b, the region that met the specification for the CS and SP was between 0.5-1.4% for the NI/B and 36-37% for the W/B when the FA/B was held at 28.5%. On the other hand, when the W/B was fixed at its optimum level of 35.1%, the desirable responses were also obtained at two different regions. A wider region at the upper right half of the design was predicted for the desired responses when NI/B ranged between 1.5-3% and the FA/B was between ~33-36%. On the contrary, the second region was found at the lower left half at the lower levels of the FA/B and ~1.1-1.6% for the NI/B (Figure 28c).

In contrast, Figure 29a, when the NI/B was held at its optimum level of 0.55%, the responses for the Type IP cement achieved the desired ranges when FA/B was higher than 30% while the W/B was lower than 36.5%. In the Figure 29b, the region that met the specification for the CS and SP was between 0.5-1.5% for the NI/B and ~35-36.5% for the W/B when the FA/B was held at 40.0%. On the other hand, when the W/B was fixed at its optimum level of 35.0%, the desirable responses were only obtained at a very narrow range, with the NI/B at its lower level of 0.5 and the W/B set at ~35.0% (Figure 29c).

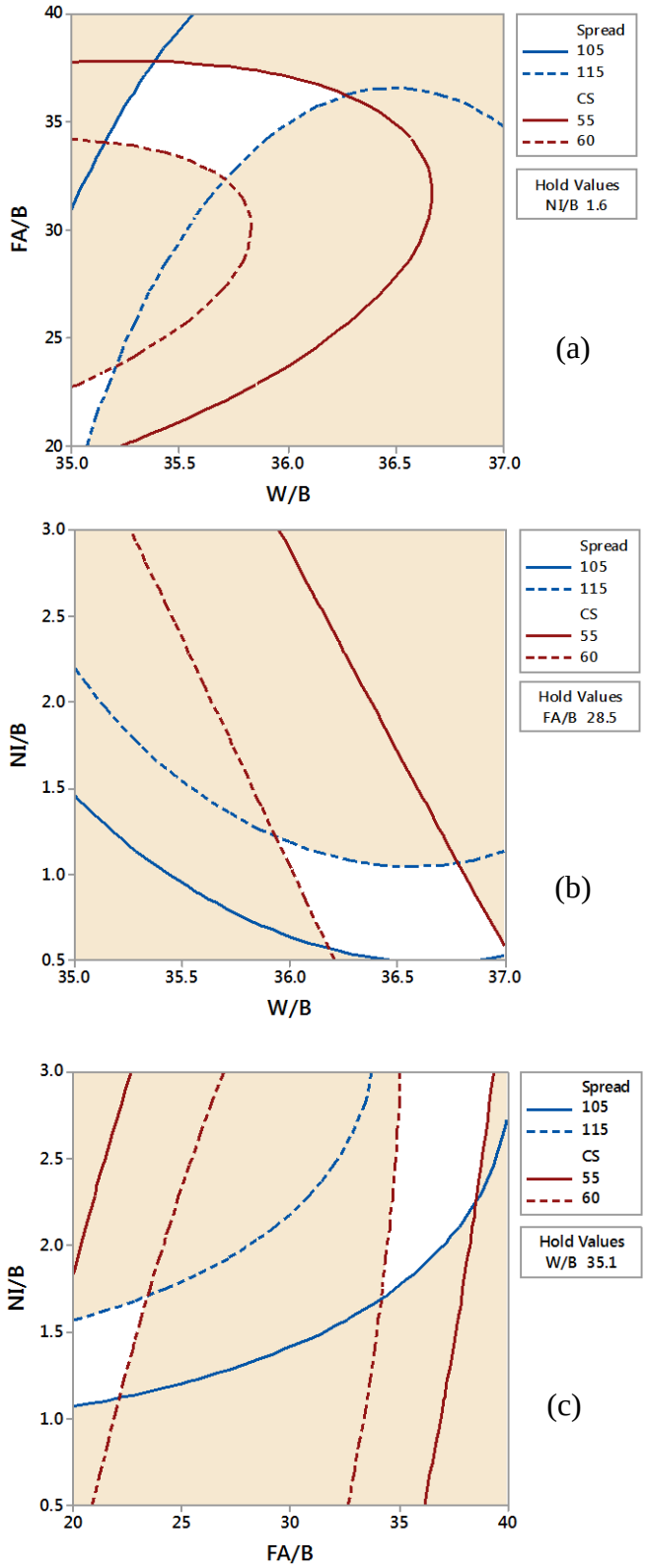

Figure 28. Overlay contour plots of the Type IP cement response variables in a function of two independent variables while the third one was held at its optimum level.

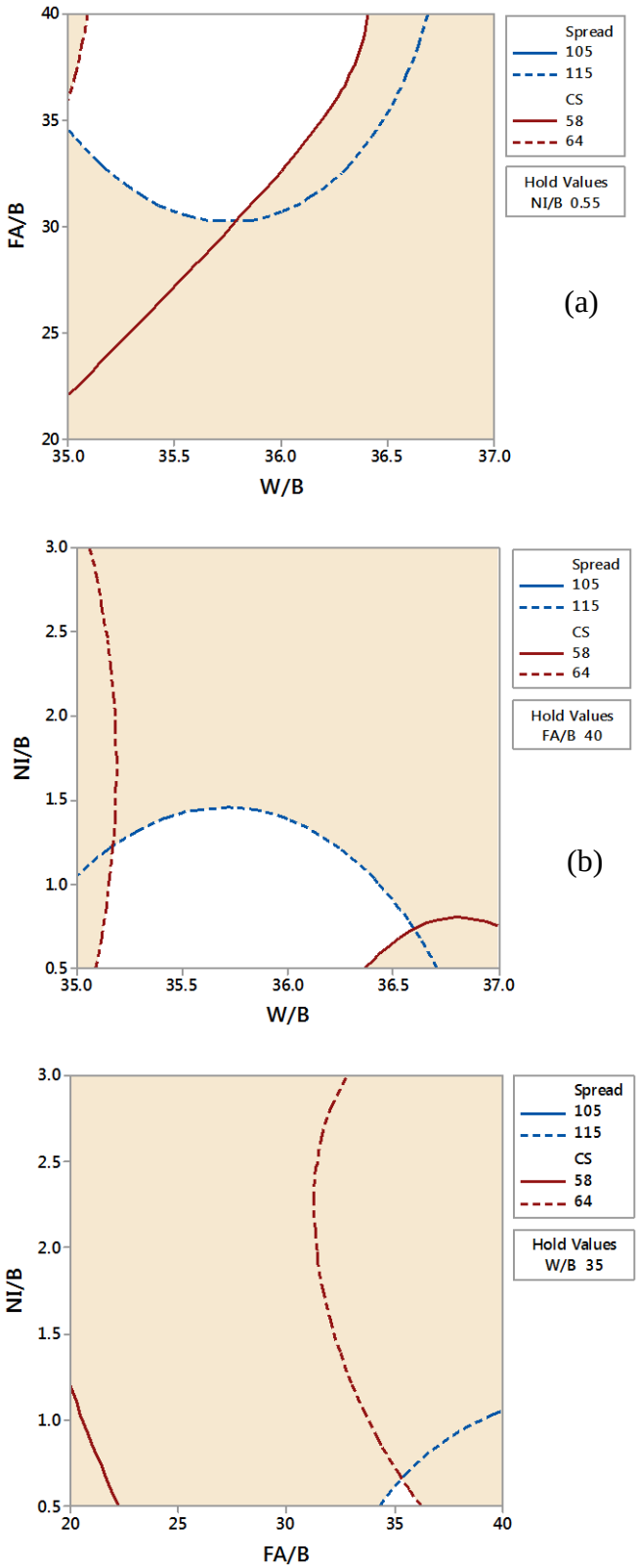

Figure 29. Overlay contour plots of the Type GU cement response variables in a function of two independent variables while the third one was held at its optimum level.

3.5.Conclusions

In this investigation, the mix ratio of two different cement types were optimized for a desired spread percentage and the maximum possible compressive strength of the hardened pastes cured for 28 days. The following conclusions can be drawn from the experimental results:

- The CS's were measured in the range of 27.9-64.3 MPa and 52.7-66.7 for the hardened pastes, while the SP's ranged in between 84.8-150% and 111.5 to 154% for the fresh paste of the Type IP and GU cements, respectively.
- The spread percentage of fresh pastes increased with the increase of NI/B or W/B but with the decrease of FA/B for both types of cements.
- The compressive strength of both the Type IP and GU cements decreased with the increment of W/B, while it was not affected by the addition of NI/B.
- The optimum variable settings for the Type IP cement were at 35.1 % W/B, 28.5% FA/B and 1.6% NI/B, which resulted in a predicted 28 day CS at 62.78 MPa while meeting the desirable SP at 109.24%.
- The optimum variable settings for the Type GU cement was achieved at a higher FA% addition at 40% and a lower NI/B addition at 0.55%, while similar W/B at 35.1%, resulting in slightly higher predictive strength at 64.72 MPa and a 110.13% of SP since Type GU cement did not contained any pozzolans and higher amounts could be added without compromising the strength of the specimen.
- Quadratic and interaction effects of the factors resulted playing a significant role in the development of the prediction models of the responses for both types of cements.

3.6. References

Baş D, Boyacı IH. Modeling and optimization I: Usability of response surface methodology. Journal of Food Engineering 2007; 78:836-845.

Cyr M, Trinh M, Husson B, Casaux-Ginestet G. Effect of cement type on metakaolin efficiency. Cement and Concrete Research 2014, 64:63-72.

Jiménez-Quero VG, León-Martínez FM, Montes-García P, Gaona-Tiburcio C, Chacón-Nava JG. Influence of sugar-cane bagasse ash and fly ash on rheological behavior of cement pastes and mortars. Construction and Building Materials 2013; 40:691-701.

Meng B, Wiens U, Schiessl P. Significance of the type of cement on the reaction mechanisms of pozzolans. American Concrete Institute 1998; 178:109-128.

Nematzadeh M, Naghipour M. Compressing fresh concrete technique and the effect of excess water content on physical–mechanical properties of compressed concrete. Materials & Design 2012; 37:256-267.

Montgomery D. Design and Analysis of Experiments. 8th Ed. John Wiley & Sons, Inc.; 2013.

Ouyang X, Guo Y, Qiu X. The feasibility of synthetic surfactant as an air entraining agent for the cement matrix. Construction and Building Materials 2008; 22:1774-9.

Popovics, S. Effects of the Fineness of Fly Ash on the Flow and Compressive Strength of Portland Cement Mortars. American Concrete Institute 1993; 141:205-226.

Sybertz F. Comparison of different methods for testing the pozzolanic activity of fly ashes. American Concrete Institute 1989; 114:477-497.

CHAPTER 4

The effect of aggregate grading on the properties of fly ash pervious concrete

4.1. Abstract

When making Portland cement pervious concrete (PCPC), the quality of the aggregates used is very important since it could affect the compressive strength and permeability of the specimens. In this regard, the effect of aggregate type and grading size on the manufacture of PCPC and its performance permeability were evaluated in order to select the best aggregate type and gradation that would produce the strongest PCPC with good hydrologic characteristics. The uniform gradation of the gray gravel resulted ideal for the making of pervious concrete with less man-hours being needed to prepare the aggregates. The abrasion resistance of both the gray and the reddish gravels resulted in very similar results, with average mass losses by 29.4 and 30.7%, respectively. The partial substitution of cement with FA didn't have a direct correlation to the permeability of the PCPC, although it significantly reduced the compressive strength at 7 days of curing. Partial clogging due to the drainage of the binder materials was obtained due to an excess in the W/B ratios and the reduction of FA/B in the PCPC. The reduction of the aggregate size caused a decrease in permeability but an increase in the compressive strength of the PCPC. Therefore, the gravels retained in the sieve with the opening size of 4.74 mm were better for the PCPC production.

4.2. Literature Review

4.2.1. Portland cement pervious concrete

Portland cement pervious concrete (PCPC) is made by eliminating or reducing the fine aggregates and incrementing coarse aggregates, resulting in greater void content and allowing the storm water to infiltrate into the ground, controlling storm water pollution, reducing storm water runoff and recharging groundwater (Deo and Neithalath, 2010). PCPC has been used in the construction of streets, low traffic roads, surface of parks and tennis courts, among others due to the wide environmental benefits that possess. Some other benefits of using PCPC are: enhance of vehicle traction, reduce of the tire-pavement noise, trap of the oil spilled by vehicles and reduce of the urban heat island effect (Metha and Monteiro, 2014). Other applications in which PCPC has been used are: bridge embankments, greenhouses, drains, beach structures and artificial reefs (ACI, 2010).

The construction of retention ponds, swales and lagoons for controlling storm water runoff as measures for controlling storm water runoff can be eliminated with the implementation of pervious pavements, representing a great economical advantage over conventional impervious pavements. Despite of all the benefits of using PCPC, there are some challenges that still present when making the mixture. Some examples are: requirement of special construction practices, extended curing times, aware of expansive soils, lack of standardized test methods and limited application to low traffic loads (Metha and Monteiro, 2014).

4.2.2. PCPC materials

The coarse aggregates that are commonly used for PCPC are either uni-size or graded aggregates ranging from 19 mm to 2.36 mm (ACI, 2010; Deo and Neithalath, 2010). Fine aggregates are limited when making pervious concrete since it reduces the porosity of the specimen, although in some cases they are added to increase the strength of the specimen (ACI, 2010). The quality of the aggregates used to make PCPC is very important since flaky and elongated particles should be avoided. Since the contact zone between the cement paste and the aggregates is the matrix's weakest point, a rough and porous aggregate is recommended to form a stronger bond between them (Ćosić et al., 2015). A flaky aggregate may cause the specimen to

break through the gravel and not through the paste, reducing the strength of the material. In addition, a clean aggregate surface is recommended by the ACI (2010) in order to improve the paste to aggregate bond and cement hydration.

The water content in PCPC ranges from 0.26 to 0.45 by mass in order to provide a good coating and paste stability (ACI 2010). Moreover, the aggregate absorption capacity must be considered when quantifying the water necessary to make the mixture since a dry aggregate will absorb water, resulting in a lower W/C ratio than what it was accounted for. This may cause to obtain a dryer mixture, thus reducing its workability for placing and compaction (ACI, 2010). Conversely, if the aggregate is wet and the humidity is not considered in the design, draining of the paste from the aggregates may occur due to the excess of water in the mixture.

Water reducing (WR) admixtures, also known as plasticizers or super-plasticizers, are commonly used to increase the fluidity of a mixture. If water is added to the mixture with the purpose of increasing its fluidity, the strength of the concrete will decrease due to the increment in porous that this will generate (Toledano-Prados et al., 2013). Since super-plasticizers are used to significantly reduce the W/C ratio and increase the flowability of a mixture, special concretes with high mechanical strengths and self-consolidating properties have been developed (Mardani-Aghbaglou et al., 2013). WR's can also control the settling time and increase impermeability and durability of cement paste (Ma et al., 2014).

There is a wide variety of WR, for which it is very important to determine the affinity of a certain WR with the cement and mineral admixtures, and the dosage that will be used for the fabrication of concrete in order to obtain a good performance of the final product (Mardani-Aghbaglou et al., 2013). Particle dispersion due to an electro-steric mechanism is known to be obtained from WR with base of naphthalene, melamine and lignosulfonate. On the other hand, polycarboxylate-based WRs are known to form a steric obstacle to any direct inter-particle contact; in other words, super-plasticizer molecules absorbed onto the cement particles creates negative charges that repulse each other, increasing the dispersion of cement by creating a space-steric effect (Ma et al., 2014; Toledano-Prados et al., 2013).

4.2.3. PCPC properties

When making PCPC, it is desired to obtain an optimum among the compressive strength, void content, workability and permeability of the material. Both hydrological and mechanical properties of PCPC have a strong dependence on its pore structure, which depends on its aggregate size, water-to-cement (W/C) ratio and method of compaction. The typical volume fraction of the pores formed using these aggregate sizes can range between 15 to 35% of the total volume (Deo and Neithalath, 2010), for which values of permeability in the range of 2.06 to 5.44 mm/s are obtained, depending on the compaction effort. Due to its high porosity, PCPC can only reach compressive strength of 2.8 to 28 MPa (ACI, 2010), limiting its uses to non-structural applications. Higher compressive strength can only be obtained with the incorporation of fine aggregates, mineral admixtures and water reducing agents in the PCPC (Lian and Zhuge, 2010). Studies have shown that mechanical strength increases as aggregate size is reduced, which also is directly related to a reduction in void fraction and permeability (ACI, 2010).

An increase in compressive strength implied a reduction in permeability due to a reduction in the pore structure of the specimen (Bhutta et al., 2012; Huang et al., 2010; Tho-in et al. 2012), although compressive strength is not always proportional to permeability. As mentioned before, another factor affecting PCPC properties is the selection of the proper W/C ratio. Lian and Zhuge (2010) tested five different W/C ratios and found that as the W/C ratio increased, the compressive strength was reduced and also found that permeability increased as the W/C ratio increased. This phenomenon may not always be true because an excess of water in the mixture can cause the binders to drain out of the aggregates, clogging the bottom of the specimen and thereby causing a reduction in its permeability.

4.3. Materials and Experimental Methodology

4.3.1. Materials

Portland cement (PC) Type IP in compliance with ASTM C595 was used and fly ash (FA) was obtained from a local coal-fueled power plant (AES Puerto Rico). Two different limestone gravels in sizes of 4.75-12.5 mm were used as a coarse aggregate. The main difference between the gravels was their carbonate and iron oxide contents. The grey gravels had a higher amount of carbonates, while the ones that had a reddish color was due to high amounts of iron oxides.

4.3.2. Specimen design and preparation

No specific standard procedure is available for the making of PCPC's. For this reason, the standard practice for making and curing concrete test specimens in the laboratory (ASTM C192) was followed for the making of the PCPC specimens. The mixtures were prepared in a mechanical mixer and then cast into cylindrical molds of 20.32 cm in length and 10.16 cm in diameter. Compaction of the specimens was made using the standard rodding consolidation method in accordance to ASTM C192. After 24 hours, specimens were demolded and cured for 28 days in lime-saturated tap water at ambient temperature (24±2 ^{o}C).

The independent variables tested in this experiment were the gravel size and type, and the fly ash-to-binder (FA/B) ratios of 0, 20 and 40%. In this study, the binding material was defined as the total of the powder materials (i.e., cement + FA), and its mass ratio to coarse aggregates was fixed at 1:4. The W/B ratio was fixed to 40% based on the results of the OFAT study on Chapter 1 and considering the addition of coarse aggregates to the mixture.

4.3.3. Aggregate characterization

The aggregate grading, absorption capacity and abrasion resistance were tested for both gravel types. The determination of the average particle size distribution of the bags for each gravel type was done following the standard test method for sieve analysis of coarse aggregates (ASTM C136). The gravel retained in the sieves with a square opening size of 25, 19, 12.5, 9.5, 4.75, 2.36 and 0 mm was quantified and the cumulative weight was calculated.

The absorption capacity of both gravels was calculated following the ASTM C127. Since the gravels had a nominal maximum size of 12.5 mm, a total of 2,000 g were used to calculate the

absorption capacity. The aggregates were dried in an oven at a temperature of 110±5℃ for 24 hours. After 24 hour in the oven, the aggregates were taken out and cooled at room temperature until they were comfortable to handle and the weight was measured and reported as the oven-dry weight (W_{OD}). The sample was then put in the water and removed after 24 hours. The saturated-surface-dry weight (W_{SD}) was calculated after drying the surface of each aggregate individually until all the visible films of water were removed. Equation (11) was used to calculate the absorption (A) percentage of each gravel:

$$A = \left(\frac{W_{SD} - W_{OD}}{W_{OD}}\right) \times 100$$

The Los Angeles abrasion machine was used to evaluate abrasion resistance of pervious concrete in accordance to the ASTM C131, which is specific for gravels with sizes smaller than 37.5 mm. The gravel used for the testing was washed and oven dry at 100±5 ℃ for 24 hours. Then the gravels were sieve to collect 2,500 g of the aggregates retained in each of the sieves with a square opening size of 6.3 and 4.75 mm. A total of 8 spheres were used as specified by the ASTM C131. A total of 500 revolutions at a speed of 30 r/min were completed for the testing. The material coarser than 1.70 mm was collected, washed and oven dry to quantify the mass loss by abrasion with equation (12):

$$W_{loss}\ (\%) = \left(\frac{W_i - W_f}{W_i}\right) \times 100 \qquad (12)$$

Where W_{loss} is the weight lost by abrasion, W_i is the initial weigh of the sample (5,000 g) and W_f is the weight of the gravel retained in the sieve with an opening of 1.70 mm after the abrasion test.

4.3.4. Permeability and Compressive Strength of the PCPC

In accordance to ASTM C39, compressive strength was tested for the PCPC specimens in triplicate after they were cured for 7 days in $Ca(OH)_2$-saturated tap water. Capping rubber pads (Gilson HM-362) were placed during the compressive strength test on the top and bottom sides of the specimens to provide a uniform load distribution by a 3000 kN Forney universal testing machine.

The permeability of the specimens in triplicate was measured by quantifying the flow of water passing through the PCPC, under a constant head difference. ASTM D2434 was modified to accommodate the experiment with PCPC specimens. Darcy's law was used to calculate the permeability coefficient, as is shown in equation (13):

$$k = \frac{V \cdot L}{A \cdot h \cdot t} \tag{13}$$

Where k is the permeability coefficient (mm/hr), V is the collected volume of water (mm^3), L is the length of the PCPC specimen (mm), A is the area of the specimen (mm^2), h is the head difference (mm) and t is the time required to get the collected volume of water (hr). Figure 30 shows the experimental set-up that will be used in the laboratory to measure the permeability.

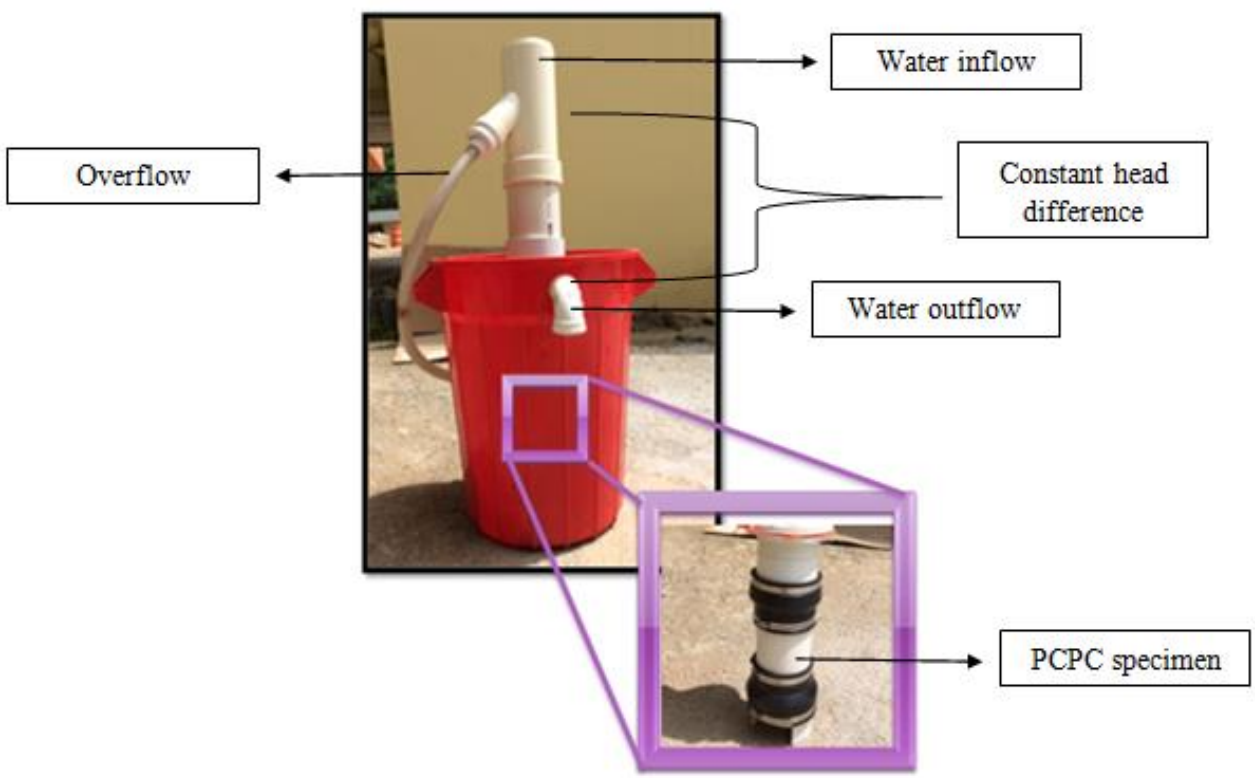

Figure 30. Schematic representation of the permeability test experiment.

4.4. Results and Discussion

4.4.1. Aggregate characterization

The average of three gravel bags was used to calculate the mass retained in each sieve. As shown in

Table 23, 93% of the total mass of the grey gravel was retained in the sieves with a square opening size of 9.5 and 4.75mm. In Figure 31 it can be observed that the grey gravel curve is very steep, which means that the bag has a uniform gradation since most of the particles are in a very narrow size range.

On the other hand, the reddish gravel had more distributed gradation (Figure 31), although a 43% of the gravel was retained in the sieve with a square opening of 12.5mm, and only 37.2% of the total mass was retained in the sieves of 9.5 and 4.75 mm. In this regard, higher man-hours were needed to collect the sufficient amount of reddish gravel to make the PCPC specimens.

Table 23. Cumulative weight percentages of the coarse aggregates.

Sieve Size (mm)	Grey gravel		Reddish gravel	
	Mean weight per sieve (%)	Cumulative weight (%)	Mean weight per sieve (%)	Cumulative weight (%)
25	0.0	0.0	0.4	0.4
19	0.0	0.0	12.5	12.9
12.5	3.9	3.9	43.0	55.9
9.5	42.2	46.1	22.6	78.6
4.75	51.0	97.1	14.6	93.2
2.36	0.9	98.0	4.3	97.6
0	2.0	100.0	2.4	100.0

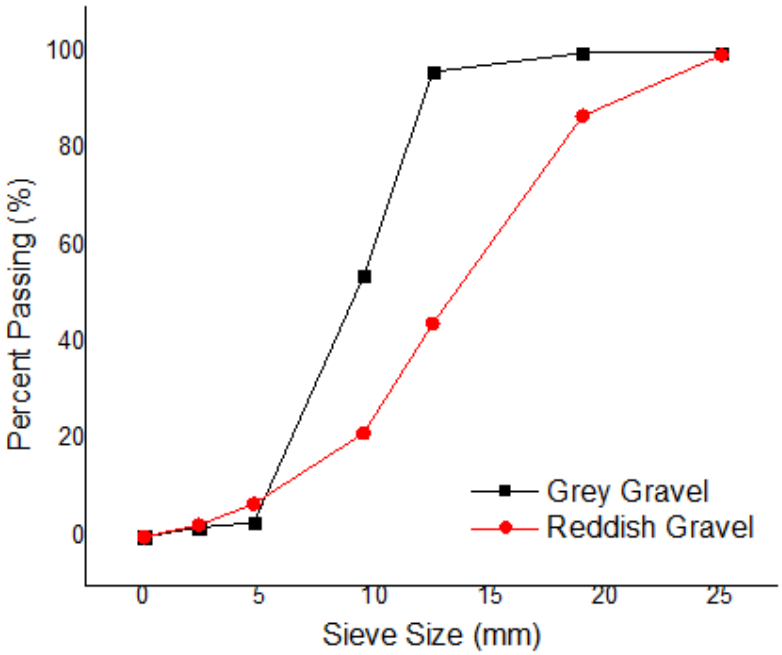

Figure 31. Aggregate gradation for each gravel type.

The water absorption capacity of each aggregate was 0.7 and 2% for the grey and reddish gravel, respectively. Reported values for the absorption capacity of limestone gravels when immersed in water for 24 hour ranged between 0.48-1.62% (Huang et al., 2010; Alhozaimy, 2009).

Los Angeles testing machine (Figure 32) was used to perform the resistance to degradation of both gravel types. The abrasion resistance for the grey gravel was slightly higher than for the reddish gravel, with values of 29.4 and 30.7 for the loss by abrasion after 500 revolutions, respectively. These results were in good agreement with Ugur et al. (2010), who obtained abrasion results for different limestone gravels in the range of 23.5 to 34.3 after 500 revolutions.

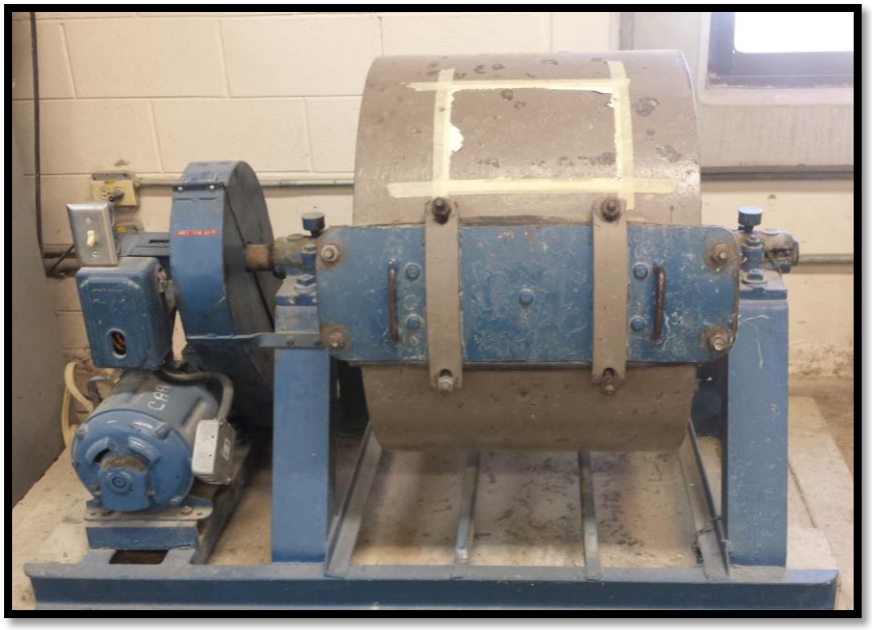

Figure 32. Los Angeles abrasion and impact testing machine.

4.4.2. Permeability and compressive strength of the PCPC

The permeability of both types of gravels were very similar, although the reddish gravel obtained slightly higher permeability rates, values ranging between 4.5-13.9 mm/s and 7.8-15.1 mm/s for the grey and reddish gravel, respectively (Table 24). As shown in Figure 33, no consistent influence was found between the partial substitution of cement with FA and the permeability of the specimens. Although some of the PCPC specimens with no FA addition resulted in lower permeability rates due to drain of the paste and partially clogging the bottom of the specimen. Thoin et al. (2012) reported a reduction in permeability of fly ash geopolymer concrete with the increment of the liquid in the mixtures due to void filling.

In Chapter 1 it was mentioned that the addition of FA to the mixture reduced its fluidity due to greater amount of binder volume and to the high LOI value for the FA, which increases the requirement for water on the mixtures (Jimenez-Quero et al., 2013). This behavior was clearly observed in the PCPC specimens, and as a result the specimen containing 40% FA and the 4.75 mm grey gravel was not possible to cast in the mold. The binders were not completely hydrated, resulting in a dry mixture with no cementitious capacity.

Table 24. Values for the 7 day compressive strength and permeability of the PCPC specimens.

Gravel Type	Gravel size (mm)	F.A. (%)	Average Compressive Strength (MPa)	Average Permeability (mm/s)
Grey	9.5	0	8.3	7.6
		20	7.0	11.6
		40	4.1	13.9
	4.75	0	10.0	4.5
		20	8.1	12.2
		40	-[a]	-[a]
Reddish	9.5	0	7.2	11.2
		20	6.8	15.1
		40	4.6	12.9
	4.75	0	10.5	8.5
		20	6.9	7.8
		40	5.3	9.4

[a]The binding material was very dry and the mixture was not able to be cast into the molds.

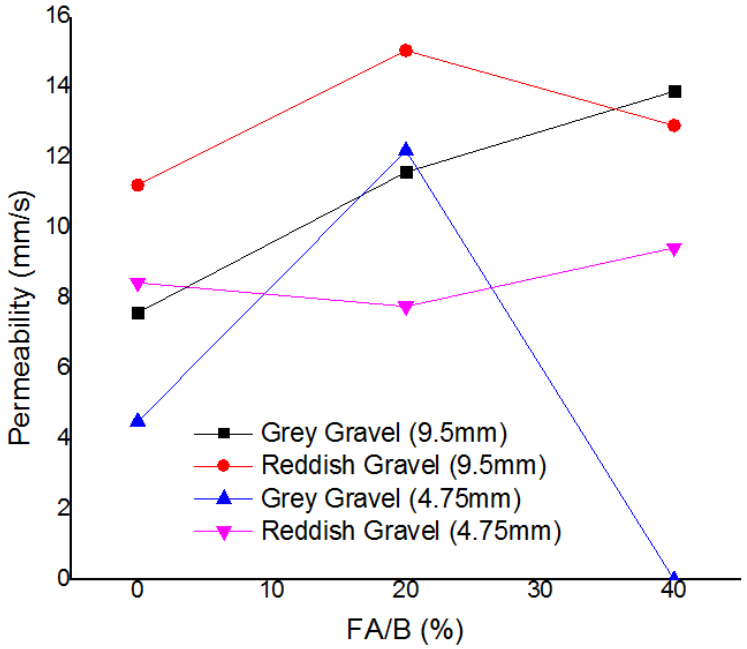

Figure 33. Effect of FA substitution on the permeability of the PCPC specimens.

The reduction in gravel size resulted in a decrease in the permeability for most of the PCPC specimens (Figure 33). These results were in agreement with Sumanasooriya and Neiththalath (2011), who reported that a decrease in aggregate size resulted in a reduction of pore size, and consequently obtaining lower permeability rates on the PCPC specimens. However, some researchers have not found a direct influence on the permeability of PCPC due to different aggregate gradation (Huang et al., 2010).

The 7 day compressive strength was not affected by the gravel type, and values ranged between 4.1-10.0 MPa and 4.6-10.5 MPa for the grey and reddish gravels, respectively (Table 24). On the contrary, smaller particle size slightly increased the 7 day compressive strength of the PCPC specimens, as shown in Figure 34. These results were in agreement with Crouch et al. (2007), who reported that smaller aggregate sizes produced a higher compressive strength than larger aggregates. An increase in compressive strength also implied a reduction in permeability due to a reduction in the pore structure of the specimen (Bhutta et al., 2012).

The greatest effect on the compressive strength was made by the partial substitution of the cement with FA. In Figure 34 it is observed how the compressive strength decreases dramatically with the increment of the FA/B. This behavior was resulted from the slow pozzolanic reaction of FA occurring at late ages (Donatello et al., 2013). Consequently low compressive strengths were obtained at the early stage of the reaction.

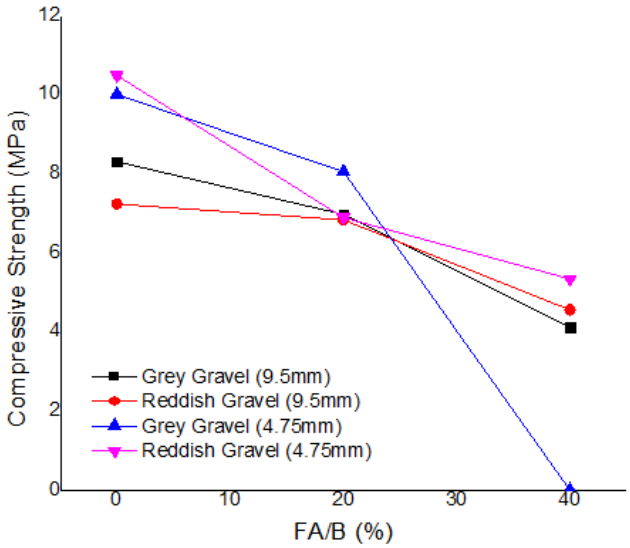

Figure 34. Effect of FA substitution on the compressive strength of the PCPC specimens.

4.5. Conclusions

The effect of aggregate type and grading size on the manufacture of PCPC and performance in terms of compressive strength and permeability were evaluated and the following conclusions were drawn from the experiments:

- A gravel with a uniform gradation was ideal for the making of pervious concrete since the particle sizes were in a very narrow range and also resulted in a less packing of the aggregates and consequently better permeability due to more interconnected voids in the specimens.
- The abrasion resistance of both gravel types resulted in very similar results, with average values at 29.4 and 30.7 % for the mass loss of the grey and reddish gravel, respectively.
- No consistence relationship was found between the partial substitution of cement with FA and the reduction or increase of the permeability of the PCPC.
- Partial clogging due to the drainage of the binder materials was obtained due to an excess in the W/B ratios and the reduction of FA/B in the PCPC, while the lack of water and the excess of FA resulted in a very dry mixture and consequently an incomplete hydration of the binder materials was achieved.
- The reduction of the aggregate size resulted in a decrease in permeability but an increase in the compressive strength of the PCPC.

4.6. References

ACI, American Concrete Institute Committee 522. *Report on Pervious Concrete*. 1st Ed., ACI 522R-10. American Concrete Institute, Michigan; 2010.

Alhozaimy AM. Effect of absorption of limestone aggregates on strength and slump loss of concrete. Cement and Concrete Composites 2009; 31(7):470-473.

Bhutta M AR, Tsuruta K, Mirza J. Evaluation of high-performance porous concrete properties. Construction and Building Materials 2012; 31:67-73.

Ćosić K, Korat L, Ducman V, Netinger I. Influence of aggregate type and size on properties of pervious concrete. Construction and Building Materials 2015; 78:69-76.

Crouch LK, Pitt J, Hewitt R. Aggregate effects on pervious Portland cement concrete static modulus of elasticity. Journal of Materials in Civil Engineering 2007; 19(7):561-567.

Deo O, Neithalath N. Compressive behavior of pervious concretes and a quantification of the influence of random pore structure. Materials and Science and Engineering A 2010; 528:402-412.

Donatello S, Palomo A, Fernández-Jiménez A. Durability of very high volume fly ash cement pastes and mortars in aggressive solutions. Cement and Concrete Composites. 2013; 38:12-20.

Huang B, Wu H, Shu X, Burdette EG. Laboratory evaluation of permeability and strength of polymer-modified pervious concrete. Construction and Building Materials 2010; 24:818-823.

Jiménez-Quero VG, León-Martínez FM, Montes-García P, Gaona-Tiburcio C, Chacón-Nava JG. Influence of sugar-cane bagasse ash and fly ash on rheological behavior of cement pastes and mortars. Construction and Building Materials 2013; 40:691-701.

Liann C, Zhuge Y. Optimum mix design of enhanced permeable concrete - An experimental investigation. Construction and Building Materials 2010; 24:2664-2671.

Ma B, Ma M, Shen X, Li X, Wu X. Compatibility between a polycarboxylate super-plasticizer and the belite-rich sulfoaluminate cement: Settling time and the hydration properties. Construction and Building Materials 2014; 51-47-54.

Mardani-Aghbaglou A, Tuyan M, Yilmaz G, Arioz O, Ramyar K. Effect of different types of super-plasticizer on fresh, rheological and strength properties of self-consolidating concrete. Construction and Building Materials 2013; 47:1020-1025.

Metha P, Monteiro P. *Concrete microstructure, properties and materials*. 4th Ed. McGraw-Hill Education; 2014.

Sumanasooriya MS, Neiththalath N. Pore structure features of pervious concretes proportioned for desired porosities and their performance prediction. Cement and Concrete Composites 2011; 33(8):778-787.

Tho-in T, Sata V, Chindaprasirt P, Jaturapitakkaul C. Pervious high-calcium fly ash geopolymer concrete. Construction and Building Materials 2012; 30:366-371.

Toledano-Prados M, Lorenzo-Pesqueira M, González-Fonteboa B, Seara-Paz S. Effect of polycarboxylate super-plasticizers on large amounts of fly ash cements. Construction and Building Materials 2013; 48:628-635.

Ugur I, Demirdag S, Yavuz H. Effect of rock properties on the Los Angeles abrasion and impact test characteristics of the aggregates. Materials Characterization 2010; 61(1):90-96.

CHAPTER 5

Green pervious concrete optimization by RSM for the removal of nutrients and fecal coliforms from water

5.1. Abstract

A green pervious concrete surface (GPCS) capable of removing contaminants from water was developed in a four factor, two level central composite design to investigate the main, quadratic and interaction effects of the independent variables on the permeability and compressive strength. The independent variables were percentage of water-to-binder (W/B), fly ash-to-binder (FA/B) iron-oxide nanoparticles-to-binder (NI/B) and water reducer-to-binder (WR/B). Two optimum mix ratios at 36% W/B, 35% FA/B, 6% NI/B and 1.2 % WR/B for Opt A and 32% W/B, 10% FA/B, 0.5% NI/B and 0.8% WR/B for Opt B were found to achieved the maximum possible compressive strength while maintaining the permeability between the range 2 to 12.2 mm/s. Opt A and Opt B resulted in an average measured compressive strength and permeability in the ranges of 17.8 and 19.2 MPa and 10.0 and 11.9 mm/, respectively. The increment of W/B and the reduction of FA/B independently of the settings of NI/B and WR/B resulted in a decrease of the permeability. The addition of high amounts of FA/B required a large addition NI/B in order to achieve a compressive strength higher than 20.7 MPa, while lower additions of NI/B were found to required less amount of NI/B. Phosphorus and FC removals were achieved at a high pH, with average values for FC inactivation of 74.2%, 67.9% 95.4% at 2 hour contact time, and for phosphorus removal of 84.6 and 100% for Opt A, Opt B and Control, respectively. The increase of contact time improved the nitrate reduction, achieving removals up to up to 79.0, 48.8 and 54.3 % by the Opt A, Opt B and Control, respectively.

5.2. Literature Review

5.2.1. Storm-water Runoff

The water quality of surface waters near urban areas has deteriorated as a result of the increase of impervious surfaces and the abundant sources of contamination such as urban runoff, storm sewers and land disposal of waste. As for the Environmental Protection Agency, stormwater runoff is defined as the water generated by rain precipitation or melting snow that doesn't percolate through impervious surfaces and accumulates debris, sediments, chemical compounds and other pollutants, affecting the water quality of waters where runoff is discharged (EPA, 2012).

The quantity and type of contaminants found in runoff greatly depended on the land use, rainfall intensity, and previous dry days, among others. Preventive practices such as covering storage areas, diverting runoff from pollutant sources and recycling programs have been established in order to minimize the pollutants entering to the runoff (Kim et al., 2005). Some of the contaminants associated with urban development are sediments, heavy metals, nutrients and bacteria (Schoonover and Lockaby, 2006). Other researchers have also reported concentrations of suspended solids, phosphorous, nitrogen, copper lead and zinc in asphalt driveways runoff (Gilbert and Clausen, 2006). Data collected by the Nationwide Urban Runoff Program have also revealed that pollutants such as organic nutrients, pesticides, herbicides and heavy metals were present in runoff near urban areas (Kim et al., 2005). Toxic metals can be accumulated in food crops due to irrigation with contaminated water. If food is ingested, human heath can be disturbed, causing liver, kidney, cardiovascular, nervous and bone disorders (Mahmood and Malik, 2013).

These contaminants represent a great danger to the human and environmental health. For example, even though nutrients such as nitrogen (N) and phosphorous (P) are necessary for plant growth, high concentrations of these nutrients into water greatly induce eutrophication. The eutrophication causes water quality to degrade due to change in color and smell, and reduction in the amount of dissolved oxygen, thus causing fish death (Wang and Wang, 2009; Luck et al., 2009).

The maximum allowable concentration of N in water is 10mg/L (EPA, 2014). High concentrations of nitrate in drinking water cause health problems such as methemoglobinemia in infants and stomach issues in adults (Ensie and Samad, 2014). On the other hand, the maximum allowable concentration for P in water is in the range of 0.05 to 0.10 mg/L (EPA, 2014). Municipal

waste waters have been found to contain large concentrations of P (Litter et al., 2013). Several studies have been made to test materials for P uptake from water. Some material that have been tested are slags (Xue et al., 2009), fly ashes (Ragheb, 2013) and hydrated ferric oxide sludge (Litter et al., 2013).

5.2.2. Fecal Coliforms

Pathogenic micro-organism contamination of surface water from livestock slurries and manure, runoff from pastures, animal confinement facilities and animal feedlots is a serious environmental problem due to the possible human exposure to these micro-organisms through drinking and bathing waters (Ramos et al., 2006; Luck et al., 2009). Possible fecal contamination can be identified due to excessive bacterial growth in stream environment. The presence of FC also indicates the possibility of the presence of other harmful contaminants and organisms (Luck et al., 2009). The EPA considers that a concentration of FC above 2,000 mg/L is considered to be of concern for the human health (EPA, 2014). High concentrations of FC in runoff waters have been found during the first phases of rainfall events. Ramos et al. (2006) found that the rate of transport was very high during the first 15 minutes of the event and it decreased significantly afterwards. They also found that there was a linear relationship between the transport of FC and organic sediment.

The use of porous media for removing pathogenic bacteria has been widely employed since they have shown very effective at reducing bacteria in water through adsorption. The removal is controlled by physical factors such as grain size and specific surface area, hydraulic loading and residence time (Tawfik et al., 2006). The process is usually accompanied by another disinfection process, for example, chlorination. Metallic oxides/hydroxides are also known to be very efficient for bacteria and virus removal due to its good adsorption characteristics and are commonly used as sand coating for biosand filters (Ahammed and Davra, 2011).

5.3. Materials and Experimental Methodology

5.3.1. Materials

Portland cement (PC) Type IP in compliance with ASTM C595 was used and fly ash (FA) was obtained from a local coal-fueled power plant (AES Puerto Rico). Limestone gravel in the range size of 4.75-9.5 mm was used as a coarse aggregate. The NI solution was purchased from the Ferrotec (Bedford, NH). The BASF Glenium 3030 NS water-reducing admixture was supplied by a local company in Puerto Rico. Its chemical and physical characteristics are unknown. Treated final effluent prior to disinfection was collected from Mayagüez Waste Water Treatment Plant and was used as the target water containing FC. A commercial fertilizer (15-50-5) was used to increase the concentration of phosphate and nitrate ions in the target water for the nutrient removal experiment.

5.3.2. Specimen design and preparation

The preparation of the GPCS specimens was designed in a four factor, two level (2^4) central composite design (CCD). To measure the responses of permeability and the compressive strength after 28 days of curing, a total of 20 experiments in triplicate were run, with 6 replicates at the center points. The four factors used were the water-to-binder (W/B), fly ash-to-binder (FA/B), NI-to-binder (NI/B) and water reducer-to-binder (WR/B) ratios. In this study, the binding material is defined as the total of the powder materials (i.e., cement + FA), and its mass ratio to coarse aggregates was fixed at 1:4. The ratios used at the center and axial points and the low and high levels for each of the factors are listed in Table 25.

Table 25. Low and high levels of the 2^4 central composite design RSM.

Factors	**Levels**				
	Axial	**Low**	**Center**	**High**	**Axial**
W/B	30	32	34	36	38
FA/B	0	10	20	30	40
NI/B	0	1.7	3.4	5.1	6.8
WR/B	0	0.4	0.8	1.2	1.6

The mixtures were prepared in a mechanical mixer in accordance to the ASTM C192 and then cast into cylindrical molds of 20.32 cm in length and 10.16 cm in diameter. Compaction of the specimens was made using the standard rodding consolidation method in accordance to ASTM C192. After 24 hours, specimens were demolded and cured for 28 days in lime-saturated tap water at ambient temperature (24±2 ^{o}C).

5.3.3. Compressive strength and permeability tests

In accordance to ASTM C39, compressive strength was tested for the GPCS specimens after they were cured for 28 days in $Ca(OH)_2$-saturated tap water. Capping rubber pads (Gilson HM-362) were placed during the compressive strength test on the top and bottom sides of the specimens to provide a uniform load distribution by a 3000 kN Forney universal testing machine.

The permeability of the specimens was measured by quantifying the flow of water passing through the GPCS, under a constant head difference as specified in Chapter 4. ASTM D2434 was modified to accommodate the experiment with GPCS specimens.

5.3.4. Fecal coliform and nutrient removal analysis

Fed-batch experiments were conducted in triplicate for FC removal with the optimum GPCS specimens selected from the CCD analysis. The fed-batch systems were replenished with 400 mL of fresh FC-containing target water (1 load) for a total of 21 loads. The first 10 loads of the fed-batch systems had a contact time of 2 hrs, followed by 8 loads with a contact time of 4 hrs, and the last 3 loads had a 24 hrs contact time. Treated water was decanted for FC, pH, phosphorus as PO_4^{3-} (P) and nitrogen as NO_3^- (N) analysis. The target water was also analyzed for the same water quality parameters prior to treatment with the GPCS specimens.

An Orion pH meter was used to record the pH to the nearest 0.05 of the aqueous samples. Fecal coliform analysis was done by a membrane filtration technique with a 0.45-μm cellulose ester membrane. The filtered membrane was placed into Petri dishes containing the HACH m-FC broth and incubated for 24 hours at 44.5℃. Blue colonies were counted as FC colonies that were expressed as colony-forming units (CFU) per 100 mL of sample.

A Shimadzu Prominence IC system (Kyoto, Japan) (Figure 35) was used for the nutrient analysis. It consisted of an LC-20AD quaternary pump, a CDD-10AVP conductivity detector, a

SIL-20A autosampler, a CTO-20AC column oven, and a DGU-20A3R degasser. LabSolutions Lite Single LC-PDA software was used for system control and data processing. Phosphorus and nitrate were detected by suppressed conductivity with a SAMS anion suppressor and a CARS continuous anion regeneration system. Chromatographic separation was attained at 45 ℃ with a Shodex SI-52 4E anion column (4.0 mm i.d.×250 mm) (Showa Denko, Tokyo, Japan). The mobile phase had 3.6 mM sodium carbonate and was passing through the column at a flow rate of 0.9 mL/min. The sample injection volume was 20 µL.

Figure 35. Shimadzu Prominence IC system.

5.4. Results and Discussion

5.4.1. Responses of the RSM

For the testing of the compressive strength and permeability responses, specimens were made in triplicate for each of the variable settings and the averaged results were studied. The measured compressive strengths were in the ranges of 6.0 to 24.3 MPa while the permeability ranged between 0.0 and 12.2 mm/s (Table 26).

The suitability of the model was corroborated by the inspection of residual analysis and the lack-of-fit-test at a significance level of 5%. Residual plots confirmed that the results were independent, followed a normal distribution and had equal variances. The lack-of-fit-test for each of the responses resulted in high p-values, indicating that the model was suitable. These results were confirmed with the regression coefficients of the models (R^2), which were 87.49% and 86.44% for permeability and the 28 day compressive strength, respectively.

5.4.2. Statistical models for the RSM

The main, quadratic and interactive effects of the independent variables on the dependent variables were considered as statistically relevant at p-values < 0.05 (Table 27). The estimated regression models after removing non-relevant terms for the permeability and compressive strength responses are given by the Equations 14 and 15, respectively.

$$P = 40.75 - 0.926W/B + 0.0831FA/B - 4.843\mathrm{WR/B} \tag{14}$$

$$\begin{aligned} CS_{28d} = 44.3 &- 0.70W/B - 3.37FA/B - 12.33NI/B + 73.1WR/B - 6.88WR/B^2 \\ &+ 0.0816W/B * FA/B + 0.382W/B * NI/B - 2.054W/B * WR/B \\ &+ 0.467FA/B * WR/B \end{aligned} \tag{15}$$

Equation (14) shows that only the linear terms of W/B, FA/B and WR/B significantly affected the permeability of the specimens. It can be observed that both terms of W/B and WR/B negatively affected the response, with WR/B having the greatest effect. These results show that an increase of W/B and WR/B would lead to a reduction of the permeability of the specimens.

Table 26. Matrix of 2^4 CCD and the measured dependent response variables.

Run	Independent variables Actual (% wt.)				Dependent variables	
	W/B	FA/B	NI/B	WR/B	Compressive Strength (MPa)	Permeability (mm/s)
1	36	10	1.7	0.4	22.2	5.0
2	32	30	1.7	0.4	6.0	10.9
3	32	10	5.1	0.4	16.8	12.2
4	36	30	5.1	0.4	18.3	8.9
5	32	10	1.7	1.2	20.1	5.6
6	36	30	1.7	1.2	14.3	3.7
7	36	10	5.1	1.2	17.4	2.4
8	32	30	5.1	1.2	13.0	8.5
9	34	20	3.4	0.8	17.7	7.7
10	34	20	3.4	0.8	22.7	5.7
11	32	10	1.7	0.4	18.7	9.8
12	36	30	1.7	0.4	12.6	6.4
13	36	10	5.1	0.4	23.2	5.1
14	32	30	5.1	0.4	8.2	9.2
15	36	10	1.7	1.2	14.4	0.0
16	32	30	1.7	1.2	15.6	9.1
17	32	10	5.1	1.2	21.3	5.4
18	36	30	5.1	1.2	24.3	4.8
19	34	20	3.4	0.8	16.6	7.9
20	34	20	3.4	0.8	17.3	9.7
21	30	20	3.4	0.8	14.2	10.2
22	38	20	3.4	0.8	14.9	5.2
23	34	0	3.4	0.8	14.4	7.4
24	34	40	3.4	0.8	9.0	9.5
25	34	20	0	0.8	13.8	6.8
26	34	20	6.8	0.8	17.9	5.2
27	34	20	3.4	0	10.0	12.0
28	34	20	3.4	1.6	10.3	2.8
29	34	20	3.4	0.8	15.5	6.7
30	34	20	3.4	0.8	13.4	7.2

This reduction is attributed to the excess of fluidity in the mixture, causing the binders to drain out of the aggregates and thereby clogging the bottom of the specimen and reducing its permeability. On the contrary, an increment of the FA/B resulted in an increment of permeability, counteracting the effect of the W/B and WR/B terms.

Table 27. ANOVA and full regression statistics.

Term	Permeability		Compressive Strength 28-day	
	P-value	Coefficients[a]	P-value	Coefficient
Constant		40.75		44.3
W/B	0.000	-0.926	0.037	-0.7
FA/B	0.019	0.0831	0.001	-3.37
NI/B	0.721	NR[b]	0.048	-12.33
WR/B	0.000	-4.843	0.235	73.1
W/B^2	0.810	NR	0.912	NR
FA/B^2	0.701	NR	0.126	NR
NI/B^2	0.108	NR	0.596	NR
WR/B^2	0.646	NR	0.029	-6.88
W/B*FA/B	0.280	NR	0.021	0.0816
W/B*NI/B	0.335	NR	0.057	0.382
FA/B*WR/B	0.890	NR	0.020	-2.054
FA/B*NI/B	0.571	NR	0.252	NR
FA/B*WR/B	0.149	NR	0.010	0.467
NI/B*WR/B	0.941	NR	0.659	NR
Lack-of-Fit	0.291		0.462	
R-sq (%)		87.49		86.44

[a] Uncoded values for the relevant terms
[b] NR: Not statistically relevant

The 28 day compressive strength prediction followed a second order polynomial behavior, as shown in equation (15). All of the linear terms except for the WR/B resulted to be statistically relevant (Table 27). However, the WR/B was also incorporated in the regression equation to maintain hierarchy in the model (Montgomery, 2013). The only quadratic term that resulted to be statistically relevant was WR/B, which produced a significant impact on the compressive strength

response. Several interactions between the independent variables resulted to be relevant, as noted in Table 27. The interactions of W/B*FA/B, W/B*WR/B and FA/B*WR/B had a very strong effect on the response while W/B*NI/B had a relatively marginal effect since its p-value was very close to 0.05.

5.4.3. Response optimization of the RSM

The response optimizer tool of Minitab 17 was used to generate the optimization plots that simultaneously optimized the dependent variables to equally maximize the compressive strength while targeting 7 mm/s for the water permeability. As shown in Table 28, two different optimums were found to meet with the specifications: one near the high levels of each factor and the other close to its low levels. The predicted compressive strength after 28 days of curing was slightly higher for Opt A than for Opt B, with values of 22.8 and 21.3 MPa, respectively. An increase in compressive strength implied a reduction in permeability due to a reduction in the pore structure of the specimen (Bhutta et al., 2012). Therefore, Opt B resulted to have a higher predicted permeability than Opt A, with values of 7.6 and 5.5, respectively, which falls in the reported range of 1.4 to 12.2 mm/s (ACI, 2010).

Table 28. Compositions of the optimum GPCS specimens.

GPCS ID	W/B	FA/B	NI/B	WR/B	Prediction	
					Permeability (mm/s)	28 day CS (MPa)
Control	34	0	0	0	-	-
Opt A	36	35	6	1.2	5.5	22.8
Opt B	32	10	0.5	0.8	7.6	21.3

5.5.3. Overlay contour plots for the RSM

The overlay plots were obtained by expressing the two responses in a binary function of two independent variables and the other two held at its optimum settings. By overlaying both responses it was possible to find not only one set of variable settings, but regions where the responses would obtain values in the ranges were specified. The regions in white shown in Figure 36 represents the areas where the permeability and the 28 day compressive strength achieved values between the ranges of 3 to 12.3 mm/s and 20.7 and 25 MPa, respectively.

As shown in Figure 36a, the permeability of the specimens decreased with the increment of W/B and the reduction of FA/B when NI/B and WR/B were held at 6 and 1.2%, respectively. A similar effect was observed when NI/B and WR/B were held close to their low levels (Figure 37a), with the difference that the permeability was higher for the Opt B specimens when FA/B was increased, and significantly lower when simultaneously W/B was increased and FA/B was reduced. The higher permeability of Opt B was attributed to an increment in the fluidity of the mixture due to the addition of a greater volume of superplasticizer (Mardani-Aghbaglou et al., 2013) and NI/B, which is coated with surfactants that are also known to increase the fluidity of concrete (Ouyang et al. 2008). On the other hand, the reduction of permeability was caused by the drainage of the binding materials to the bottom, and therefore clogging the specimen due to an excess of water. When comparing Figure 36a with Figure 32a it can be observed that the compressive strength of Opt A was higher when both W/B and FA/B were in their high levels, while for the Opt B a greater compressive strength was achieved at the lower ratios of W/B and FA/B.

Figure 36b and 32b shows that the permeability was in a rising ridge pattern, which was more prominent for Opt A, where the increment or reduction of the NI/B from the middle levels of the design and the increase of W/B reduced the permeability of the specimens. The addition of large amounts of FA/B required an addition of more than 4% of NI/B in order to meet the specification of achieving a compressive strength higher than 20.7 MPa. On the contrary, Figure 37b shows that when the FA/B was held at 10%, a compressive strength higher than 20.7 MPa could be achieved by simultaneously increasing the W/B and NI/B or by the decrease of both, with the lowest strengths at the saddle points near the center of the design.

The response of permeability was found to be significantly high when both WR/B and W/B decreased while the FA/B and NI/B where held at both of their optimum levels (Figure 36c and 32c). The desired compressive strength response was met for Opt A when increasing the W/B due to the high amount of FA/B in the mixture. On the contrary, Opt B specimens required low amounts of W/B and the WR/B near to the middle levels of the model to comply with the values of the compressive strength. Figure 38a and 34a clearly show how the NI/B affected the compressive strength response with respect to the FA/B amount. When a high FA/B was applied, a minimum of 5% NI/B was required in order to obtain a compressive strength higher than 20.7 MPa when W/B and WR/B were held at 36 and 1.2 respectively. Conversely, when the W/B and WR/B were

held at their low values, it was necessary to decrease both the NI/B and the FA/B near to their lower levels in the model.

Figure 38b shows that the permeability in the range between 4 to 8 mm/s and the compressive strength in the range of 20.7-25 MPa can be obtained for any FA/B ratios, depending on the amount of WR/B added, when holding the NI/B and the W/B and the levels of 6 and 36%, respectively. It also shows that in order to obtain the responses between the desired ranges, both the FA/B and WR/B must be increased simultaneously. On the contrary, when the W/B and the NI/B were fixed at 32 and 0.5%, respectively; only a maximum of 10% of FA/B could be added in order to achieve desired compressive strength (Figure 39b). For the permeability in the range of 5 to 12 mm/s could be achieved for an addition of NI/B from 0.1 to 1.2 %.

While the independent variables of W/B and FA/B were held at their optimum levels, the permeability greater than 5 mm/s was observed in a very wide range. The increment or the decrease of NI/B from the middle level of the model resulted in a reduction in the permeability, whereas the increment of WR/B resulted in a lower permeability in both of the optimum specimens. Figure 38c and 34c also show that at a high FA/B in the mixture it was required to add more than 5% of NI/B to the mixture. However, for a low FA/B less than 2% NI was required to achieve a compressive strength over 20.7 MPa.

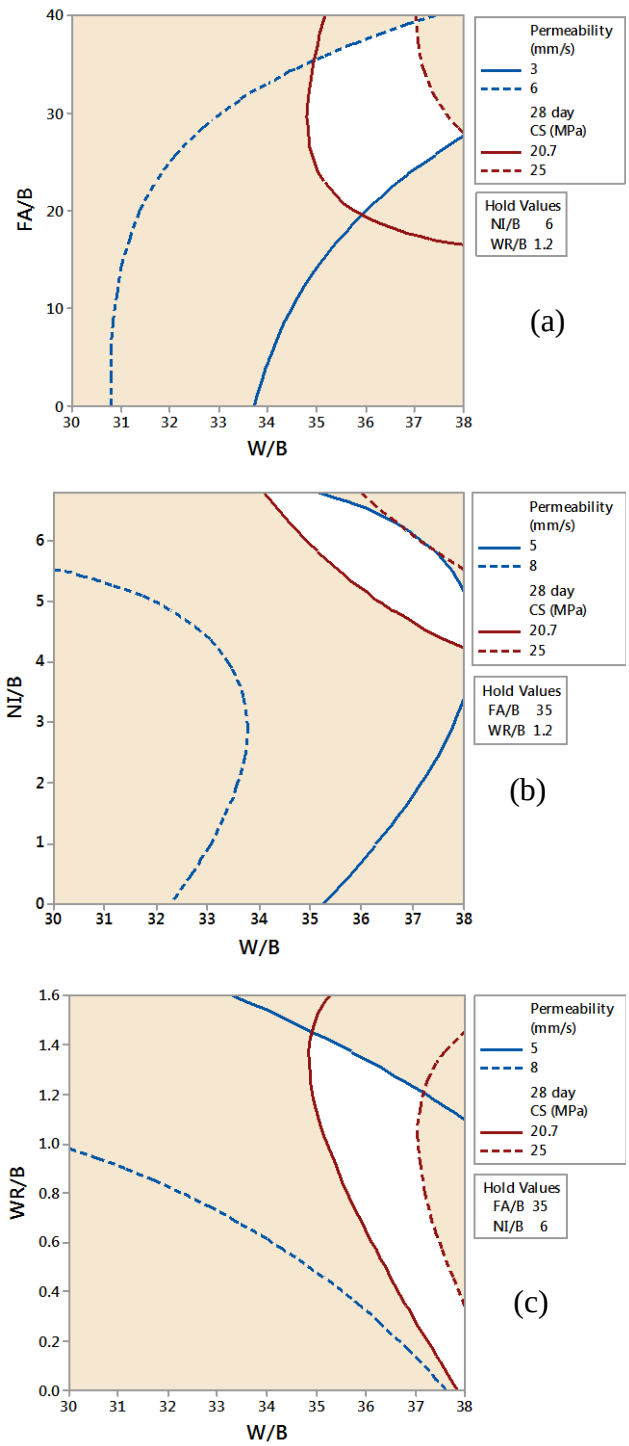

Figure 36. Overlay contour plots of the permeability and the compressive strength for the Opt A specimens.

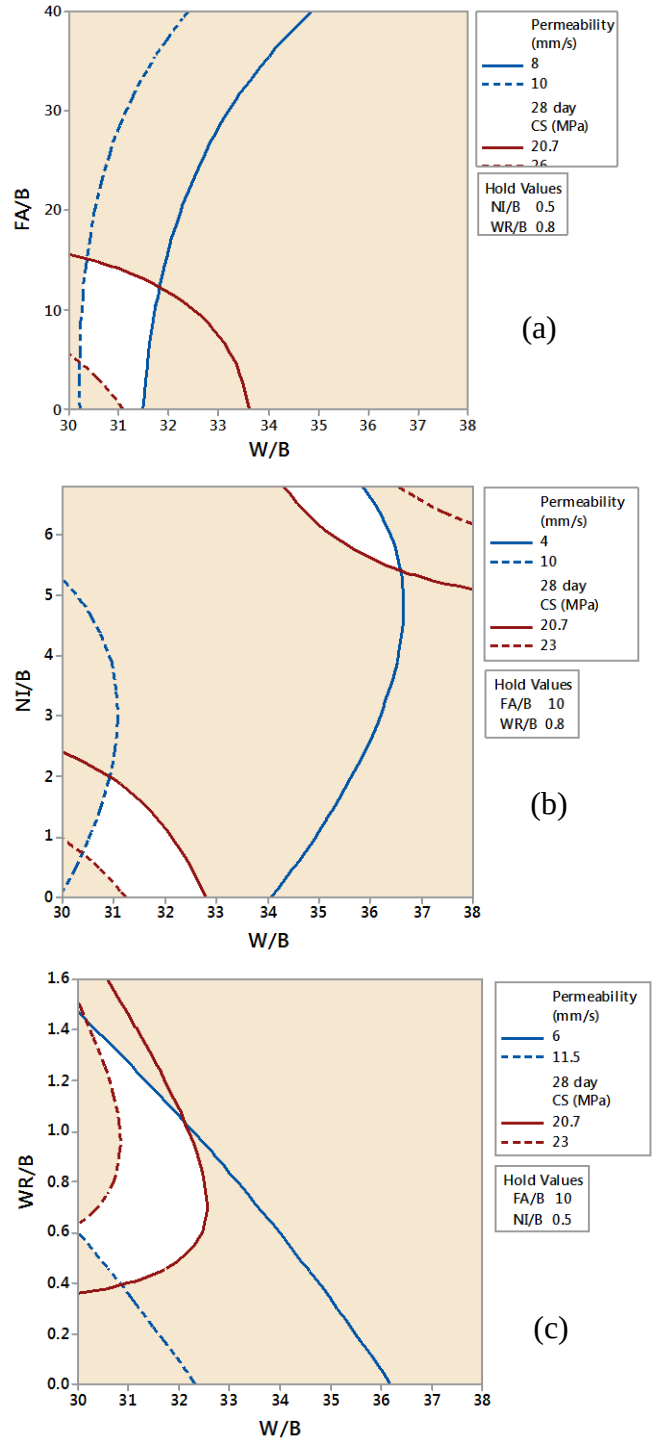

Figure 37. Overlay contour plots of the permeability and the compressive strength for the Opt B specimens.

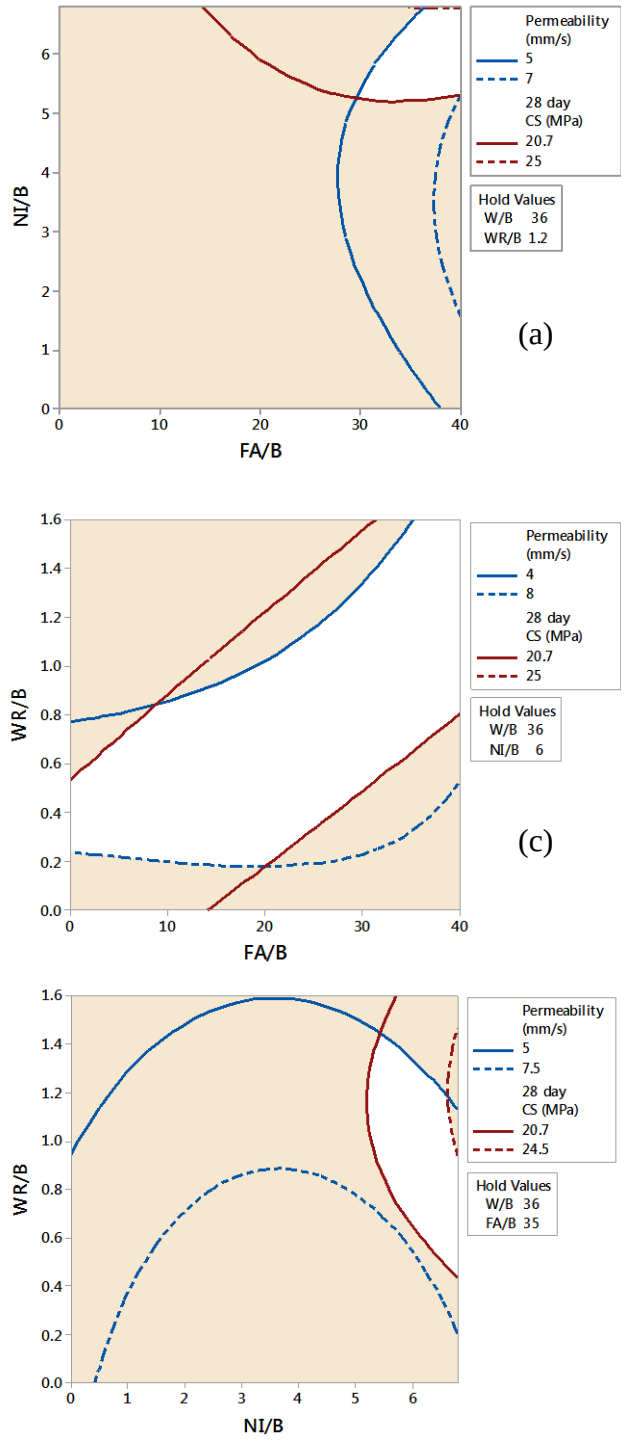

Figure 38. Overlay contour plots of the permeability and the compressive strength for the Opt A specimens.

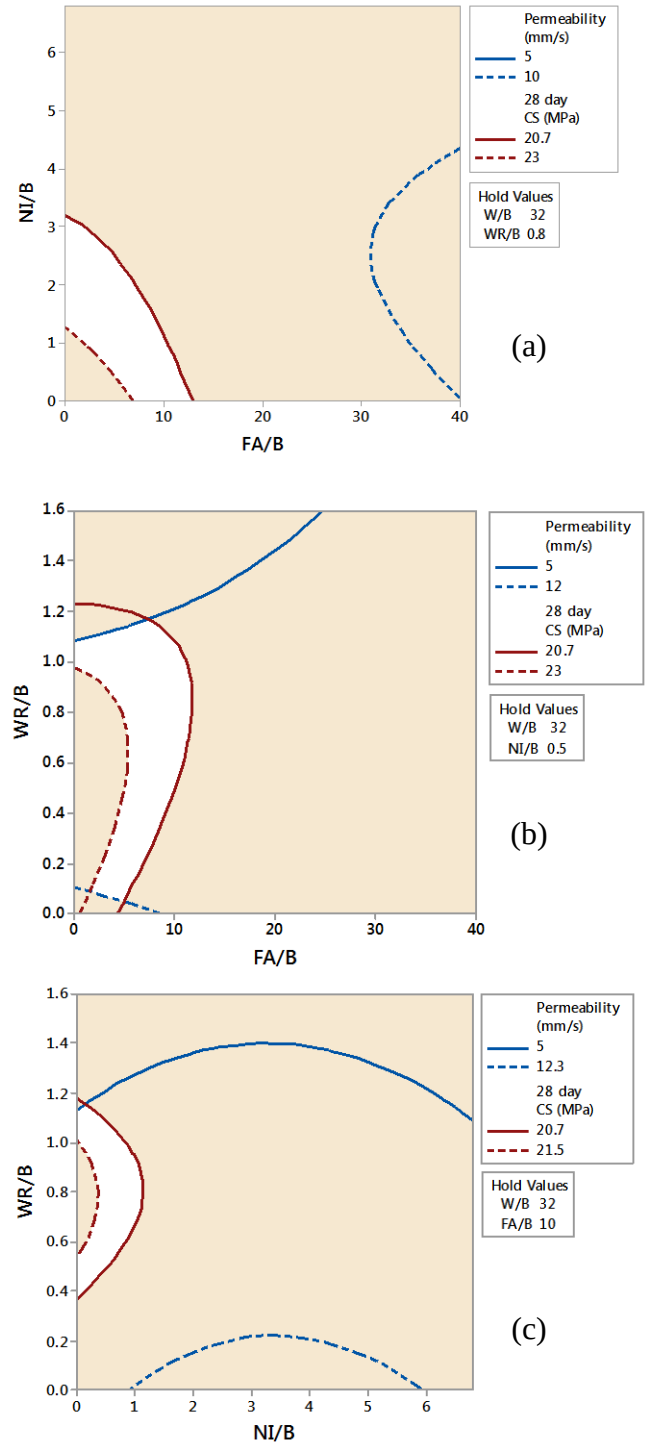

Figure 39. Overlay contour plots of the permeability and the compressive strength for the Opt B specimens

5.5.4. Statistical models validation

The prediction of the RSM model was validated by performing another set of experiment where three specimens where made at the optimum settings found in Section 5.4.3 and the control specimen from Table 28. As shown in Figure 40, the Opt A specimens resulted in slightly lower compressive strength compared to the Opt B specimens, with average values of 17.8 and 19.2 MPa, respectively. Although the predicted values for the compressive strengths of Opt A and B where slightly higher than the measured values, they were in the range of the 95% confidence intervals (CI), which were 16.3 to 29.3 MPa and 16.4 to 26.3 MPa, respectively. Control specimens resulted in significantly lower compressive strength than the Opt A and B specimens, with an average value of 12.0 MPa. Figure 40 also shows that as compressive strength increased, permeability was lowered due to a reduction in the pore structure of the PCPC (Tho-in et al. 2012).

The average permeability's of the Opt A and Opt B specimens were 10.0 and 11.9 mm/s, respectively. As predicted by the model, Opt B resulted in a slightly higher permeability than the Opt A specimens. The predicted value for the permeability's of Opt A and B specimens where 5.5 and 7.7, with a 95% CI of 1.52 to 9.51 mm/s and 4.61 to 10.64 mm/s, respectively.

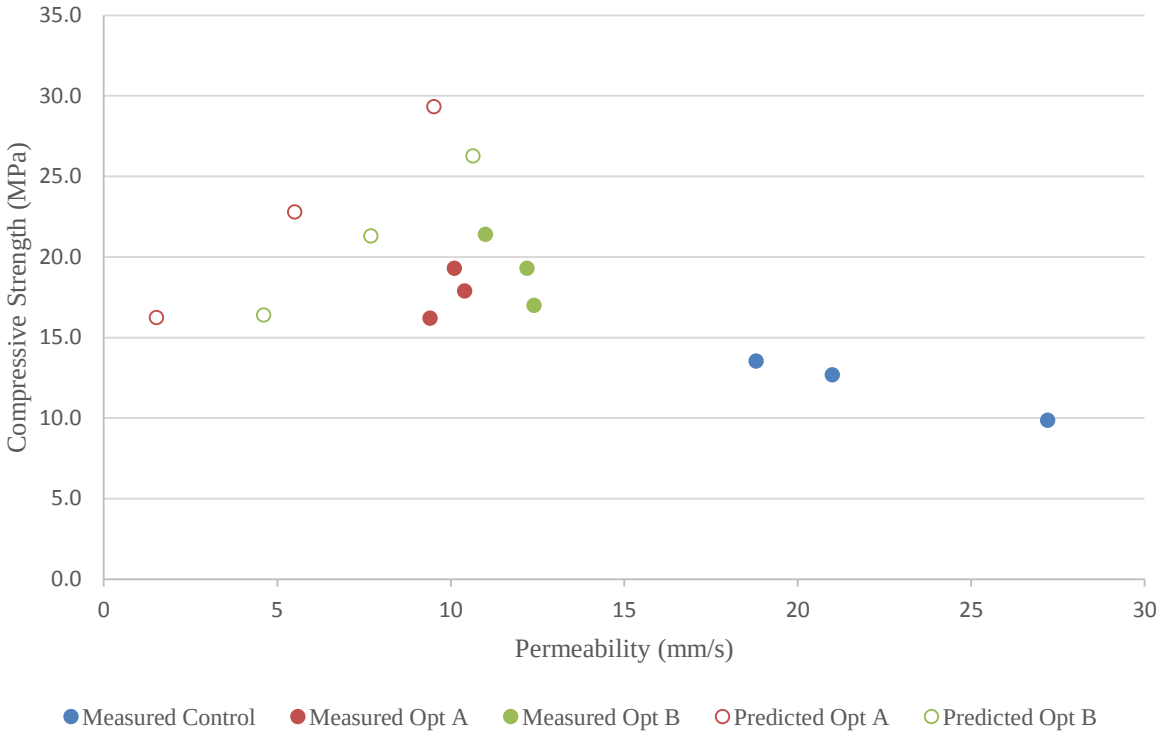

Figure 40. Relationship between permeability and compressive strength of the GPCS specimens.

5.5.5. FC inactivation by optimum GPCS

For a contact time of 2 hours, the Control specimens obtained a higher percentage of FC inactivation throughout the experiment, with an average of 95.4% inactivation for a total of 10 loads. Although FC inactivation with the Opt A and Opt B specimens was lower than for the Control (Figure 41), they were able to inactivate an average of 74.2% and 67.9%, respectively. When a contact time of 24 hours was given after 20 loads a higher FC inactivation was achieved, with values of 85.5, 97.4 and 97.1% for the Opt A, Opt B and Control specimens, respectively.

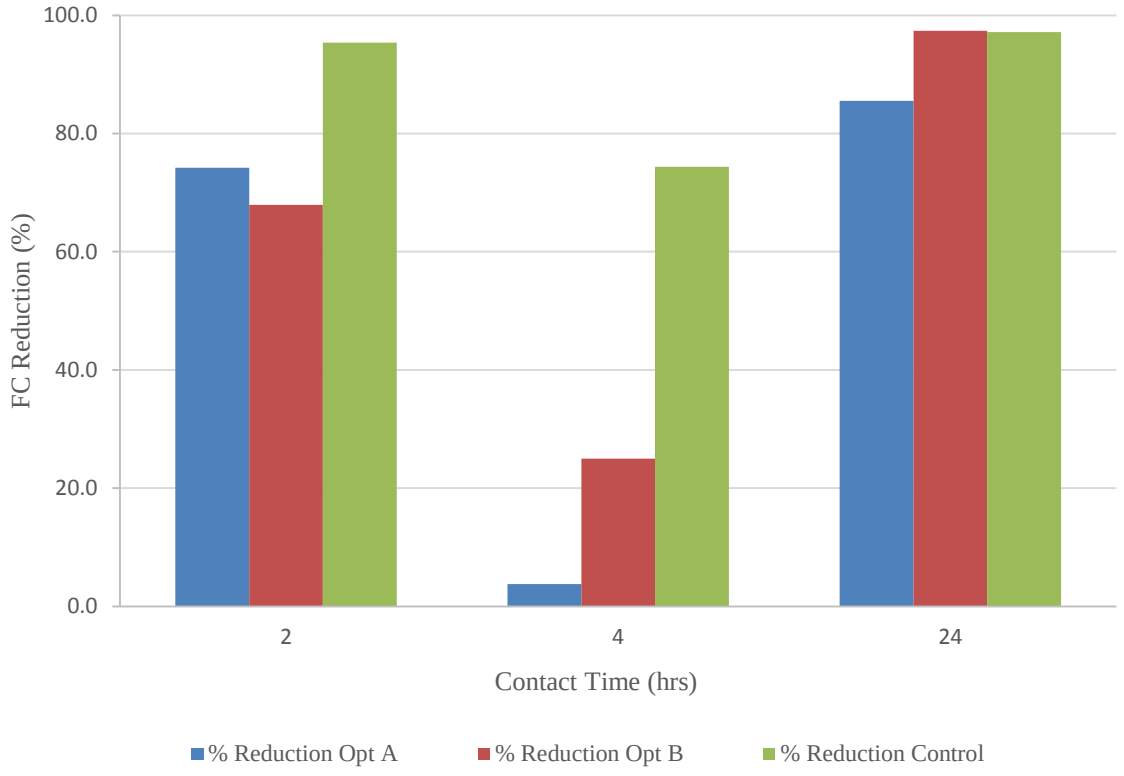

Figure 41. FC reduction in water after treatment with GPCS specimens.

It is important to notice that FC inactivation was achieved better at higher water pHs. Calcium hydroxide (CH) is one of the principal hydration products of concrete and is highly soluble in water, contributing to the high alkalinity of concrete (Mehta and Monteiro, 2014). This behavior was clearly noticed in Figure 42, which shows that after treating the target water with the GPCS specimens, pH increased significantly. After a 2-hour contact time, the pH increased from ~7.5 to ~10.0, and it slightly decreased as loads of water pass through the specimens. A minor increase in pH was also observed at the 19th load, since the contact time was increased from 4 to 24 hours, although a notable decreased was observed on the following loads. The water treated with the Opt A and B specimens resulted in lower pH than the control specimens. This behavior can be attributed to the partial substitution of cement with FA. Since SiO_2 contained in FA reacts with the CH available in the hydrated paste to form the C-S-H gel, less CH leaches out of the specimen thus resulting in a less alkaline effluent (Deschner et al., 2012).

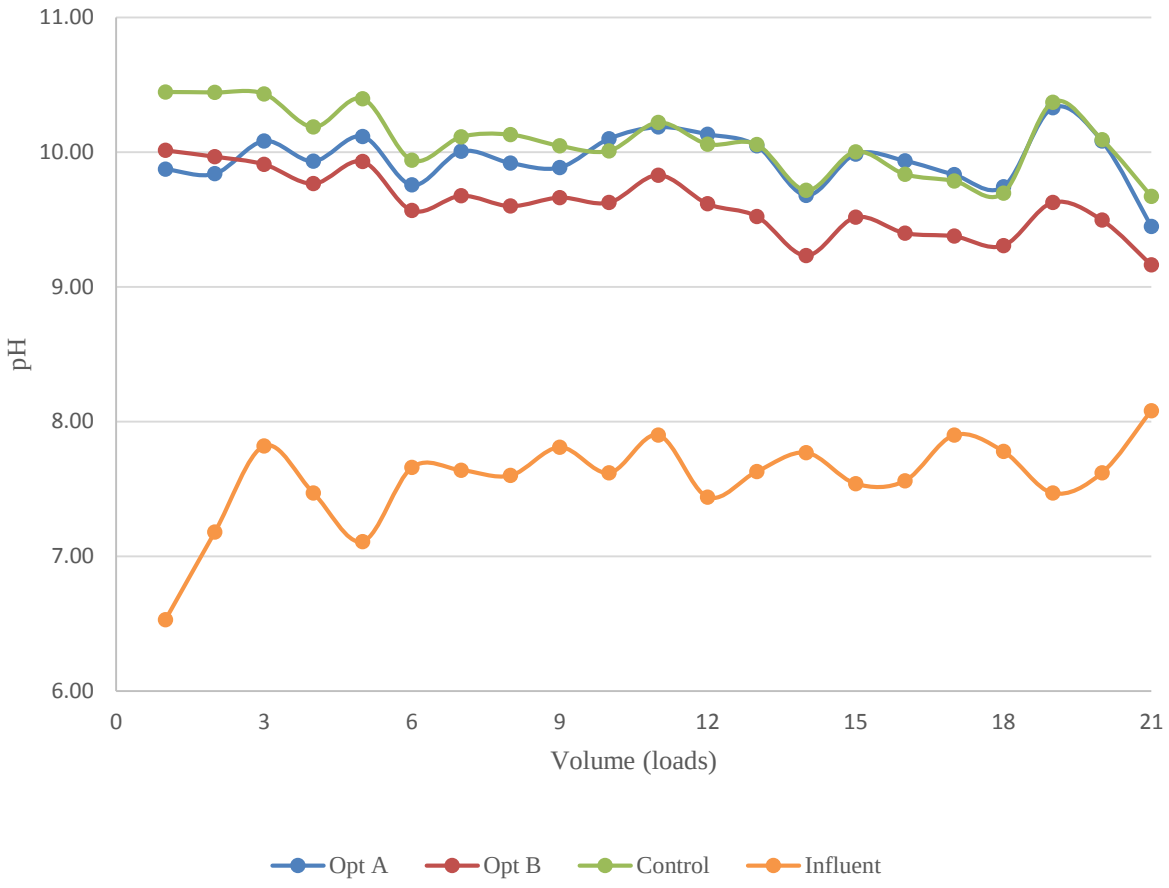

Figure 42. pH change of treated influent water over volume (1 load = 400 mL of FC containing water.

5.5.6. Phosphate and nitrate reduction with optimums GPCS

Results of phosphorous removal showed that the higher the initial concentration of phosphate ions, the better was its removal from water. As the initial concentration of phosphorus increased, the solution became more turbid with time. As shown in Figure 43, the specimen with the lowest phosphorous removal was Opt B, with a maximum and minimum average removal of 84.6 and 13.4 % respectively. On the other hand, the Control specimens were the ones that achieved the highest phosphorous removal, followed by the Opt A, with a range of 54.2 % to 100.0 and 26.6% to 92.6, respectively. Most likely phosphorus was removed by adsorption and co-precipitation with calcium ions that were leached from the PCPC cementitious matrix (Luck et al., 2008).

The nitrate removal from water was significantly influenced by the pH and contact time. This was in good agreement with Ensie and Samad (2014), who also found that the removal of nitrate with nano SiO_2–FeOOH–Fe core–shells increased in acidic environments, since at alkaline pH's iron oxide precipitated, reducing its percentage of removal. Average nitrate removals for the Opt A, Opt B and Control specimens where 18.8, 13.8 and 20.1%, respectively. Reductions up to 79.0, 48.8 and 54.3 % were achieved by the Opt A, Opt B and Control, with the increment of the contact time up to 24 hours (Figure 44).

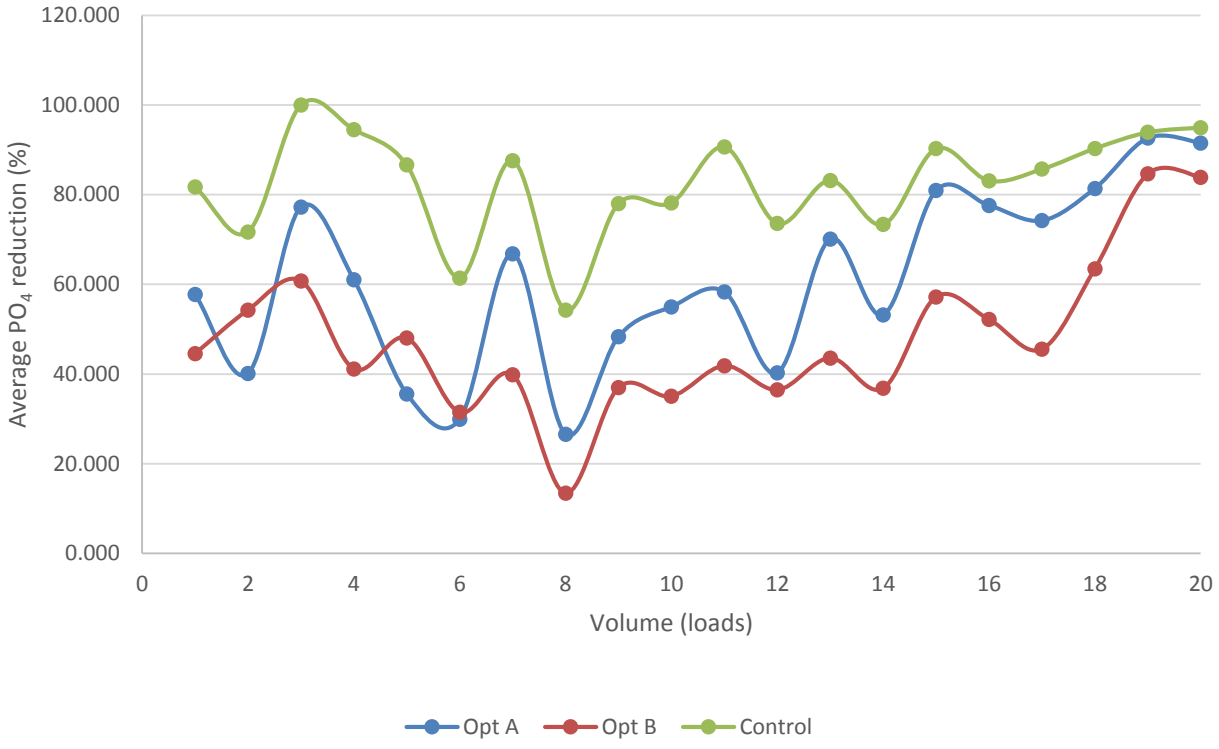

Figure 43. Phosphorous removal with the GPCS specimens over volume of treated influent.

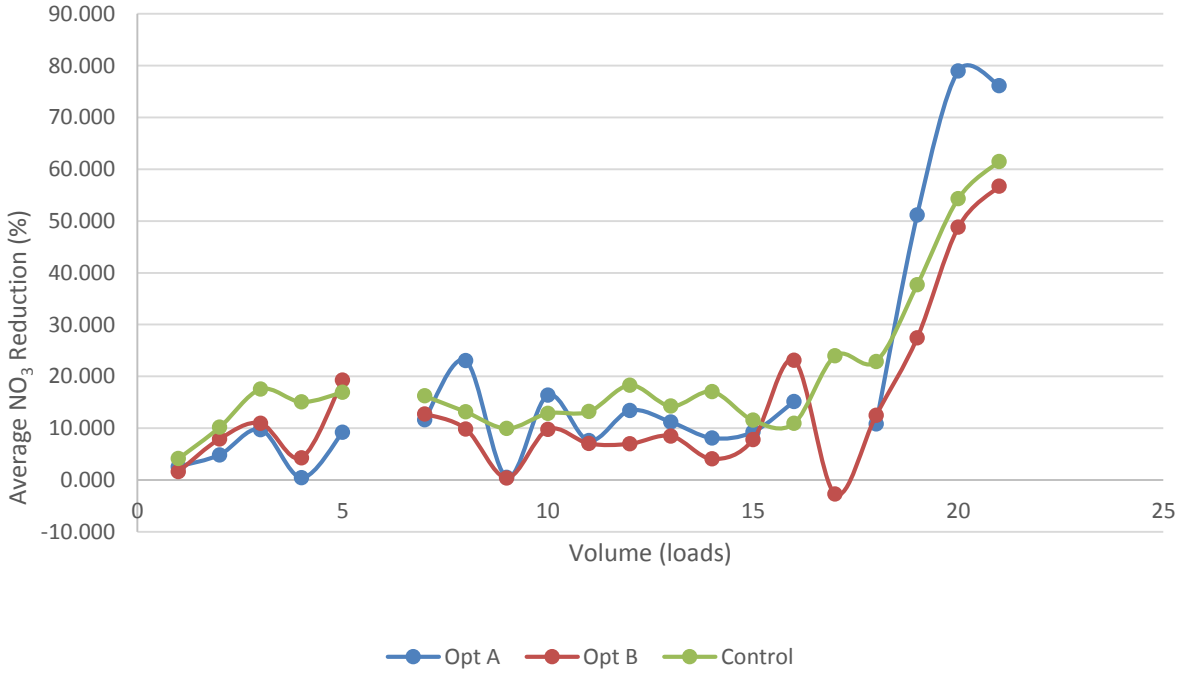

Figure 44. Nitrate removal with the GPCS specimens over volume of treated influent.

5.5. Conclusions

The following conclusions can be made from this study:

- The optimum mix ratios at 36% W/B, 35% FA/B, 6% NI/B and 1.2 % WR/B for Opt A and 32% W/B, 10% FA/B, 0.5% NI/B and 0.8% for Opt B resulted in an average measured compressive strength and permeability in the ranges of 17.8 and 19.2 MPa and 10.0 and 11.9 mm/s, respectively.
- The increment of W/B and the reduction of FA/B independent of the settings of NI/B and WR/B resulted in a decrease of the permeability of the specimens due to drainage of the binder material and clogging of the bottom of the specimens.
- The addition of large amounts of FA/B required an addition of more than 4% NI/B in order to achieve a compressive strength higher than 20.7 MPa.
- Compressive strength increased with the decrease of permeability due to pore structure reduction of the specimens.
- Greater FC and phosphorus removals were achieved at a higher pH's, with average values for FC inactivation of 74.2%, 67.9%, 95.4% at 2 hour contact time, and for phosphorus removal 92.6, 84.6 and 100% for Opt A, Opt B and Control, respectively.
- The increase of contact time improved the nitrate reduction, achieving removals up to 79.0, 48.8 and 54.3 % by the Opt A, Opt B and Control, respectively.

5.6. References

ACI, American Concrete Institute Committee 522. Report on Pervious Concrete. 1st Ed., ACI 522R-10. American Concrete Institute, Michigan, 2010.

Ahammed MM, Davra K. Performance evaluation of biosand filter modified with iron oxide-coated sand for household treatment of drinking water. Desalination 2011; 276:287-293.

Bhutta MAR, Tsuruta K, Mirza J. Evaluation of high-performance porous concrete properties. Construction and Building Materials 2012; 31:67-73.

Deschner F, Winnefeld F, Lothenbach B, Seufert S, Schwesig P, Dittrich S, Goetz-Neunhoeffer F, Neubauer J. Hydration of Portland cement with high replacement of siliceous fly ash. Cement and Concrete Research 2012; 42:3989-1400.

Ensie B, Samad S. Removal of nitrate from drinking water using nano SiO_2-FeOOH-Fe core-shell. Desalination 2014; 347:1-9.

EPA (2014). US Environmental Protection Agency. Drinking water contaminants. http://water.epa.gov/drink/contaminants/index.cfm. Retrieved on February 2, 2015.

EPA. (2012). US Environmental Protection Agency. National Pollutant Discharge Elimination System (NPDES). http://cfpub.epa.gov/npdes/home.cfm?program_id=6. Retreived on April 20, 2014.

Gilbert JK, Clausen JC. Stormwater runoff quality and quantity from asphalt, paver and crushed stone driveways in Connecticut. Water Research 2006; 40:826-832.

Kim LH, Kayhanian M, Zoh KD, Stenstrom MK. Modeling of highway stormwater runoff. Science of the Total Environment 2005; 348:1-18.

Litter J, Geroni JN, Sapsford DJ, Coulton R, Griffiths AJ. Mechanisms of phosphorus removal by cement-bound ochre pellets. Chemosphere 2013; 90:1533-1538.

Luck JD, Workman SR, Coyne MS, Higgins SF. Solid material retention and nutrient reduction properties of pervious concrete mixtures. Biosystems Engineering 2008; 100:401-408.

Luck JD, Workman SR, Coyne MS, Higgins SF. Consequences of manure filtration through pervious concrete during simulated rainfall events. Biosystems Engineering 2009; 102: 417-423.

Mahmood A, Malik RN. Human health risk assessment of heavy metals via consumption of contaminated vegetables collected from different irrigation sources in Lahore, Pakistan. Arabian Journal of Chemistry 2013:7:91-99.

Mardani-Aghbaglou A, Tuyan M, Yilmaz G, Arioz O, Ramyar K. Effect of different types of super-plasticizer on fresh, rheological and strength properties of self-consolidating concrete. Construction and Building Materials 2013; 47:1020-1025.

Metha P, Monteiro P. *Concrete microstructure, properties and materials*. 4th Ed. McGraw-Hill Education, 2014.

Ouyang X, Guo Y, Qiu X. The feasibility of synthetic surfactant as an air entraining agent for the cement matrix. Construction and Building Materials 2008; 22:1774-1779.

Ragheb, SM. Phosphate removal from aqueous solution using slag and fly ash. HBRC Journal 2013; 9:270-275.

Ramos MC, Quinton JN, Tyrrel SF. Effects of cattle manure on erosion rates and runoff water pollutionby feacal coliforms. Journal of Environmental Management 2006; 78:97-101.

Schoonover JE, Lockaby BG. Land cover impacts on stream nutrients and feacal coliform in the lower Piedmont of West Georgia. Journal of Hydrology 2006; 331:371-382.

Tawfik A, El-Gohary F, Ohashi A, Harada H. The influence of physical–chemical and biological factors on the removal of faecal coliform through down-flow hanging sponge (DHS) system treating UASB reactor effluent. Water Research 2006; 40:1877-1883.

Tho-in T, Sata V, Chindaprasirt P, Jaturapitakkaul C. Pervious high-calcium fly ash geopolymer concrete. Construction and Building Materials 2012; 30:366-371.

Xue Y, Hou H, Zhu S. Characteristics and mechanisms of phosphate adsorption onto basic oxygen furnace slag. Journal of Hazardous Materials 2009; 162:973-980.

Sumanasooriya MS, Neithalath N. Pore structure features of pervious concretes proportioned for desired porosities and their performance prediction. Cement and Concrete Composites 2011; 33(8):778-787/

Wang H, Wang H. Mitigation of lake eutrophication: Loosen nitrogen control and focus on phosphorus abatement. Progress in Natural Science 2009; 19:1445–1451.

CHAPTER 6

Durability of green pervious concrete under acidic environments

6.1. Abstract

Concrete structures can be exposed to acidic environment that deteriorates the quality of concrete such as changes in the weight, the compressive strength and the concrete microstructure depending on the type of the acids to which was exposed and the composition of the concrete mixture. No information is available on the effects of acetic and sulfuric acids in terms of compressive strength and weight for pervious concrete containing chemical admixtures and high volumes of FA. In this regard, the effect of these acids on the two optimum and the control GPCS, used in Chapter 5, were evaluated. Weight increment in all GPCS's was observed when exposed to either water or sulfuric acid, although the increment was more noticeable for the specimens placed in water. On the contrary, GPCS placed in the acetic acid solution resulted in a rapid weight loss from the beginning of the experiment. The simultaneous addition of FA and NI resulted in a higher compressive strength for the GPCS even after the exposition to acids.

6.2. Literature Review

6.2.1. Sulfuric acid attack to concrete

Sulfuric acid attack to concrete structures is due to two primary reasons: discharge from chemical industries and the decomposition of sulfur containing compounds in wastewaters into hydrogen sulfide (H_2S) by anaerobic bacteria which then is dissolved in water or metabolized with oxygen by aerobic bacteria to produce sulfuric acid (Li et al., 2009; Girardi et al., 2010). Concrete elements such as sewers, foundations, industrial floors of chemical plants, basements walls of buildings near chemical plants, and superstructures (due to acid rain) can be susceptible to sulfuric acid attack (Chang et al., 2005).

The sulfuric acid first attacks the CH found on the hardened concrete to form gypsum and when there is no CH available, it attacks the C-S-H gel to form gypsum and an incoherent mass of hydrated silicate, as expressed by reactions (1) and (2) in Chapter 1 (Metha and Monteiro, 2014). This type of sulfate attack occurs at high sulfate concentrations, otherwise the CAH gel or the monosulfates present in concrete reacts with the sulfuric acid to form ettringite as shown in reactions reactions (3) and (4) from Chapter 1, respectively (Girardi and Di Maggio, 2011).

In order to control the sulfate attack to concrete, either a cement with less than 8% of tricalcium aluminate (C_3A) or the addition of pozzolan such as FA, slag, volcanic ash or volcanic pumice is required (Hossian and Lachemi, 2006). The C_3A reacts with the sulfate originally present in cement to form ettringite. An excess of C_3A in the cement will yield to the formation of monosulfate after all the sulfate in consumed, leaving a susceptible concrete to late ettringite formation if exposure to rich sulfate environments occurs (Metha and Monteiro, 2014).

6.2.2. Organic acids attack to concrete

Organic acids are weak acids that partially dissociate in water and react with the hydrated and anhydrous phases of the cement paste to form calcium salts (Oueslaty and Duchesne, 2012). Concrete agricultural structures can be damaged by agricultural effluents containing organic acids such as acetic, propionic, butyric and lactic acid, to name a few. Bertron et al. (2005) found that the aggressiveness of organic acids depends on their dissociation constant values (pKa), for which lower values result in a greater aggressiveness in regard to the pH increase and release of elements

of the cement paste matrix. Moreover, they found that a solution of acetic acid at pH 4 could mimic effectively the aggressiveness of organic acids in manure (Bertron et al., 2005).

The durability of concrete against the exposure to acetic acid also depends on the amount CH in the hardened concrete. The reaction of acetic acid with CH leads to the formation of a highly soluble salt in water (43.6 g in 100 g water at 25 ℃) (Chatveera and Lertwattanaruk, 2014) as shown in the reaction (5):

$$2(CH_3COOH) + Ca(OH)_2 \rightarrow (Ca(CH_3COO)_2) + 2H_2O \qquad (5)$$

6.2.3. Concrete additives on the chemical durability

As mentioned before, the solubility of calcium salts play an important role in the degradation of hardened concrete. The addition of mineral admixtures such as silica fume, FA and furnace slag have shown to be very effective to the resistance against acid attack in terms of the reduction of the calcium hydroxide (CH), which is highly soluble in water and does not contribute to the strength in concrete (Metha and Monteiro, 2014; Oueslati and Duchesne, 2012). The pozzolanic reaction produces C-S-H or C-A-H gel, which reduces the pores sizes, resulting in a denser and stronger concrete that is more resistant to acid attack (Makhloufi et al., 2012; Sata et al., 2012). Pacheco-Torgal and Jalali (2009) studied the durability of polymer modified and polymer impregnated concrete when exposed to sulfuric acid. They found minor benefits on the durability and acid resistance of concrete pipes, although the increase in cost made the use of polymers not feasible.

6.3. Materials and Experimental Methodology

6.3.1. Materials

Portland cement (PC) Type IP in compliance with ASTM C595 was used and fly ash (FA) was obtained from a local coal-fueled power plant (AES Puerto Rico). Limestone gravel in the range size of 4.75-9.5 mm was used as a coarse aggregate. The NI solution was purchased from the Ferrotec (Bedford, NH). The BASF Glenium 3030 NS water-reducing admixture was supplied by a local company in Puerto Rico. Certified ACS-grade sulfuric acid and acetic acid were purchased from the Fisher Scientific and were diluted with DI water to make acid solutions at pH 3 to test durability of the GPCS under acidic environments.

5.3.2. Specimen design and preparation

The composition of the GPCS from the optimum specimens found in Chapter 5 were used for this experiment, and are shown in Table 29.

Table 29. Mixture composition of the GPCS.

GPCS ID	W/B	FA/B	NI/B	WR/B
Control	34	0	0	0
Opt A	36	35	6	1.2
Opt B	32	10	0.5	0.8

The mixtures were prepared in a mechanical mixer in accordance to the ASTM C192 and then cast into cylindrical molds of 20.32 cm in length and 10.16 cm in diameter. Compaction of the specimens was made using the standard rodding consolidation method in accordance to ASTM C192. After 24 hours, specimens were demolded and cured for 28 days in lime-saturated tap water at ambient temperature (24±2 ^{o}C).

5.3.3. Compressive strength test

In accordance to ASTM C39, compressive strength was tested for the GPCS specimens after they were cured for 28 days in $Ca(OH)_2$-saturated tap water. After the acid exposure, specimens were tested for the compressive strength in order to calculate the strength change after

the acid attack. Capping rubber pads (Gilson HM-362) were placed during the compressive strength test on the top and bottom sides of the specimens to provide a uniform load distribution by a 3000 kN Forney universal testing machine.

6.3.4. Durability

The method for testing chemical resistance of concrete mortars (ASTM C267) was modified to accommodate the experiment with the GPCS specimens. Chemical resistance of the specimens were tested in terms of changes in the weight and compressive strength by exposing the specimens to tap water and two different acid solutions at pH 3: sulfuric acid and acetic acid. Three specimens per mixture were placed in a container filled with 5 liters of the test solution. Weight monitoring was done after 1, 7, 28, 56, and 90 days of immersion and, after each monitoring, the test solution was replenished with the fresh solution. After talking out specimens from the test solutions, they were shortly rinsed and brushed with running DI water and blot dried with a paper towel in order to record the saturated weight of the specimens. Solution pH was also recorded and cumulative mass loss was calculated between each monitoring period.

6.4. Results and Discussion

6.4.1. Durability in terms of weight change

Figure 45 shows the weight changes when the GPCS were placed in tap water at pH 7.5 and acid solutions at pH 3.0. The GPCS were cured for 28 days prior to the durability experiment. In tap water, the Opt A and Control specimens had a greater weight gain than the Opt B specimen. This can be attributed to the ongoing hydration of cement, to the pozzolanic reactions to form more C-S-H and calcium aluminate hydrate (CAH) gels or to the formation of gypsum and ettringite. Studies have shown that a faster and higher weight gain is achieved for the specimens containing natural pozzolana (Makholoufi et al., 2012), resulting in a denser material due to pore reduction and thus enhancing the durability of the concrete specimens.

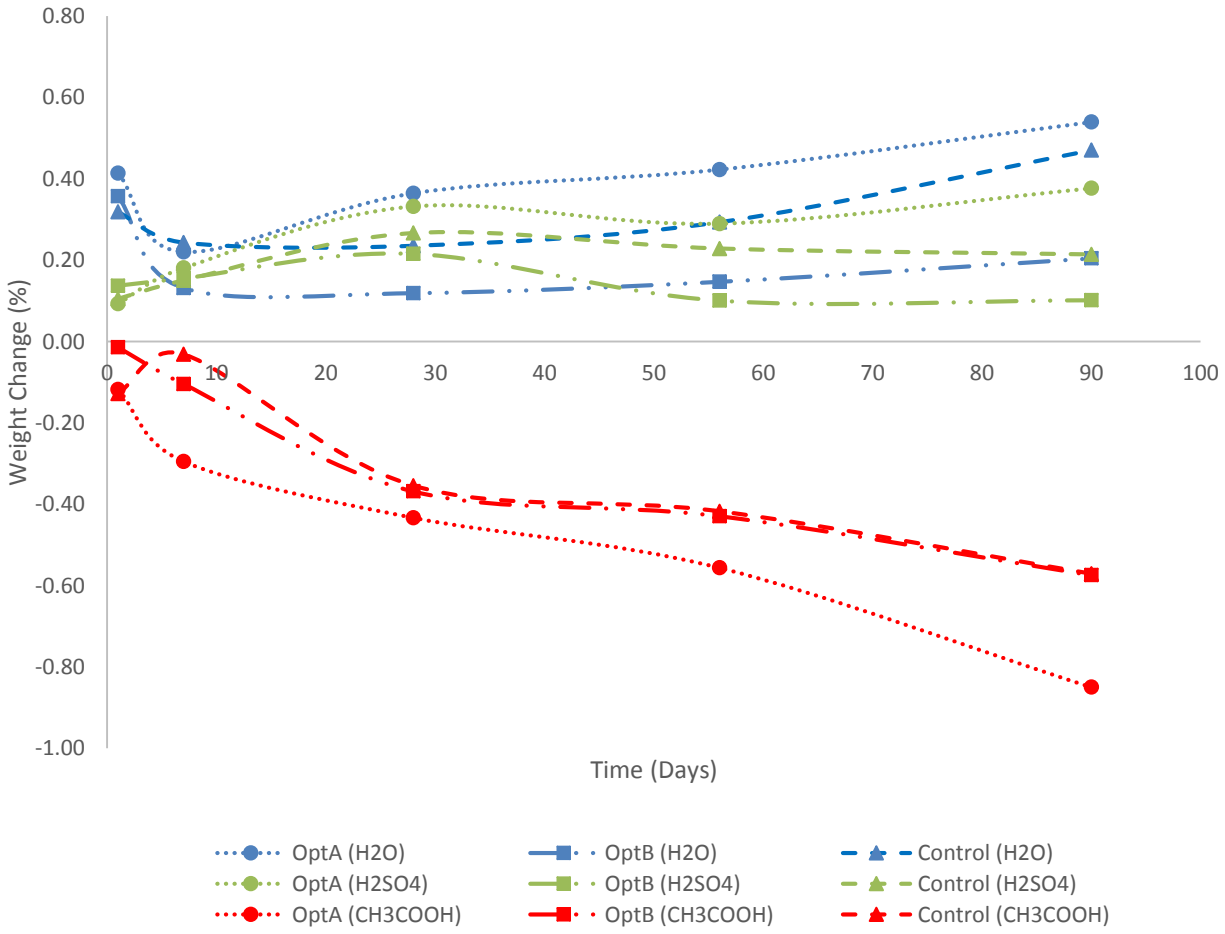

Figure 45. Weight changes of the GPC specimens in water and acid solutions.

All the GPCS in the sulfuric acid solution gained weight, although the magnitude of weight gain was less than 0.4% and smaller than weight increment when exposed to water. Similarly to the specimens exposed only to water, the least weight gain was found for the Opt B followed by the Control specimen, whereas Opt A gained weight the most. These results are in agreement with the results for the cement paste specimens, in which it was also found that the specimen containing both FA and NI resulted to have the highest weight change. This implies that the simultaneous addition of FA and NI in high amounts helped to improve the durability of the specimens when exposed to sulfuric acid in terms of densification of the specimen. As previously discussed in Chapter 1, this behavior is primarily due to the dual attack of the acid and the sulfate ions, which increase the weight due to the formation of expansive products such as ettringite, contracting the weight loss produced by the decalcification by the acid (Metha and Monteiro, 2014). Early ettringite formation by sulfate attack on monosulfate hydrates ($C_3A{\cdot}C\underline{S}H_{12\text{-}18}$) can be responsible for weight increase at the beginning of the exposure.

Similarly to the cement pastes specimens studied in Chapter 1, when the GPCS were exposed to acetic acid solution at pH 3, weight loss was immediately observed (Figure 45). Since acetic acid tends to form calcium salts ($Ca(CH_3COO)_2$), which are highly soluble in water and easily leach out of the paste specimens, weight loss is rapidly observed (Metha and Monteiro, 2014). After 90 days in acetic acid, the Opt A GPCS showed a higher weigh loss in comparison to the other two specimens, which resulted in the same weight loss after 90 days of exposure. Deterioration and spalling on the specimens surface was visually noticed on all GPCS after 90 days in the acetic acid solution

6.4.2. pH changes during exposure in tap water and acid solutions

In tap water, pH rapidly increased from 7.3 to ~9.6 at day 1 and then quickly stabilized at ~10.0 for all the pastes regardless of FA substitution or NI addition (Figure 46). The increase of the pH was due to the water absorption/transport through the pores, dissolving and leaching CH to the solution.

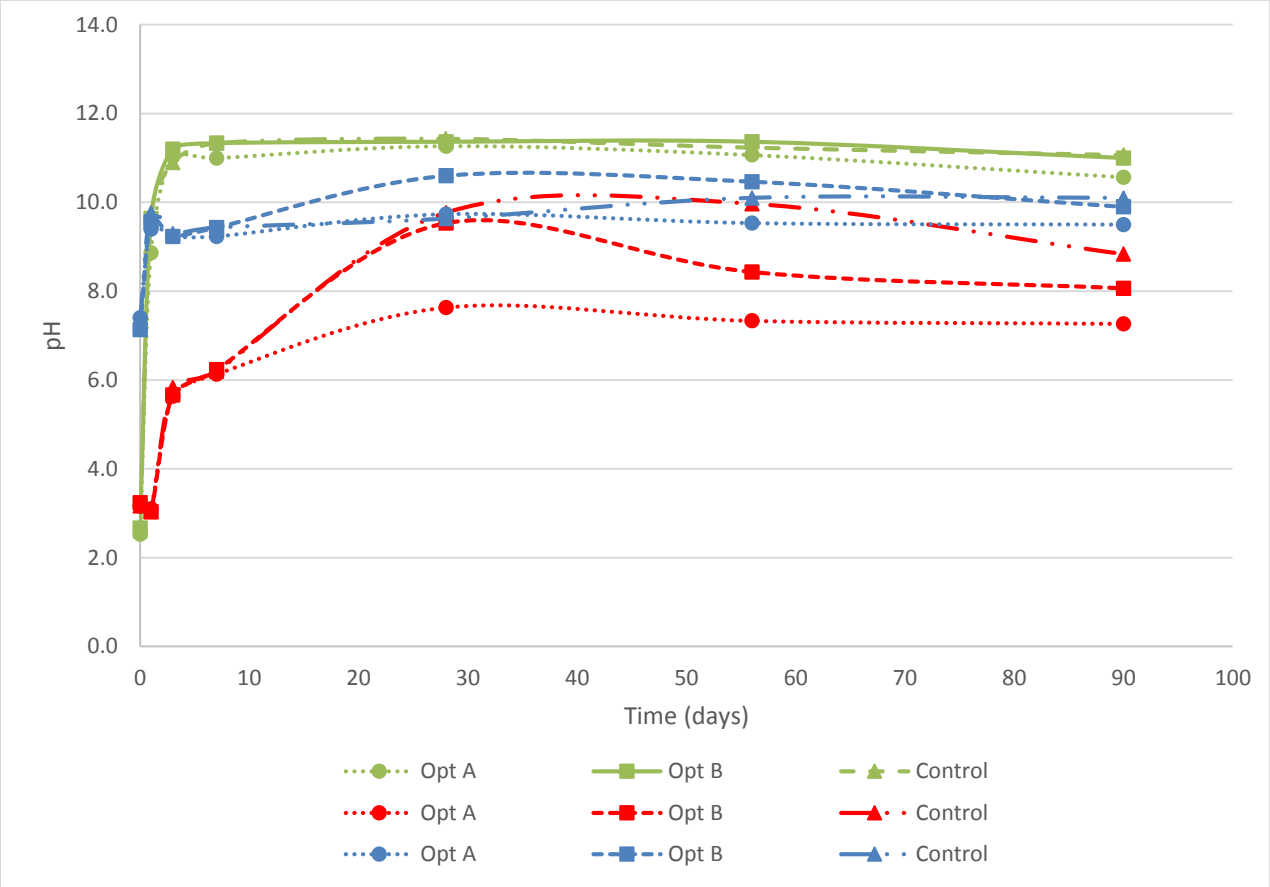

Figure 46. pH profiles when the paste specimens were in contact with tap water and acid solutions.

In the sulfuric acid solution, the pH of all of the GPCS increased from 2.6 to ~9.4 at day 1 (Figure 46) and then it stabilized at pH ~11.0 for the rest of the experiment. A much lower pH development was found in acetic acid solution than in the sulfuric acid (Figure 46). After one day of exposure, no change in the pH was observed. The Opt A GPCS had lower pHs in acetic acid solution, followed by the Opt B and then the Control. The highest pHs at ~9.7 were found at day 28 for the GPCS Opt B and Control, while the Opt A had the pH at 7.6. After day 56, the GPCS had slightly lower pHs than at day 28 and continued to decrease until the end of the experiment. These results were in good agreement with Bertron et al. (2005), who reported that acids with lower pKa values (strong acids) dissociated better in the solution, increasing the kinetics of pH increase in the solutions. Consequently, solution with GPCS exposed to sulfuric acid, which pKa

value is 1.987, resulted to have a faster pH increment than the acetic acid solutions (pKa = 4.756) (Harris, 2009).

6.4.3. Durability in terms of compressive strength change

Changes in compressive strength of the GPCS were tested after exposure in tap water and acid solutions for 90 days (Figure 47). The 28-day compressive strengths of the pastes measured prior to the durability experiment were used as the initial values for this purpose.

The type of chemical solution influenced the changes in the compressive strength. For example, all of the Opt A and Control GPCS that were exposed either to tap water or sulfuric acid gained compressive strength, whereas the Opt B GPCS lost the compressive strength in both solutions (Figure 47). Some of the specimens of the Opt A and Control GPCS slightly gained the compressive strength in acetic acid, although a significant weight loss was observed. This was consistent with the trend of weight changes (Figure 45) where the GPCS in tap water gained the weight the most and those in sulfuric acid solution the second, whereas those in acetic acid solution lost the weight.

Although sulfuric acid is a strong acid capable of decalcifying the binders of the GPCS, the sulfate ions present in the solution tend to form expansive products such as gypsum and ettringite when in contact with the GPCS, consequently incrementing the weight of the specimens. On the other hand, acetic acid tend to only form calcium salts (Mehta and Monteiro, 2014). The formation of highly soluble calcium salts ($Ca(CH_3COO)_2$) by the reaction of acetic acid with hydration products such as CH and C-S-H gel would have facilitated leaching of these soluble salts, leaving a more porous material, and therefore reducing the compressive strength as well as the weight of the GPCS.

Additionally, depending on the type of chemical solution, the FA and NI addition produced a mixed effect on the changes in the compressive strength. For example, when the GPCS had been exposed to tap water, the greatest gain of the compressive strength was found for the Control followed by the Opt A specimens and Opt B with the least compressive strength gain. On the other hand, when exposed to the sulfuric acid, Opt A the Control specimens obtained similar compressive strength changes, while Opt B resulted in a compressive strength reduction. The exposition to acetic acid attack also lead to very similar results for the Opt A and Control

specimens, although one of the Opt A specimens lost the compressive strength. The Opt B resulted in compressive strength reduction for only two of the specimens.

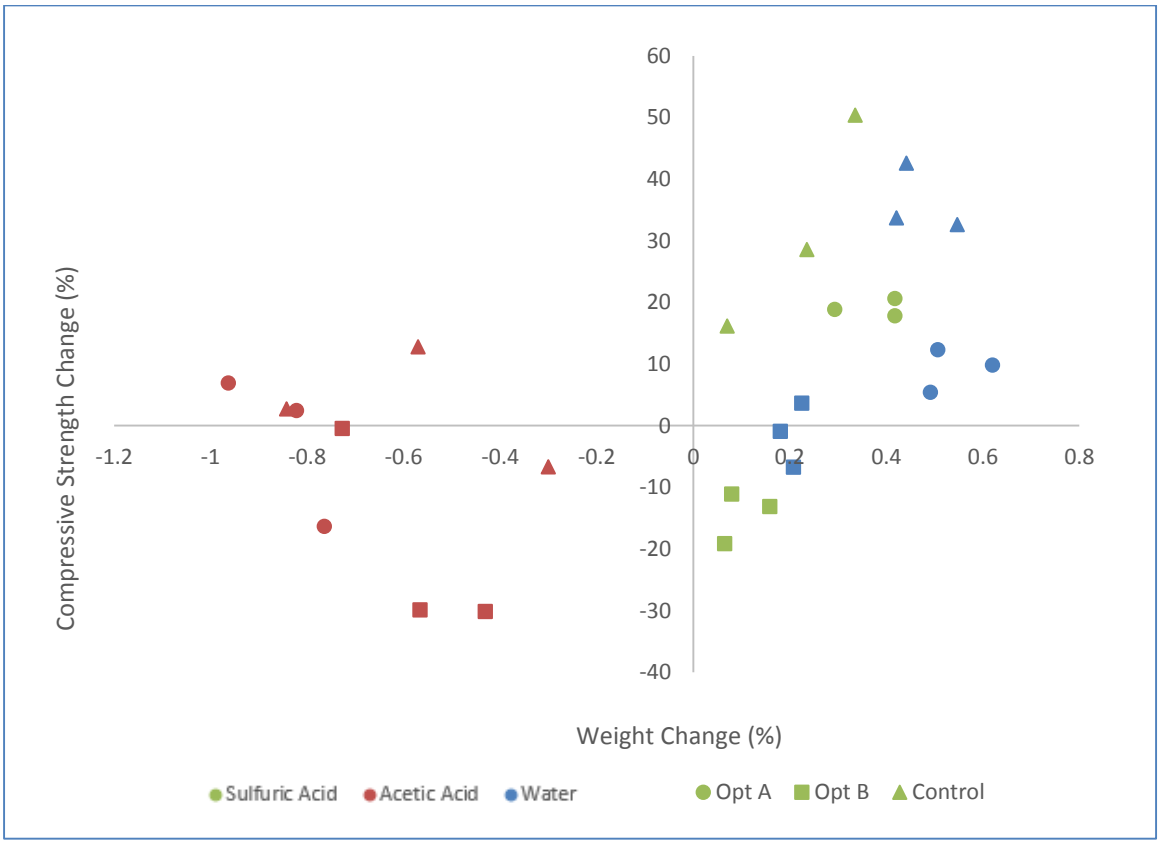

Figure 47. Changes in the compressive strength and weight of the specimens after a 90-day exposure in tap water and acid solutions.

Despite these results, it cannot be concluded that the simultaneous addition of FA and NI were not beneficial for the compressive strength improvement of the GPCS specimens. These results only show that the magnitude of the compressive strength increase was higher for the Control GPCS than for the Opt A and B, although the highest compressive strength after acid exposure were obtained for Opt A and Opt B, as shown in Table 30. It is also important to mention that after 3 months of exposure, weight loss was very low for all GPCS when exposed to acetic acid, ranging between 0.30 to 0.85% losses.

Table 30. Compressive strength development after acidic environment exposure.

Solution	Time (days)	Compressive Strength (MPa)		
		Opt A	Opt B	Control
Water	28	17.8	19.2	12.0
	90	22.0	16.8	18.0
Acetic acid	28	17.8	19.2	12.0
	90	17.7	16.4	12.4
Sulfuric Acid	28	17.8	19.2	12.0
	90	19.6	19.1	18.8

6.5. Conclusions

The physical and chemical changes such as variations in the weight, the compressive strength and the concrete microstructure were examined for three different mixture compositions. The following conclusions can be derived from the current study:

- Weight increment was observed for all the GPCS's when exposed to either water or sulfuric acid. It was lower than 0.6% and 0.4% when exposed to water and sulfuric acid, respectively.
- GPCS placed in the acetic acid solution resulted in a rapid weight loss, with values of weight reduction up to 0.85%.
- pH increment was found to have a higher rate for the sulfuric acid which had a lower pKa value.
- The simultaneous addition of FA and NI resulted in a higher compressive strength of the GPCS even after the exposition to acids.
- The addition of FA and NI was not beneficial in terms of preventing the weight and compressive strength loss of the GPCS when exposed to acidic environments.

6.6. References

Bertron A, Duchesne J, Escadeillas G. Attack of cement pastes exposed to organic acids in manure. Cement and Concrete Composites 2005; 27:898-909.

Chang JT, Song XJ, Munn R, Marosszeky M. Using limestone aggregates and different cements for enhancing resistance of concrete to sulphuric acid attack. Cement and Concrete Research 2005; 35:1486-94.

Chatveera B, Lertwattanaruk P. Evaluation of nitric and acetic acid resistance of cement mortars containing high-volume black rice husk ash. Journal of Environmental Management 2014; 133:365-373.

Girardi F, Di Maggio. Resistance of concrete mixtures to cyclic sulfuric acid exposure and mixed sulfates: Effect of the type of aggregate. Cement & Concrete Composites 2011; 33:276-285.

Girardi F, Vaona W, Di Maggio. Resistance of different types of concretes to cyclic acid and sodium sulfate attack. Cement & Concrete Composites 2010; 32:596-602.

Harris DC. *Exploring Chemical Analysis.* 4th Ed. W.H. Freeman and Company, 2009.

Hossain KMA, Lachemi M. Performance of volcanic ash and pumice based blended cement concrete in mixed sulfate environment. Cement and Concrete Research 2006; 36:1123-1133.

Makhloufi Z, Kadri EH, Bouhicha A, Benaissa A. Resistance of limestone mortars with quaternary binders to sulfuric acid solution. Construction and Building Materials 2012; 26:497-504.

Metha P, Monteiro P. *Concrete microstructure, properties and materials*. 4th Ed. McGraw-Hill Education, 2014.

Li G, Xiong G, Lü Y, Yin Y. The physical and chemical effects of long-term sulfuric acid exposure on hybrid modified cement mortar. Cement & Concrete Composites 2009; 31:325-330

Oueslati O, Duchesne J. The effect of SCMs and curing time on resistance of mortars subjected to organic acids. Cement and Concrete Research 2012; 42:205-214.

Sata V, Sathonsaowaphak A, Chindaprasirt P. Resistance of lignite bottom ash geopolymer mortar to sulfate and sulfuric acid attack. Cement & Concrete Composites 2012; 34:700-708.

Conclusions and Recommendations

The physicomechanical and durability properties of cement pastes containing different additives, the optimization of different mixture components, the mechanical and hydrological properties of a reactive PCPC, and the FC inactivation and nutrients removal from water were evaluated. The important remarks of each chapter are summarized as follows:

- The increment of W/B ratios resulted in a reduction of the compressive and tensile strength of the cement paste specimens. The FA substitution had a negative effect on the mechanical strength at early ages of curing, although a long term curing was beneficial as the pastes compressive strength was improved. The FA addition resulted in a lower fluidity, a delayed setting time and a faster initial water absorption rate. The NI addition enhanced the workability and reduced water absorption rate. The FA substitution with and without the NI addition deteriorated durability of the hardened pastes in acid solutions, whereas the NI addition alone enhanced durability, increasing the compressive strength.

- The extent of contribution that W/B, FA/B and NI/B ratios had on the compressive strength responses was time-dependent for the cement pastes containing FA and NI as admixtures. The spread percentage of fresh pastes increased with the increase of NI/B or W/B but with the decrease of FA/B. The slow pozzolanic reaction of FA that occurs at late ages produced a decrease of the compressive strength at early age of curing. The NI/B did not play a significant role in the development of compressive strength at early age, whereas it was effective in supporting the chemistry in cement paste at later curing stages. SEM images showed areas were a very dense microstructure was achieved for the specimens containing both the NI and FA. The developed statistical model predicted the dependent variables of spread percentage and compressive strength with good accuracy.

- The mix ratio of two different cement types was successfully optimized for a desired spread percentage and the maximum possible compressive strength of the hardened pastes cured for 28 days. The compressive strength of both the Type IP and GU cements decreased with the increment of W/B, while it was not affected by the addition of NI/B. The optimum variable settings for the GU cement was achieved at a higher FA% addition at 40% and a lower NI/B

addition at 0.55%, while similar W/B at 35.1%, resulting in slightly higher predictive strength at 64.72 MPa and a 110.13% of SP. These findings were attributed to the absence of pozzolans in the GU cement. The quadratic and interaction effects of the factors resulted to play a significant role in the development of the prediction models of the responses for both types of cements.

- The gravel with a uniform gradation was ideal for the making of pervious concrete since the particle sizes were in a very narrow range and resulted in a less packing of the aggregates while attaining a higher permeability. The reduction of the aggregate size resulted in a decrease in permeability but an increase in the compressive strength of the PCPC. The excess in W/B resulted in the partial clogging of the PCPC due to the drainage of the binder materials, whereas the lack of water and the excess of FA resulted in a very dry mixture and consequently an incomplete hydration of the binder materials resulted in lower CS's.

- The increment of W/B and the reduction of FA/B independent of the settings of NI/B and WR/B resulted in a decrease of the permeability of the specimens due to drainage of the binder material and clogging of the bottom of the GPCS's. The compressive strength increased with the decrease of permeability due to pore structure reduction of the specimens. The addition of large amounts of FA/B required an addition of more than 4% NI/B in order to achieve a compressive strength higher than 20.7 MPa. A greater FC and phosphorus removals were achieved at a higher pH, while the increase of contact time improved the nitrate reduction from water.

- The physical and chemical changes such as variations in the weight, the compressive strength and the concrete microstructure showed that weight was increased in all of the GPCS when exposed to either water or sulfuric acid. GPCS placed in the acetic acid solution resulted in a rapid weight loss. The pH increment was found to have a higher rate for the specimens placed in the solution with lower pKa values. The simultaneous addition of FA and NI resulted in a higher compressive strength of the GPCS even after the exposition to acids, although it was not beneficial in terms of preventing the weight and compressive strength loss of the GPCS when exposed to acidic environments.

In order to further support the findings in this study, it is recommended that further studies be made on:

- Microstructural analysis of the paste matrix by SEM coupled with energy-dispersive X-ray spectroscopy.
- Impact assessment of pervious concrete with respect to microbial population and dynamics in subsurface.
- Technical improvement of pervious concrete that could produce a neutral pH (6.5 – 8.5) in resulting water.